# INVESTIGATION OF PARAMETRIC INSTABILITY IN ELASTIC STRUCTURES

*By*

**SIVA SRINIVAS KOLUKULA**

**(PHYS02200804010)**

**Indira Gandhi Centre for Atomic Research, Kalpakkam**

***A thesis submitted to the***

***Board of Studies in Physical Sciences***

***In partial fulfillment of requirements***

***For the Degree of***

**DOCTOR OF PHILOSOPHY**

***of***

**HOMI BHABHA NATIONAL INSTITUTE**

**December, 2013**

# Homi Bhabha National Institute

## Recommendations of the Viva Voce Board

As members of the Viva Voce Board, we certify that we have read the dissertation prepared by Siva Srinivas Kolukula entitled "Investigation of parametric instability in elastic structures" and recommend that it may be accepted as fulfilling the dissertation requirement for the Degree of Doctor of Philosophy.

____________________________ **Date:**

Chairman - Dr. T. Jayakumar

____________________________ **Date:** 09/05/15

Guide / Convener - Dr. P. Chellapandi

____________________________ **Date:** 09/5/2015

Member 1 - Dr. A. K. Bhaduri

____________________________ **Date:**

Member 2 - Dr. C. Lakshman Rao

____________________________ **Date:** 09/05/2015

External Examiner: Dr. Jebaraj Chidambaram

Final approval and acceptance of this dissertation is contingent upon the candidate's submission of the final copies of the dissertation to HBNI.

## CERTIFICATE

I hereby certify that I have read this dissertation prepared under my direction and recommend that it may be accepted as fulfilling the dissertation requirement.

P. Ch

Guide – Dr. P. Chellapandi

**Date:** 09/05/15

## STATEMENT BY AUTHOR

This dissertation has been submitted in partial fulfillment of requirements for post doctoral degree at Homi Bhabha National Institute (HBNI) and is deposited in the Library to be made available to borrowers under rules of the HBNI.

Brief quotations from this dissertation are allowable without special permission, provided that accurate acknowledgement of source is made. Requests for permission for extended quotation from or reproduction of this manuscript in whole or in part may be granted by the Competent Authority of HBNI when in his or her judgment the proposed use of the material is in the interests of scholarship. In all other instances, however, permission must be obtained from the author.

K. Siva Srinivas

(Siva Srinivas Kolukula)

# DECLARATION

I, hereby declare that the investigation presented in the thesis has been carried out by me. The work is original and has not been submitted earlier as a whole or in part for a degree / diploma at this or any other Institution / University.

K. Siva Srinivas

(Siva Srinivas Kolukula)

**DEDICATED to**

*To those who never give up*

(Siva Srinivas Kolukula)

# ACKNOWLEDGEMENTS

First and foremost I offer my sincerest gratitude to my supervisor, **Dr. P. Chellapandi**, *Director, Reactor Design Group, IGCAR* who has supported me throughout my thesis with his patience and knowledge whilst giving me the space to work in my own way. The enthusiasm he has towards the research was contagious and motivational for me during the PhD pursuit. One simply could not wish for a better supervisor.

I convey my sincere gratitude to **Dr. P. R. Vasudev Rao**, *Director, IGCAR* and **Sri. S. C. Chetal,** *former Director, IGCAR* for their constant support and encouragement to research fellows of *IGCAR*. I appreciate the amenities and environment created by **Dr. Baldev Raj**, *former Director, IGCAR* towards pursuing high-end research. I acknowledge him for creating an opportunity for many research fellows to be a part of this wonderful institution and pursue enterprising research.

I thank **Dr. M. Saibaba**, *Associate Director, Resource Management Group* for his constant support and encouragement during the time.

I express my sincere gratitude to all the teachers who taught me during the course work in training school. Especially my sincere thanks to **Sri M. Valsakumar**, **Dr. S. Sivakumar**, **Sri. S. Kanmani**, **Dr. K. Raghavan**, **Prof. Jebraj** (*Anna-University*).

I gratefully acknowledge **Sri T. Selvaraj**, *Head, PFRP Design Section*, **Sri S. Jalaaldeen**, *Head, Structural Mechanics Section* for their valuable contributions and kind help sharing their scientific and technical knowledge through clearing my doubts whenever I approached them.

I would like to thank my Doctoral Committee members **Prof. C. Lakshmana Rao** (*IIT Madras*), **Dr. T. Jayakumar**, *Director, Metallurgy and Materials Group*, **Dr. A. K. Bhaduri**, *Associate Director, Material Development and Technology Group* who provided encouraging and constructive feedback towards thesis work giving insightful suggestions and advice.

I thank **Sri P. Selvaraj**, *Associate Director, Reactor Analysis Group*, **Sri V. Rajan Babu**, *Head, Reactor Assembly Section* for facilitating the official formalities.

I am deeply indebted to **Mr. S. D. Sajish**, *SO (F)*, *Structural Mechanics Section* for his help in conducting shake table experiments. He has also helped me providing insightful discussions about the subject.

I thank **Mr. R. Suresh Kumar** and **Mr. Raghavendran** for taking care of the official activities while conducting shake table experiments.

I acknowledge crew of *Structural Mechanics Laboratory***, Mr. Aravind**, **Mr. Babu Rao**, **Mr. Venkatiah**, **Mr. Raja**, **Mr. Ramesh Selam, Mr. Rajesh**, **Mr. Mano and Mr. Devraj** for their help in shake table experiments in their own ways and keeping a homely environment at my work place.

I acknowledge **Mr. Govindraj**, **Mr. Nithya**, **Mr. Veera** for providing me assistance in office hold works during my office hours.

A good support and surroundings are important for surviving and staying sane; my time at *IGCAR* was made enjoyable in large part due my friends who became a part of my life providing support and friendship that I needed.

I acknowledge my friend **Mr. Ashok Kumar** for his healthy discussions on subject and my research related aspects constantly at coffee breaks and listening to my ideas, grievances related to numerical aspects of coding providing me ideas and help to best of his knowledge.

I am thankful to my friends **Mr. D. Uday Kumar, Mr. Ranjit Jovin Cyriac** and **Mr. Nimala Sundaran** for their discussions on the subject which were helpful to clear my ambiguities on the subject. My special thanks to **Mr. D. Uday Kumar** for proofreading my research related articles and giving me suggestions.

I am grateful for time spent with my backpacking buddies **Mr. P. Srijan Babu** and **Mr. A. Santhana Raj** and our memorable trips to different places. My special thanks to **Mr. A. Santhana Raj** for sharing tips on MATLAB and checking my MATLAB codes irrespective of his field. My special thanks to **Mr. P. Srijan Babu** for being supportive, helpful throughout my time here.

To my dear comrades **Mr. D. Sharath**, **Mr. Ilairaja**, **Mr. Naveena**, **Mr. Mariyappa Narayanan**, **Mr. Bubathi Muruganatntham** thanks for being friends, awesome officemates and thanks for being there to listen, console, bearing the brunt of the frustrations and sharing the joy of the successes.

I thank **Mr. Ashustosh Mishra** and **Mr. L. Ravi** for their constant support. I am thankfull to my senior friends **Dr. Pandian Chelliah** and **Dr. Kamalakanta Sathpathy** for their advices and sharing their experiences during my early stage of research.

Lastly, I would like to thank my family for all their love and encouragement. For my parents who raised me with love and supported me in all my pursuits. And most of all for my loving, supportive, encouraging and patient wife **Sreedevi** whose faithful support during the final stages of this PhD is highly appreciable.

K. Siva Srinivas

**Siva Srinivas Kolukula**

# CONTENTS

ABSTRACT

In many engineering applications it is essential to know the maximum response of the system and the nature of the oscillations under external excitations, during design in order to meet fundamental requirements. Under external excitations the system may show maximum response under resonance and or parametric resonance. Resonance corresponds to the tendency of the system to oscillate with greater amplitude, when the external excitation frequency is equal to natural frequency of the system. In resonance, the rate of increase of systems amplitude is linear. Parametric resonance refers to an oscillatory motion in a mechanical system due to time-dependent variation of the system parameters caused due to external excitation. The response of the system is orthogonal to the direction of external excitation. In parametric resonance, the rate of increase of systems response is generally exponential and grows without limit. This exponential unlimited increase of amplitude is potentially dangerous to the system. Although parametric resonance is secondary, the system may undergo failure near the critical frequencies of parametric resonance. Parametric resonance is also referred as parametric instability or dynamic instability.

The general mathematical equation of a mechanical system under parametric excitation is given by

$$M(t)\ddot{q} + C(t)\dot{q} + K(t)q = 0 \tag{1}$$

where $q$ is amplitude of response of the system, dots denote differentiation with respect to time $t$. $M(t)$, $C(t)$ and $K(t)$ are inertial, damping and stiffness matrices respectively. The mechanical system described by Eq. (1) can experience

parametric instability when the excitation frequency $\Omega$ is twice or any integral multiple of the system natural frequency $\omega$, i.e.

$$\Omega = m\omega, \; m = 2, 3 \ldots \tag{2}$$

The case $\Omega = 2\omega$, is most important in the application and is known as principal parametric resonance. Also system undergoes parametric instability when excitation frequency is equal to combination of systems natural frequencies i.e.

$$\Omega = m\left(\omega_i \pm \omega_j\right) \tag{3}$$

The main objective of analysis of the parametrically excited systems described by Eq. (1) is to establish the relationship between the system parameters at which the solution is unstable. The solution of Eq. (1) can be represented by the regions in the parameter space in which the system becomes unstable. These regions are known as regions of dynamic instability. The boundary separating a stable region from an unstable one is called a stability boundary. Plot of these boundaries on the parameter space is called a stability diagram.

**Outline of the present work**

The present work mainly deals with investigation of parametric instability of elastic structures, free surface of liquid and liquid-filled shells. The computer programs have been written for this purpose. The governing equations of motion are solved employing finite element method. Theoretical investigations have been carried out where ever possible and an experimental investigation of dynamic stability of plane free surface of liquid on shake table is reported. The stability boundaries for the elastic structures have been established by using Floquet's theory, Bolotin's method and Hsu's conditions. For numerical computations computer programs have been developed using MATLAB and CAST3M.

This thesis contains seven chapters.

In chapter 1 a detailed introduction to parametric instability and its governing equation of motion classified as Hill's equation is given. The objective of the Hill's equation is not to get the exact form of solution but to know under what parameters system undergoes instability. Various methods employed to obtain stability boundary diagrams are discussed along with detailed survey of relevant literature in this chapter.

In chapter 2 dynamic stability of a parametric oscillator is considered i.e. dynamic instability of a single degree of freedom (SDOF). A parametric oscillator is a simple pendulum or an inverted pendulum excited vertically at its pivot; it is a harmonic oscillator whose parameters oscillate in time. This study helps in understanding the basics of parametric instability. The governing equation for the parametric oscillator is Mathieu equation. Stability diagram is plotted using Bolotin's approach and reliability of the stability diagram is checked via simulation of response of Mathieu equation employing Runge-Kutta method.

Chapter 3 deals with the investigation of dynamic stability of a slender beam. The instability regions are obtained using finite element Bolotin's approach. To check the reliability of the procedure direct time integration using Newmark's method is carried out. The instability regions are checked by plotting time vs. displacement plots at different integration points.

In chapter 4 dynamic stability of simply supported plate under uniform edge loading is investigated. The governing Mathieu-Hill equation is obtained by employing finite element formulation. Mindlin plate theory is used for the formulation of global system matrices. The effects of static load factor of edge loading and aspect ratio on the dynamic stability of plate are studied.

Chapter 5 deals with dynamic stability of bottom clamped cylindrical shells under uniform periodic compressive force. The governing Mathieu-Hill equation is obtained by employing finite element formulation. 3D degenerated four noded shell elements are used for the formulation of global system matrices. Two shells of different aspect ratio are considered for investigating the dynamic stability.

In chapter 6 dynamic stability of plane free-surface of liquid in rectangular tanks is investigated numerically considering fully non-linear equations. Dynamic stability chart is plotted from the linear governing equations and response of the fluid is simulated employing arbitrary Eulerian-Lagrangian finite element method. The slosh response is simulated for horizontal, vertical and combined base excitations of the tank. An experiment on shake table is carried out to validate the stability chart obtained.

Chapter 7 addresses the dynamic stability of bottom clamped cylindrical shells filled with fluid under vertical base excitation taking fluid-structure interaction into consideration. The governing Mathieu-Hill equation is obtained by employing finite element formulation. Two tanks of different aspect ratio are taken and analysis is carried out in CAST3M.

Finally in chapter 8 important conclusions drawn from the present investigations reported in chapters 3-7 along with suggestions for future work are presented.

# LIST OF FIGURES

# LIST OF TABLES

# LIST OF ANIMATIONS / VIDEOS

| No. | Animation / Video | Link |
|---|---|---|
| 1 | Stable response of vertically excited simple pendulum | http://youtu.be/QwSHhknz9ys |
| 2 | Unstable response of vertically excited simple pendulum | http://youtu.be/L-Q6xg2KbCA |
| 3 | Stable response of vertically excited inverted pendulum | http://youtu.be/GwlegJHI4vQ |
| 4 | Unstable response of vertically excited inverted pendulum | http://youtu.be/ytkwtTaWOq0 |
| 5 | Stable response of beam under parametric excitation | http://youtu.be/mOAmeDxQq9w |
| 6 | Unstable response of beam under parametric excitation | http://youtu.be/xW065jvw_wg |
| 7 | Stable response of plate under parametric excitation | http://youtu.be/zg508alVhbA |
| 8 | Unstable response of plate under parametric excitation | http://youtu.be/iU_XbJJzZeQ |
| 9 | Free-surface response under resonance | http://www.youtube.com/watch?v=LlwUOWMmVtc |
| 10 | Free-surface response under parametric resonance | http://youtu.be/VTsA0I7Ry4s |
| 11 | Free-surface response under detuning effect | http://youtu.be/ylRHuxKt3rw |
| 12 | Stable response of liquid free-surface under vertical excitation | http://youtu.be/L1LADAPVKG4 |
| 13 | Unstable response of liquid free-surface under vertical excitation | http://youtu.be/4ft_jd5dkvQ |

# LIST OF PUBLICATIONS

## JOURNALS

1. **Siva Srinivas Kolukula** and P. Chellapandi, Nonlinear Finite Element Analysis of Sloshing, Advances in Numerical Analysis, Vol. 2013, Article ID 571528, 10 pages, 2013. doi:10.1155/2013/571528.
2. **Siva Srinivas Kolukula** and P. Chellapandi, Dynamic Stability of Plane Free Surface of Liquid in Axisymmetric Tanks, Advances in Acoustics and Vibration, Vol. 2013, Article ID 298458, 16 pages, 2013. doi:10.1155/2013/298458.
3. **Siva Srinivas Kolukula** and P. Chellapandi, Finite element simulation of plane free-surface of a liquid under vertical excitation, Modelling and Simulation in Engineering, Vol. 2013, Article ID 252760, doi:10.1155/2013/252760.
4. **Siva Srinivas Kolukula,** S. D. Sajish and P. Chellapandi, Experimental investigation of slosh parametric instability in liquid filled vessel under seismic excitations, Annals of Nuclear Energy, Vol. 76, February 2015, pages. 218-225, doi:10.1016/j.anucene.2014.09.056.
5. **Siva Srinivas Kolukula** and P. Chellapandi, Finite element simulation of sloshing motion in excited tanks. (Under review).
6. **Siva Srinivas Kolukula** and P. Chellapandi, Dynamic stability of elastic structures under combined parametric and forcing excitations: a finite element approach. (Under review).
7. **Siva Srinivas Kolukula**, and P. Chellapandi, Non-linear finite element analysis of sloshing in liquid-filled containers with submerged components. (To be communicated).
8. **Siva Srinivas Kolukula** and P. Chellapandi, Investigation of parametric instability of thin shells with fluid-structure interaction. (Manuscript under preparation).
9. **Siva Srinivas Kolukula** and P. Chellapandi, Non-linear finite element analysis of sloshing considering fluid-structure interaction. (Manuscript under preperation)

## CONFERENCE PROCEEDINGS

1. **Siva Srinivas Kolukula**, S. D. Sajish and P. Chellapandi, Seismic behaviour of liquid filled cylindrical tanks considering fluid-structure interaction, Mathematical Modelling and Applications to Industrial Problems (MMIP 2011), 28$^{th}$-31$^{st}$ March 2011, NIT Calicut, Kerala, India.
2. **Siva Srinivas Kolukula** and P. Chellapandi, Dynamic stability of elastic structures, International Conference on MATLAB Applications in Engineering and Technology (ICMAET 2012) , 9$^{th}$-10$^{th}$ March 2012, Hyderabad, India.
3. **Siva Srinivas Kolukula** and P. Chellapandi, Nonlinear finite element analysis of sloshing, International Conference on Recent Advances in Science and Engineering (ICRASE 2012), 30$^{th}$-31$^{st}$ October 2012**,** Hyderabad, India.
4. C. Vishnu Pandi and **Siva Srinivas Kolukula**, Dynamic Analysis of liquid in rectangular container, International Congress on Computational Mechanics and Simulation (ICCMS 2012), 9$^{th}$-12$^{th}$ December 2012, IIT Hyderabad, India.
5. **Siva Srinivas Kolukula** and P. Chellapandi, Dynamic stability of rectangular plates subjected to edge loading, Structural Engineering Convention (SEC 2012), 9$^{th}$-21$^{st}$ December 2012NIT Surat, Gujarat, India.
6. **Siva Srinivas Kolukula** and P. Chellapandi, Dynamic stability of plane free-surface of liquid under vertical excitation: An experimental study, International Conference on Pressure Vessel and Piping (OPE 2013), 13$^{th}$-16$^{th}$ February 2013, Mamallapuram, Chennai, India.
7. **Siva Srinivas Kolukula** and P. Chellapandi, Non-linear slosh dynamics of liquid-filled containers with submerged components, Indian Conference on Applied Mathematics (INCAM 2013), 4$^{th}$-6$^{th}$ July 2013, IIT Madras, India.

## AWARDS

**Best oral presentation award**

1. **Siva Srinivas Kolukula** and P. Chellapandi, Dynamic stability of elastic structures, International Conference on MATLAB Applications in Engineering and Technology (ICMAET 2012), Hyderabad, India, 9$^{th}$-10$^{th}$ March 2012.

2. **Siva Srinivas Kolukula** and P. Chellapandi, Nonlinear finite element analysis of sloshing, International Conference on Recent Advances in Science and Engineering (ICRASE 2012), Hyderabad, India, 30th-31st October 2012.

# Chapter 1

# INTRODUCTION

## 1.1 Parametric Instability

In many engineering applications it is of immense interest to study the vibratory motion of a mechanical system under external excitations. In all the mechanical systems under going oscillatory or vibratory motion, it is essential to know the time history, or the maximum response of the system, and the nature of the oscillations i.e. if it is periodic, chaotic or not. It is very important to know the different resonance frequencies of the system for an efficient and safe design of the structures so that harmful resonances can be avoided during the working conditions. External excitations can cause the system to undergo two kinds of oscillations; forced oscillations and parametric oscillations. Forced oscillations correspond to the oscillatory response of the system in the direction of external excitation and system undergoes resonance when the external excitation frequency is equal to natural frequency of the system. In resonance, the rate of increase of systems amplitude is linear. The amplitude attained under resonance can be effectively reduced by including damping in the system. Parametric oscillations refer to an oscillatory motion of a mechanical system due to time-dependent variation of the system parameters caused due to external excitation. The external excitation enters into the system and changes the geometry of the system which in turn results in variation of system parameters, due to which forces or torques do work on the system and energy flows into the system from external source, depending on the frequency of system parameter variation and the natural frequencies of the system; such a state created is called parametric resonance.  The system parameters can be inertia, damping or stiffness. Under parametric resonance, when certain energy flows into the system, the amplitude of the system response increases. The response of the system is orthogonal to the direction of external excitation. In parametric resonance, the rate of increase of the system's response is generally exponential and grows without limit. This exponential unlimited increase of amplitude is potentially dangerous to the system. This behaviour is referred to as parametric instability or dynamic instability. Introducing damping can reduce only rate of increase of amplitude and thus have little or no effect on final amplitudes. System undergoes parametric resonance when the frequency of external excitation is equal to integral multiple of natural frequency of the system. The resonance condition is considered primary and given utmost importance during designing of the structures. Although parametric resonance is secondary, the system may undergo failure near the critical frequencies of parametric resonance. The general mathematical equation of a mechanical system under parametric excitation is given by

$$M(t)\ddot{q}(t)+C(t)\dot{q}(t)+K(t)q(t)=0 \tag{1.1}$$

and

$$M(t+T)=M(t),\;\; C(t+T)=C(t),\;\; K(t+T)=K(t) \tag{1.2}$$

where *q(t)* is amplitude of response of the system, dots denote differentiation with respect to time *t*. *M(t)*, *C(t)* and *K(t)* are inertial, damping and stiffness matrices respectively with a time period *T*. Eq. (1.1) is a second order homogenous differential equation with time dependent coefficients; such type of equation is called Hill's equation. The mechanical system described by Eq. (1.1) can experience parametric instability when the excitation frequency Ω is twice or any integral multiple of the system natural frequency $\omega$, i.e.

$$\Omega = m\omega,\ m = 2, 3\ldots \tag{1.3}$$

The case $\Omega = 2\omega$, is most important in design point of view and it is known as principal parametric resonance. Not only at these discrete frequencies, parametric instability can occur over a spectrum of frequencies which are away from natural frequencies of system for a given external excitation amplitude. In case of multi degrees of freedom (MDOF), parametric instability can occur when the excitation frequency equals to sum or difference of systems natural frequencies of different modes.

$$\Omega = \frac{1}{n}\left(\omega_i \pm \omega_j\right) \tag{1.4}$$

The above relation defines the condition of parametric combination resonance. Combination resonance is of first order when $n = 1$; otherwise, it is of $n$-th order.

The main objective of analysis of the parametrically excited systems Eq. (1.1) is to establish the relationship between the system parameters at which the solution will become unstable. The solution of Eq. (1.1) can be represented by the regions in the parameter space in which the system becomes unstable. These regions are known as regions of dynamic instability. The boundary separating a stable region from an unstable one is called a stability boundary. Plot of these boundaries on the parameter space is called stability diagram.

In practice, parametric excitation can occur in structural systems subjected to vertical ground motion, air craft structures subjected to turbulent flow, marine crafts subjected to longitudinal waves and in machine components and mechanisms. Other examples are liquid sloshing in tanks subjected to longitudinal excitation, thin shells filled with fluid under horizontal and vertical excitations and spinning satellites in elliptic orbits passing through a periodically varying gravitational field. In industrial machines and mechanisms, their components and instruments are frequently subjected to periodic or random excitation transmitted through elastic coupling elements. A few examples include those associated with electromagnetic and aeronautical instruments, vibratory conveyers, saw blades, belt drives and robot manipulators etc.

## 1.2 Difference between resonance and parametric instability

Although parametric resonance has a term resonance, its features are completely different from typical resonance. Parametric resonance differs as follows compared to normal resonance.

**Table 1.1**: Difference between parametric instability and resonance

| | **Parametric Resonance** | **Resonance** |
|---|---|---|
| 1. | External excitation enters into the system; the excitation is called parametric excitation. | External excitation remains outside as a forcing term; the excitation is called forcing excitation. |
| 2. | The excitation makes the system properties time dependent. | System properties are constant and are time independent. |
| 3. | Systems response is orthogonal to direction of excitation. | Systems response is along the direction of excitation. |
| 4. | The rate of increase of systems response is exponential. | The rate of increase of systems response is linear. |
| 5. | Damping has no control on the peak amplitude. Damping can reduce only the rate of increase of amplitude. | Damping can control the peak value of amplitude. |

| | | |
|---|---|---|
| 6. | Governing equation is second order homogenous differential equation with time dependent coefficients. | Governing equation is second order inhomogeneous differential equation with constant coefficients. |
| 7. | $M(t)\ddot{q}+C(t)\dot{q}+K(t)q=0$ | $M\ddot{q}+C\dot{q}+Kq=F(t)$ |

## 1.3 Historical background of parametric instability

The early work on parametric instability was reported in fluid mechanics. The credit of first work on parametric resonance goes to Faraday [1] way back in 1831. Faraday observed that when a thin sheets of fluid like mercury, ink, water, alcohol, turpentine, milk and egg white covering a horizontal plate subjected to vertical vibration forms elevations, waves or crispations with a peculiar character on the plate projecting directly out of the plate. Faraday reported that these waves had a frequency equal to half the excitation frequency. Such waves generated under vertical excitation are sometimes referred to as Faraday waves. On a similar ground, parametric resonance in a stretched string was demonstrated experimentally by Melde [2]. In his experiment the tension in a string is varied periodically through attachment to one of the vibrating prongs of a massive tuning fork. The theoretical explanation for Melde's experiment was given by Rayleigh [3]. Matthiessen [4] repeated Faraday's experiment and reported that the fluid free surface vibrations are synchronous to the external vertical excitation. The Faraday's study has been analyzed by Rayleigh [5, 6] and the analysis confirmed Faraday's observations. On the same context of parametric resonance in free-surface of fluid, the discrepancy between Faraday's observations and Matthiessen's observations were explained mathematically by Benjamin and Ursell [7]. Benjamin and Ursell investigated the problem theoretically and concluded that the governing equation to study the response of plane free-surface of fluid under vertical excitation is Mathieu equation [8].

The first work on parametric instability in structures was reported in an article by Beliaev [9]. Beliaev analysed the dynamic stability of a straight rod hinged on both ends and plotted the boundaries of principal region of instability theoretically. Later the problem of dynamic stability of rods with arbitrary support conditions was examined by Krylov and Bogoliubov [10]. A detailed review of the literature on the theory of dynamic stability in elastic structures till 1951 can be found in a review article by Beilin and Dzhanelidze [11]. The problem of dynamic stability is discussed in books by Stoker [12], Timoshenko [13], Bolotin [14], Nayfeh and Mook [15], Ibrahim [16] and Cartmell [17]. Bolotin [15] studied extensively on the dynamic stability of elastic systems under parametric excitations. Several review articles are published on parametric resonance, few worth noting articles are by Evan Iwanoski [18], Ariaratnam [19] and Simitses [20].

## 1.4 Mathematical methods for stability analysis

The governing equation for parametric excited system is a second order homogenous equation with time dependent coefficients as given in Eq. (1.1). The system parameters like mass, damping and / or stiffness become time dependent under parametric excitation. In the present dissertation, parametric systems with time dependent stiffness are considered. The governing equation of motion for such a system is given as

$$M\ddot{q}(t)+C\dot{q}(t)+K(t)q(t)=0 \tag{1.5}$$

and

$$K(t+T)=K(t) \tag{1.6}$$

The Eq. (1.5) is classified as Hill equation [21] and if the time varying coefficient matrices are sinusoidal it is classified as Mathieu equation [8]. To predict and determine the dynamic behavior of system, stability analysis must be implemented on Hill's equation Eq. (1.5). The main objective of solving Eq. (1.5) is to find the existence of periodic solutions and their stability. Lots of mathematical methods are available to solve Eq. (1.5). A few well known solution methods which are commonly employed are Floquet's theory, Bolotin's approach based on Floquet's theory, perturbation techniques, iteration techniques, Galerkin's method, the Lyapunov second order method and the asymptotic technique by Krylov, Bogoliubov and Mitroploskii.

The essence of Floquet's method is to examine the stability of the state transition matrix that maps an initial state to the state after one time period [22-24]. The state transition matrix can be formed from Wronskian matrix, but the numerical integrals require time consuming computations, especially for higher order dimensional systems. Bolotin [14] proposed a method based on Floquet's theory for stability boundary tracing; Bolotin considered two types of solutions with periods of T and 2T expanded using Fourier series respectively, the areas surrounded by two solutions with identical periods are unstable and by two solutions with different periods are stable. But this method can be used to get stability boundaries for simple resonance only. This method was extended to find combination resonance boundaries in [25-30].

Hsu [31-32] developed a perturbation based technique for stability analysis of parametric systems under small parameter excitations, which can be employed to obtain instability zones of simple, combination and difference type. Hsu gave conditions of stability and instability for a system with multi degrees of freedom under parametric excitation, which can be used to plot stability chart with ease. Hsu's technique works faster than Floquet and Bolotin's technique since it does not involve numerical computations.

Many researchers applied finite element method to study the dynamic stability of elastic systems. Brown [33] was the first investigator to employ finite element method to solve dynamic stability of bars. Burney [34] studied dynamic stability of plane structures. Abbas and Thomas [35], Abbas [36] analysed stability of Timoshenko beams using finite element method. Shastry [37-39] applied finite element method to study the dynamic stability of bars and cantilever columns subjected to axial loads. The finite element approach of Mathieu-Hill equation in case of shallow shells was proposed by Basar [40]. Briseghella [41] studied the dynamic stability problems of beams and frames by using finite element method. Svensson [42] studied the stability properties of a periodically loaded non-linear dynamic system, giving special attention to damping effects.

The present dissertation employs Floquet theory, finite element based Bolotin's approach and Hsu's method for stability analysis. These methods are explained below in the following sections in detail.

### 1.4.1 Floquet Theory

The state-space form of Hill's equation Eq. (1.5) is

$$\dot{X} = A(t)X \quad \text{with} \quad X = \left[ q(t)^T \quad \dot{q}(t)^T \right]^T \tag{1.7}$$

where

$$A(t)=\begin{bmatrix} 0 & I \\ -M^{-1}K(t) & -M^{-1}C \end{bmatrix} \text{ and } A(t+T)=A(t) \tag{1.8}$$

Here, $X$ is a column vector including $2n$ system state variables; $A(t)$ is a $2n \times 2n$ periodic system matrix with the period $T$; $0$ and $I$ are $n \times n$ zero and identity matrix respectively. According to Floquet theory, the stability of the periodically linear time-varying system, such as Eq. (1.7), can be represented by the stability status over only one period. The state of the system $X(t)$ at a time $t$ can be transferred to another state of time $t_0$ through a transition matrix $\Phi(t,t_0)$, and it is expressed as

$$X(t)=\phi(t,t_0)X(t_0) \tag{1.9}$$

Thus, the state after one period $T$, is

$$X(T)=\phi(T,0)X(0) \tag{1.10}$$

If the initial state is identity, $X(0) = I_{2n}$, then

$$X(T)=\phi(T,0) \tag{1.11}$$

Here, $I_{2n}$ is a $2n \times 2n$ identity matrix. In general, the state after $k$-integral periods is given by [22-24]

$$X(t+kT)=\phi(T,0)^k X(t) \tag{1.12}$$

The state transition matrix, $\Phi(T,0)$, can be obtained by numerically integrating Eq. (1.7) from 0 to $T$ with initial conditions as identity matrix. This transition matrix is called Floquet Transition Matrix (FTM), and its eigenvalues, $\lambda_i$, are Floquet multipliers. These Floquet multipliers govern the stability characteristics of the system. The stability criteria is given by [22-24]

$$\frac{\ln \lambda_i}{T}=\alpha_i+i\beta_i \text{ and } \begin{cases} \alpha_i<0 & \textit{stable} \\ \alpha_i \ge 0 & \textit{unstable} \end{cases} \tag{1.13}$$

This method can give all instabilities but need intensive computations due to numerical integration of Eq. (1.7).

### 1.4.2 Bolotin's approach

#### 1.4.2.1 Analytical Bolotin's approach

The analytical governing equation for a single degree of freedom (SDOF) for the dynamic stability of a system under periodic longitudinal force is given by

$$\ddot{q} + 2\eta\dot{q} + \Omega\,(1 - 2\mu\cos\theta t)\,q = 0 \qquad (1.14)$$

where Ω and $\mu$ are the relations given as follows

$$\Omega = \omega\sqrt{1 - \frac{P_0}{P_{cr}}}\ ; \qquad \mu = \frac{P_d}{2(P_{cr} - P_0)} \qquad (1.15)$$

and *q(t)* is the deflection, $\eta$ is damping, **Ω** is natural frequency of the system loaded with static component $P_0$, $\mu$ is the excitation parameter, $\theta$ is the frequency of external periodic force, $P_d$ is the dynamic component of external excitation and $P_{cr}$ is the buckling load of the system. Equation (1.14) is a Mathieu-Hill equation. According to Bolotin [14], Eq. (1.14) will have periodic solutions with period *T* or *2T* and can be represented by the following Fourier series expansions

$$T : q = \frac{1}{2}b_0 + \sum_{k=2,4,\ldots}^{\infty}\left(a_k \sin\frac{k\theta t}{2} + b_k \cos\frac{k\theta t}{2}\right), \qquad (1.16)$$

$$2T : q = \sum_{k=1,3,\ldots}^{\infty}\left(a_k \sin\frac{k\theta t}{2} + b_k \cos\frac{k\theta t}{2}\right), \qquad (1.17)$$

where $a_k$ and $b_k$ are time-independent Fourier coefficient vectors. They are determined by substituting Eq. (1.16-1.17) into Eq. (1.14). Substitution of Eq. (1.17) into Eq. (1.14) and a term wise comparison of sin$(k\theta t)/2$ and cos$(k\theta t)/2$ coefficients leads to the following infinite system of homogenous algebraic equations for the unknown vector sequence $a_k$ and $b_k$ ($k = 3, 5, \ldots$)

$$
\begin{aligned}
&\left(1+\mu-\frac{\theta^2}{4\Omega^2}\right)a_1-\mu a_3-\frac{\Delta}{\pi}\frac{\theta}{2\Omega}b_1=0\\
&\left(1-\mu-\frac{\theta^2}{4\Omega^2}\right)b_1-\mu b_3+\frac{\Delta}{\pi}\frac{\theta}{2\Omega}a_1=0\\
&\left(1-\frac{k^2\theta^2}{4\Omega^2}\right)a_k-\mu\left(a_{k-2}+a_{k+2}\right)-\frac{\Delta}{\pi}\frac{k\theta}{2\Omega}b_k=0\\
&\left(1-\frac{k^2\theta^2}{4\Omega^2}\right)b_k-\mu\left(b_{k-2}+b_{k+2}\right)+\frac{\Delta}{\pi}\frac{k\theta}{2\Omega}a_k=0
\end{aligned}
\tag{1.18}
$$

Similarly, substitution of Eq. (1.16) into Eq. (1.14) and term wise comparison leads to the following infinite system of homogenous algebraic equations for the unknown vector sequence $a_k$ and $b_k$ ($k = 4, 6, \ldots$)

$$
\begin{aligned}
&b_0-\mu b_2=0\\
&\left(1-\frac{\theta^2}{\Omega^2}\right)a_2-\mu a_4-\frac{\Delta}{\pi}\frac{\theta}{\Omega}b_2=0\\
&\left(1-\frac{\theta^2}{\Omega^2}\right)b_2-\mu\left(2b_0+b_4\right)+\frac{\Delta}{\pi}\frac{\theta}{\Omega}a_2=0\\
&\left(1-\frac{k^2\theta^2}{4\Omega^2}\right)a_k-\mu\left(a_{k-2}+a_{k+2}\right)-\frac{\Delta}{\pi}\frac{k\theta}{2\Omega}b_k=0\\
&\left(1-\frac{k^2\theta^2}{4\Omega^2}\right)b_k-\mu\left(b_{k-2}+b_{k+2}\right)+\frac{\Delta}{\pi}\frac{k\theta}{2\Omega}a_k=0
\end{aligned}
\tag{1.19}
$$

where $\Delta$ in Eq. (1.18) and Eq. (1.19) denotes the damping of free vibrations of a system, loaded by a constant component of longitudinal force and given by

$$
\Delta=\frac{2\pi\eta}{\omega\sqrt{1-\dfrac{P_0}{P_{cr}}}}
\tag{1.20}
$$

The system of linear homogenous equations Eq. (1.18) and Eq. (1.19) have solutions different from zero only in the case where the determinant composed of the coefficients of the system of equations is equal to zero. Thus, the necessary condition for the existence of the periodic solution of Eq. (1.14) is that the obtained determinants of the homogenous system of equations be equal to zero. The dimensions of the determinants obtained are infinite and these determinants are called Hill's infinite determinants. The required Floquent exponents discussed in section 1.4.1 are the eigenvalues of these Hill's determinants. The determinants of homogenous equations are given as follows:

$$\begin{vmatrix} \cdots & \cdots & \cdots & \cdots \\ 1-\dfrac{9\theta^2}{4\Omega^2} & -\mu & 0 & -\dfrac{\nabla}{\pi}\dfrac{3\theta}{2\Omega} \\ -\mu & 1+\mu-\dfrac{\theta^2}{4\Omega^2} & -\dfrac{\nabla}{\pi}\dfrac{\theta}{2\Omega} & 0 \\ 0 & \dfrac{\nabla}{\pi}\dfrac{\theta}{2\Omega} & 1-\mu-\dfrac{\theta^2}{\Omega^2} & -\mu \\ \dfrac{\nabla}{\pi}\dfrac{3\theta}{2\Omega} & 0 & -\mu & 1-\dfrac{9\theta^2}{4\Omega^2} \\ \cdots & \cdots & \cdots & \cdots \end{vmatrix} = 0 \qquad (1.21)$$

$$\begin{vmatrix} \cdots & \cdots & \cdots & \cdots & \cdots \\ 1-\dfrac{4\theta^2}{\Omega^2} & -\mu & 0 & 0 & -\dfrac{\Delta}{\pi}\dfrac{\theta}{\Omega} \\ -\mu & 1-\dfrac{\theta^2}{\Omega^2} & 0 & -\dfrac{\Delta}{\pi}\dfrac{\theta}{\Omega} & 0 \\ 0 & 0 & 1 & -\mu & 0 \\ 0 & \dfrac{\Delta}{\pi}\dfrac{\theta}{\Omega} & -2\mu & 1-\dfrac{\theta^2}{\Omega^2} & -\mu \\ \dfrac{\Delta}{\pi}\dfrac{\theta}{\Omega} & 0 & 0 & -\mu & 1-\dfrac{4\theta^2}{\Omega^2} \\ \cdots & \cdots & \cdots & \cdots & \cdots \end{vmatrix} = 0 \qquad (1.22)$$

These infinite eigenvalue problems can be solved for crtitical frequencies by truncating the dimensions of the determinants. For most of the problems, the first approximation gives satisfactory results. The dynamic load component $P_d$ is increased step wise, and the corresponding eigenvalues are solved for each load. Proceeding in this way, the instability charts; critical frequencies vs. dynamic load are obtained point by point.

The analytical approach of Bolotin's method is easy to apply for simple cases where the analytical equation can be derived for the system; if the system is complex and has multiple degrees of freedom with complex boundary conditions, the method cannot be employed. Employing a numerical procedure will be easy to analyze the dynamic stability behaviour of any complex system. A numerical procedure like finite element method can be applied to Bolotin's numerical approach

**1.4.2.2 Finite element Bolotin's approach**

Hill's equation Eq. (1.5) under external periodic excitation given as,

$$P(t) = P_S + P_D \cos \Omega t \tag{1.23}$$

can be written as,

$$M\ddot{q} + C\dot{q} + (K_e + K_{GS} + K_{GD} \cos \Omega t)q = 0 \tag{1.24}$$

Here $P_S$ is static component; $P_D$ is dynamic component and $\Omega$ frequency of the external parametric excitation. $M, C, K_e$ are mass matrix, damping matrix and elastic stiffness matrix respectively; $K_{GS}$, $K_{GD}$ are the geometric stiffness matrix corresponding to static load component $P_S$ and dynamic load component $P_D$ respectively.

According to Bolotin [14], Eq. (1.24) will have periodic solutions with period $T$ or $2T$ and can be represented by the following Fourier series expansions

$$T : q = \frac{1}{2}b_0 + \sum_{k=2,4,\ldots}^{\infty} \left( a_k \sin \frac{k\Omega t}{2} + b_k \cos \frac{k\Omega t}{2} \right), \tag{1.25}$$

$$2T : q = \sum_{k=1,3,\ldots}^{\infty} \left( a_k \sin \frac{k\Omega t}{2} + b_k \cos \frac{k\Omega t}{2} \right), \tag{1.26}$$

where $a_k$ and $b_k$ are time-independent Fourier coefficient vectors, which are determined by substituting Eq. (1.25-1.26) into Eq. (1.24). Substitution of Eq. (1.26) into Eq. (1.24) and a term wise comparison of sine- and cosine- coefficients leads to the following infinite system of homogenous algebraic equations for the unknown vector sequence $a_k$ and $b_k$ ($k = 3, 5, \ldots$)

$$\begin{aligned}
&\left(K_e + K_{GS} - \frac{1}{2}K_{GD} - \frac{\Omega^2}{4}M\right)a_1 - \frac{\Omega}{2}Cb_1 + \frac{1}{2}K_{GD}a_3 = 0 \\
&\left(K_e + K_{GS} + \frac{1}{2}K_{GD} - \frac{\Omega^2}{4}M\right)b_1 + \frac{\Omega}{2}Ca_1 + \frac{1}{2}K_{GD}b_3 = 0 \\
&\qquad\vdots \\
&\left(K_e + K_{GS} - \frac{k^2\Omega^2}{4}M\right)a_k - \frac{k\Omega}{2}Cb_k + \frac{1}{2}K_{GD}\left(a_{k+2} + a_{k-2}\right) = 0 \\
&\left(K_e + K_{GS} - \frac{k^2\Omega^2}{4}M\right)b_k + \frac{k\Omega}{2}Ca_k + \frac{1}{2}K_{GD}\left(b_{k+2} + b_{k-2}\right) = 0
\end{aligned} \tag{1.27}$$

Similarly, substitution of Eq. (1.25) into Eq. (1.24) and term wise comparison leads to the following infinite system of homogenous algebraic equations for the unknown vector sequence $a_k$ and $b_k$ ($k = 4, 6, \ldots$)

$$\begin{aligned}
&\left(K_e + K_{GS}\right)b_0 + K_{GD}b_2 = 0 \\
&\left(K_e + K_{GS} - \Omega^2 M\right)a_2 - \Omega Cb_2 + K_{GD}a_4 = 0 \\
&\left(K_e + K_{GS} - \Omega^2 M\right)b_2 + \Omega Ca_2 + K_{GD}\left(2b_0 + b_4\right) = 0 \\
&\qquad\vdots \\
&\left(K_e + K_{GS} - \frac{k^2\Omega^2}{4}M\right)a_k - \frac{k\Omega}{2}Cb_k + \frac{1}{2}K_{GD}\left(a_{k+2} + a_{k-2}\right) = 0 \\
&\left(K_e + K_{GS} - \frac{k^2\Omega^2}{4}M\right)b_k + \frac{k\Omega}{2}Ca_k + \frac{1}{2}K_{GD}\left(b_{k+2} + b_{k-2}\right) = 0
\end{aligned} \tag{1.28}$$

Both the above sets of equations Eq. (1.27-1.28) possess non-trivial solutions, if the infinite determinants of the corresponding coefficient matrices vanish identically, yielding two eigenvalue problems of infinite order for the critical frequencies **Ω**. The condition of solvability of an infinite eigenvalue problem can be approximated by a simplified and finite one by considering the first few terms. The simplified eigenvalue problems for the above infinite equations are

$$\begin{vmatrix} K_e + K_{GS} - \frac{1}{2}K_{GD} - \frac{\Omega^2}{4}M & -\frac{1}{2}\Omega C \\ \frac{1}{2}\Omega C & K_e + K_{GS} + \frac{1}{2}K_{GD} - \frac{\Omega^2}{4}M \end{vmatrix} = 0 \qquad (1.29)$$

$$\begin{vmatrix} K_e + K_{GS} - \Omega^2 M & 0 & -\Omega C \\ 0 & K_e + K_{GS} & K_{GD} \\ \Omega C & \frac{1}{2}K_{GD} & K_e + K_{GS} - \Omega^2 M \end{vmatrix} = 0. \qquad (1.30)$$

After some suitable transformation and adjustment of terms in the above determinants, the following eigenvalue problems are obtained for solution with period *2T* and *T* respectively [40],

$$\left\| \begin{bmatrix} K_e + K_{GS} - \frac{1}{2}K_{GD} & 0 \\ 0 & K_e + K_{GS} + \frac{1}{2}K_{GD} \end{bmatrix} + \Omega \begin{bmatrix} 0 & -\frac{1}{2}\Omega C \\ \frac{1}{2}\Omega C & 0 \end{bmatrix} + \Omega^2 \begin{bmatrix} -\frac{1}{4}M & 0 \\ 0 & -\frac{1}{4}M \end{bmatrix} \right\| = 0$$

(1.31)

$$\left\| \begin{bmatrix} K_e + K_{GS} & 0 \\ 0 & K_e + K_{GS} - \frac{1}{2}K_{GD}\left(K_e + K_{GS}\right)^{-1} K_{GD} \end{bmatrix} + \Omega \begin{bmatrix} 0 & -C \\ C & 0 \end{bmatrix} + \Omega^2 \begin{bmatrix} -M & 0 \\ 0 & -M \end{bmatrix} \right\| = 0$$

(1.32)

Eqs. (1.31-1.32) are quadratic eigenvalue problems, which can be solved for critical excitation frequencies **Ω**, which give the boundary curve between dynamic stability and instability regions. The quadratic eigenvalue problem can be solved by reducing it to a generalized eigenvalue problem [43] as discussed in Appendix-A. In the absence of damping, the above eigenvalue problem reduces to a generalized eigenvalue problem and can be easily solved. The eigenvalue equations of Eq. (1.31) and Eq. (1.32) in the absence of damping are given in Appenidx – A. Bolotin's approach can give simple regions of parametric instability which are most dominating and dangerous. The present approach cannot capture combination parametric instability regions.

**1.4.3 Hsu's method**

Compared with the numerical integral based Floquet method and eigenvalue based Bolotin's approach, perturbation techniques provide better computation efficiency because they are based on analytical approximations. Hsu [31-32] developed a general and simple perturbation based algorithm which can trace simple and combination stability boundaries approximately. Eq. (1.5) is transformed into a standard form through normalization and diagonalization process as

$$\ddot{q}(t)+C\dot{q}(t)+\left(K^{(0)}+\varepsilon K(t)\right)q(t)=0 \tag{1.33}$$

where $\varepsilon$ is a small real number. $K^{(0)}$ is a diagonal matrix with positive real numbers which are the square of natural frequencies on its diagonal line and can be expressed as

$$K^{(0)}=\begin{bmatrix}\omega_1^2 & & & \\ & \omega_2^2 & & \\ & & \ddots & \\ & & & \omega_n^2\end{bmatrix} \text{ with } \omega_1^2\le\omega_2^2\le\ldots\omega_n^2 \tag{1.34}$$

Here, $\omega_1$, $\omega_2$ ... $\omega_n$ are system natural frequencies. $K(t)$ is periodically time varying and expanded as Fourier series as follows

$$K(t)=\sum_{s=1,2,\ldots}^{S}\left(D^{(s)}\cos s\omega t+E^{(s)}\sin s\omega t\right) \tag{1.35}$$

and damping matrix is assumed as $C = F^{(0)}$. Here, $\omega = 2\pi/T$ and $S$ is a finite integer. Substituting Eq. (1.34), Eq. (1.35) into Eq. (1.33) yields,

$$\begin{aligned}\ddot{q}(t)+K^{(0)}q(t)=-\varepsilon\sum_{s=1\ldots}^{S}\left(D^{(s)}\cos s\omega t+E^{(s)}\sin s\omega t\right)q(t)\\ -F^{(0)}\dot{q}(t)\end{aligned}\tag{1.36}$$

and its component form,

$$\begin{aligned}\ddot{q}_i(t)+\omega_i^2 q_i(t)=-\varepsilon\sum_{s=1,2\ldots}^{S}\sum_{j=1,2\ldots}^{n}\left(d_{ij}^{(s)}\cos s\omega t+e_{ij}^{(s)}\sin s\omega t\right)q_j(t)\\ +\sum_{j=1,2\ldots}^{n}f_{ij}^{(0)}\dot{q}_j(t),\quad i=1,2,\ldots,n\end{aligned}\tag{1.37}$$

where $d_{ij}^{(s)}$, $e_{ij}^{(s)}$ and $f_{ij}^{(0)}$ are the elements of matrices $D^{(s)}$, $E^{(s)}$ and $F^{(0)}$ respectively.

When $\varepsilon = 0$, Eq. (1.37) is a set of equations for s system without parametric excitation and can be solved when the initial values $q_i$ and $\dot{q}_i$ are known. The first order form of Eq. (1.37) can be written as

$$\begin{aligned}&\dot{q}_i(t)=w_i(t)\\ &\dot{w}_i(t)+\omega_i^2 q_i(t)=-\varepsilon\sum_{s=1,2\ldots}^{S}\sum_{j=1,2,\ldots}^{n}\left(d_{ij}^{(s)}\cos s\omega t+e_{ij}^{(s)}\sin s\omega t\right)q_j(t)\\ &\qquad -\sum_{j=1,2\ldots}^{n}f_{ij}^{(0)}w_j(t)\end{aligned}\tag{1.38}$$

The possible form of perturbed solution to Eq. (1.38) is,

$$\begin{aligned}q_i(t)&=A_i(t)\cos\omega_i t+B_i(t)\sin\omega_i t+\sum_{r=1,\ldots}^{\infty}\varepsilon^r q_i^{(r)}(t)\\ w_i(t)&=\omega_i\left[-A_i(t)\sin\omega_i t+B_i(t)\cos\omega_i(t)+\sum_{r=1,\ldots}^{\infty}\varepsilon^r\dot{q}_i^{(r)}(t)\right]\end{aligned}\tag{1.39}$$

First two terms on the right hand side of Eq. (1.39) are called variational part and the remaining is the perturbation part [44]. Substituting $q$, $w$ in Eq. (1.38) with the expressions in Eq. (1.39) and on truncating terms to the first order of *ε*, results into the following equations

$$\dot{A}_i \cos\omega_i t + \dot{B}_i \sin\omega_i t = 0 \tag{1.40}$$

$$\begin{aligned}
&-\omega_i \dot{A}_i \sin\omega_i t + \omega_i \dot{B}_i \cos\omega_i t + \varepsilon\left(\ddot{q}_i^{(1)} + \omega_i^2 q_i^{(1)}\right) = \\
&\qquad -\frac{\varepsilon}{2}\sum_{s=1,\ldots}^{S}\sum_{j=1,\ldots}^{n}\begin{bmatrix} H_1^{(s)}\cos\left(\omega_j t + s\omega t\right) + H_2^{(s)}\cos\left(\omega_j t - s\omega t\right) \\ +H_3^{(s)}\sin\left(\omega_j t + s\omega t\right) + H_4^{(s)}\sin\left(\omega_j t - s\omega t\right)\end{bmatrix} \\
&\qquad -\varepsilon\sum_{j=1,\ldots}^{n} \mathrm{f}_{\mathrm{ij}}^{(0)}\omega_j\left(B_j\cos\omega_j t - A_j\sin\omega_j t\right)
\end{aligned} \tag{1.41}$$

where

$$\begin{aligned}
H_1^{(s)} &= d_{ij}^{(s)}A_j - e_{ij}^{(s)}B_j \\
H_2^{(s)} &= d_{ij}^{(s)}A_j + e_{ij}^{(s)}B_j \\
H_3^{(s)} &= d_{ij}^{(s)}B_j + e_{ij}^{(s)}A_j \\
H_4^{(s)} &= d_{ij}^{(s)}B_j - e_{ij}^{(s)}A_j
\end{aligned} \tag{1.42}$$

The essential feature of Hsu's method is that, the terms which lead to instability i.e. terms of infinite magnitudes on right hand side of Eq. (1.41) are associated with the variational part and the rest of the stable terms are associated with the perturbation part [44]. The perturbation terms are always stable for all $\omega_i$ and $\omega$ being positive and the variational terms govern the system stability.

For a given $i$ ($i = 1, 2 \ldots n$), if $\omega_i \pm s\omega$ is not nearly equal to $\pm\omega_i$, for any choices of $j$ and $s$ the solution of Eq. (1.40) and Eq. (1.41) is

$$\begin{aligned}
q_i^{(1)} = -\frac{1}{2}\sum_{j=1,\ldots}^{n}\sum_{s=1,\ldots}^{S}&\left\{\frac{1}{\omega_i^2 - \left(\omega_j + s\omega\right)^2}\left[H_1^{(s)}\cos\left(\omega_j t + s\omega t\right) + H_3^{(s)}\sin\left(\omega_j t + s\omega t\right)\right]\right. \\
&\left. + \frac{1}{\omega_i^2 - \left(\omega_j - s\omega\right)^2}\left[H_2^{(s)}\cos\left(\omega_j t - s\omega t\right) + H_4^{(s)}\sin\left(\omega_j t - s\omega t\right)\right]\right\}
\end{aligned}$$

$$-\sum_{\substack{j=1,\dots\\ j\neq i}}^{n} \frac{1}{\omega_i^2-\omega_j^2} f_{ij}^{(0)} \omega_j \left(B_j \cos\omega_j t - A_j \sin\omega_j t\right) \tag{1.43}$$

Here, in obtaining the perturbation part, $A$ and $B$ are taken to be constant in the present first approximation and $A_i$, $B_i$ are determined from the equations

$$\begin{aligned} &\dot{A}_i \cos\omega_i t + \dot{B}_i \sin\omega_i t = 0 \\ &-\dot{A}_i \sin\omega_i t + \dot{B}_i \cos\omega_i t = -\varepsilon f_{ii}^{(0)} \left(B_i \cos\omega_i t - A_i \sin\omega_i t\right) \end{aligned} \tag{1.44}$$

The solution of Eq. (1.44) is given by

$$A_i = A_{i0} e^{-\frac{1}{2}\varepsilon f_{ii}^{(0)} t}, \quad B_i = B_{i0} e^{-\frac{1}{2}\varepsilon f_{ii}^{(0)} t} \tag{1.45}$$

where $A_{i0}$ and $B_{i0}$ are $2n$ constants which can be determined form the initial conditions. On substituting Eq. (1.45) and Eq. (1.43) into Eq. (1.40), we obtain the desired solution; this solution is well behaved and stable, no question of instability arises if the damping terms are positive. This implies that, the excitation frequency of the coefficient matrices in Eq. (1.33) are away from the system natural frequencies and thus response of the system is stable.

When the excitation frequency of the coefficient matrices in Eq. (1.33) is equal or close to combinations of the system natural frequencies, the parametric resonance occurs. First, the case of the excitation frequency close to sum of two natural frequencies is analyzed. Let the excitation frequency be

$$\omega = \frac{1}{s}\left(\omega_k + \omega_j\right) + \varepsilon\lambda \tag{1.46}$$

Here, $\lambda$ is a finite real number and $\varepsilon\lambda$ is a small quantity since $\varepsilon$ is small. The frequencies $\omega_k$ and $\omega_j$ terms are included in the variational equations as

$$
\begin{aligned}
&\dot{A}_k \cos\omega_k t + \dot{B}_k \sin\omega_k t = 0 \\
&-\dot{A}_k \sin\omega_k t + \dot{B}_k \cos\omega_k t = -\frac{\varepsilon}{2\omega_k}\left[H_2^{(s)}\cos\left(\omega_k t + \varepsilon\lambda st\right) - H_4^{(s)}\sin\left(\omega_k t + \varepsilon\lambda st\right)\right] \\
&\qquad\qquad\qquad\qquad\qquad -\varepsilon f_{kk}^{(0)}\left(B_k\cos\omega_k t - A_k\sin\omega_k t\right) \\
&\dot{A}_j \cos\omega_j t + \dot{B}_j \sin\omega_j t = 0 \\
&-\dot{A}_j \sin\omega_j t + \dot{B}_j \cos\omega_j t = -\frac{\varepsilon}{2\omega_j}\left[\tilde{H}_2^{(s)}\cos\left(\omega_j t + \varepsilon\lambda st\right) - \tilde{H}_4^{(s)}\sin\left(\omega_j t + \varepsilon\lambda st\right)\right] \\
&\qquad\qquad\qquad\qquad\qquad -\varepsilon f_{jj}^{(0)}\left(B_j\cos\omega_j t - A_j\sin\omega_j t\right)
\end{aligned}
\tag{1.47}
$$

where the terms $\tilde{H}_2^{(s)}, \tilde{H}_4^{(s)}$ are the terms $H_2^{(s)}, H_4^{(s)}$ with the subscripts $k$ and $j$ exchanged respectively. After decoupling $A_k$, $B_k$, $A_j$ and $B_j$ from Eq. (1.47), all resulting equations are integrated with respect to $\omega_k t$ and $\omega_j t$ over *[0, 2π]* and then on substituting their integral average, the variational equations becomes

$$
\begin{aligned}
\dot{A}_k &= -\varepsilon f_{kk}^{(0)}\frac{A_k}{2} - \frac{\varepsilon}{4\omega_k}\left[H_2^{(s)}\sin\varepsilon\lambda st + H_4^{(s)}\cos\varepsilon\lambda st\right] \\
\dot{B}_k &= -\varepsilon f_{kk}^{(0)}\frac{B_k}{2} - \frac{\varepsilon}{4\omega_k}\left[H_2^{(s)}\cos\varepsilon\lambda st - H_4^{(s)}\sin\varepsilon\lambda st\right]
\end{aligned}
\tag{1.48a}
$$

$$
\begin{aligned}
\dot{A}_j &= -\varepsilon f_{jj}^{(0)}\frac{A_j}{2} - \frac{\varepsilon}{4\omega_j}\left[\tilde{H}_2^{(s)}\sin\varepsilon\lambda st + \tilde{H}_4^{(s)}\cos\varepsilon\lambda st\right] \\
\dot{B}_j &= -\varepsilon f_{jj}^{(0)}\frac{B_j}{2} - \frac{\varepsilon}{4\omega_j}\left[\tilde{H}_2^{(s)}\cos\varepsilon\lambda st - \tilde{H}_4^{(s)}\sin\varepsilon\lambda st\right]
\end{aligned}
\tag{1.48b}
$$

Substituting Eq. (1.42) in Eq. (1.48), remembering that the index $i$ should be replaced by $k$, and then on further simplification based on the following transformation,

$$
\begin{aligned}
X_1 &= A_k + iB_k, \quad Y_1 = A_j + iB_j \\
X_2 &= A_k - iB_k, \quad Y_2 = A_j - iB_j
\end{aligned}
\tag{1.49}
$$

where $i$ is a complex number. The results are

$$
\dot{X}_1 = -\frac{1}{2}\varepsilon f_{kk}^{(0)} X_1 - \frac{\varepsilon}{4\omega_k}\left[i\left(d_{kj}^{(s)} - e_{kj}^{(s)}\right)\right]e^{-i\varepsilon\lambda st}Y_2 \tag{1.50a}
$$

$$\dot{X}_2 = -\frac{1}{2}\varepsilon f_{kk}^{(0)} X_2 - \frac{\varepsilon}{4\omega_k}\left[-i\left(d_{kj}^{(s)} - e_{kj}^{(s)}\right)\right] e^{i\varepsilon\lambda st} Y_1 \tag{1.50b}$$

$$\dot{Y}_1 = -\frac{1}{2}\varepsilon f_{jj}^{(0)} Y_1 - \frac{\varepsilon}{4\omega_j}\left[i\left(d_{jk}^{(s)} - e_{jk}^{(s)}\right)\right] e^{-i\varepsilon\lambda st} X_2 \tag{1.50c}$$

$$\dot{Y}_2 = -\frac{1}{2}\varepsilon f_{jj}^{(0)} Y_2 - \frac{\varepsilon}{4\omega_j}\left[-i\left(d_{jk}^{(s)} - e_{jk}^{(s)}\right)\right] e^{i\varepsilon\lambda st} X_1 \tag{1.50d}$$

Owing to the special structure of Eq. (1.50a) and Eq. (1.50d), we can write their solution as

$$X_1 = X_{10} e^{pt - \frac{1}{2}i\varepsilon\lambda st}, Y_2 = Y_{20} e^{pt + \frac{1}{2}i\varepsilon\lambda st} \tag{1.51}$$

where $X_{10}$ and $Y_{20}$ are constants. The indicial equation for $p$ is found as

$$\begin{aligned} p^2 + \frac{\varepsilon}{2}\left(f_{kk}^{(0)} + f_{jj}^{(0)}\right)p + \frac{\varepsilon^2}{4}\left(f_{jj}^{(0)} + is\lambda\right)\left(f_{kk}^{(0)} - is\lambda\right) \\ - \frac{\varepsilon^2}{16\omega_k\omega_j}\left(d_{kj}^{(s)} + ie_{kj}^{(s)}\right)\left(d_{jk}^{(s)} - ie_{jk}^{(s)}\right) \end{aligned} \tag{1.52}$$

and hence,

$$p = -\frac{\varepsilon}{4}\left(f_{kk}^{(0)} + f_{jj}^{(0)}\right) \pm \frac{\varepsilon}{4} P^{1/2} \tag{1.53}$$

where

$$\begin{aligned} P = \left(f_{kk}^{(0)} + f_{jj}^{(0)}\right)^2 - 4\left(f_{jj}^{(0)} + is\lambda\right)\left(f_{kk}^{(0)} - is\lambda\right) \\ + \frac{1}{\omega_k\omega_j}\left(d_{kj}^{(s)} + ie_{kj}^{(s)}\right)\left(d_{jk}^{(s)} - ie_{jk}^{(s)}\right) \end{aligned} \tag{1.54}$$

Likewise for Eq. (1.50b) and Eq. (1.50c), we get

$$X_2 = X_{20} e^{qt + \frac{1}{2}i\varepsilon\lambda st}, Y_1 = Y_{10} e^{qt - \frac{1}{2}i\varepsilon\lambda st} \tag{1.55}$$

where $X_{20}$ and $Y_{10}$ are constants. The indicial equation for $q$ is

$$q^2+\frac{\varepsilon}{2}\left(f_{kk}^{(0)}+f_{jj}^{(0)}\right)q+\frac{\varepsilon^2}{4}\left(f_{jj}^{(0)}-is\lambda\right)\left(f_{kk}^{(0)}+is\lambda\right) \\ -\frac{\varepsilon^2}{16\omega_k\omega_j}\left(d_{kj}^{(s)}-ie_{kj}^{(s)}\right)\left(d_{jk}^{(s)}+ie_{jk}^{(s)}\right) \tag{1.56}$$

and hence,

$$q=-\frac{\varepsilon}{4}\left(f_{kk}^{(0)}+f_{jj}^{(0)}\right)\pm\frac{\varepsilon}{4}Q^{1/2} \tag{1.57}$$

where

$$Q=\left(f_{kk}^{(0)}+f_{jj}^{(0)}\right)^2-4\left(f_{jj}^{(0)}-is\lambda\right)\left(f_{kk}^{(0)}+is\lambda\right) \\ +\frac{1}{\omega_k\omega_j}\left(d_{kj}^{(s)}-ie_{kj}^{(s)}\right)\left(d_{jk}^{(s)}+ie_{jk}^{(s)}\right) \tag{1.58}$$

From Eq. (1.54) and Eq. (1.58) it is evident that $Q$ is complex conjugate of $P$ and hence the roots of $q$ are the conjugates of the roots of $p$. Then it follows that the real parts of $q$ and $p$ must be same.

Looking at Eq. (1.49), Eq. (1.51) and Eq. (1.55), for the terms $A_k$, $B_k$, $A_j$ and $B_j$ to not to grow with time, none of $p$ and $q$ should have a positive real part. The system is stable if,

$$\left|\Re e P^{1/2}\right| < f_{kk}^{(0)}+f_{jj}^{(0)} \tag{1.59a}$$

and unstable if

$$\left|\Re e P^{1/2}\right| > f_{kk}^{(0)}+f_{jj}^{(0)} \tag{1.59b}$$

As $P$ is given by Eq. (1.54), the above stability conditions for the excitation frequency close to sum of $k^{th}$ and $j^{th}$ natural frequencies, $(\omega_k+\omega_j)/s$ may be written as follows after a simple calculation

$$\left[\frac{\alpha+\left(\alpha^2+\beta^2\right)^{1/2}}{2}\right]^{1/2} \Rightarrow \begin{cases} < f_{kk}^{(0)} + f_{jj}^{(0)} & stable \\ > f_{kk}^{(0)} + f_{jj}^{(0)} & unstable \end{cases} \tag{1.60}$$

where

$$\alpha = \left(f_{kk}^{(0)} + f_{jj}^{(0)}\right)^2 - 4\left(f_{jj}^{(0)} f_{kk}^{(0)} + \mathrm{s}^2\lambda^2\right) + \frac{1}{\omega_k \omega_j}\left[d_{kj}^{(s)} d_{jk}^{(s)} + e_{kj}^{(s)} e_{jk}^{(s)}\right] \tag{1.61a}$$

$$\beta = 4s\lambda\left(f_{jj}^{(0)} - f_{kk}^{(0)}\right) + \frac{1}{\omega_k \omega_j}\left[e_{kj}^{(s)} d_{jk}^{(s)} + d_{kj}^{(s)} e_{jk}^{(s)}\right] \tag{1.61b}$$

Based on the same approach, the stability criterion for the excitation frequency close to the difference of $k^{th}$ and $j^{th}$ ($j>k$) natural frequencies, $(\omega_j-\omega_k)/s$ is similar to Eq. (1.60) except that $\alpha$ and $\beta$ are now given by

$$\alpha = \left(f_{kk}^{(0)} + f_{jj}^{(0)}\right)^2 - 4\left(f_{jj}^{(0)} f_{kk}^{(0)} + \mathrm{s}^2\lambda^2\right) - \frac{1}{\omega_k \omega_j}\left[d_{kj}^{(s)} d_{jk}^{(s)} + e_{kj}^{(s)} e_{jk}^{(s)}\right] \tag{1.62a}$$

$$\beta = 4s\lambda\left(f_{jj}^{(0)} - f_{kk}^{(0)}\right) + \frac{1}{\omega_k \omega_j}\left[d_{kj}^{(s)} e_{jk}^{(s)} - e_{kj}^{(s)} d_{jk}^{(s)}\right] \tag{1.62b}$$

Similarly, the stability criterion for the excitation frequency close to twice of $k^{th}$ natural frequencies, $2\omega_k/s$ is

$$\left[\frac{\alpha+\left(\alpha^2\right)^{1/2}}{2}\right]^{1/2} \Rightarrow \begin{cases} < 2 f_{kk}^{(0)} & stable \\ > 2 f_{kk}^{(0)} & unstable \end{cases} \tag{1.63}$$

where

$$\alpha = \frac{1}{\omega_k^2}\left[\left(d_{kk}^{(s)}\right)^2 + \left(e_{kk}^{(s)}\right)^2\right] - 4s^2\lambda^2 \tag{1.64}$$

## 1.5 Summary

This chapter introduces parametric instability, its governing equation and mathematical methods to analyze the parametric system. The governing equation of motion to study parametric instability is classified as Hill's equation. The objective of solving Hill's equation is not to get the exact form of solution but to know under what parameters, the system undergoes instability. This is done by plotting stability chart.

According to Floquet theory, the state transition matrix that maps an initial state to the state after one time period determines the stability of the system. This transition matrix is Floquet Transition Matrix and it needs intensive numerical time integration to calculate. Bolotin's approach of finding eigenvalues which separate regions of stability and instability gives simple regions of parametric instability but does not give combination type of instability regions. Hsu's method which is based on perturbation technique can capture all regions (simple and combination) of stability boundaries approximately. The high-accuracy results can be achieved when the system damping and the time varying components of system stiffness are much smaller than the constant component of the system stiffness.

# Chapter 2

# PARAMETRIC OSCILLATOR

## 2.1 Introduction

A simple pendulum consists of a mass *m* suspended from a string of length *L* which is fixed at a pivot *P*. When simple pendulum is displaced to an initial angle and released, the pendulum will swing back and forth with periodic motion. The simple pendulum has two equilibrium configurations: the downward position (*m* located in the downward position) and the upright inverted position (*m* located in the upward position), they are known as simple pendulum and inverted pendulum respectively. The downward position is obviously stable, while the vertical orientation is clearly unstable. When the pivot *P* of simple pendulum is excited vertically, this vertical excitation changes the effective gravity acting on the simple pendulum; such a pendulum is called parametric oscillator or parametric pendulum. When the pivot *P* is subjected to harmonic vertical oscillation of frequency, $\omega$ and amplitude *A*, the effect of parametric excitation on the simple pendulum is that, under some system parameters ($\omega$, *A*) the parametric simple pendulum undergoes instability and the parametric inverted pendulum attains stability. It is beneficial to study the parametric pendulum since it will enable us to understand more complicated physical phenomena with ease. In addition, pendulum being a single degree of freedom, complicated mathematical concepts can be applied easily for better understanding. The pendulum can also help in understanding the nonlinear system theory and chaos [45]. Extensive research has been done on parametric oscillator. The literature reports analytical methods, numerical methods and experimental works on parametric oscillator. Few remarkable references on this context can be seen in [46-59]. In the present chapter a simple pendulum and inverted pendulum excited vertically at its support points are considered. The stability of the pendulum is analysed using Bolotin's analytical approach; stability chart is validated by simulating response of pendulums under various system parameters taken form the stability chart.

## 2.2 Governing Equations

Consider a simple pendulum and an inverted pendulum with mass *m* attached to a rod of length *L* as shown in Figure 2.1. The support of the pendulum is made to vibrate vertically by $y(t) = A\cos\omega t$, where $A$, $\omega$ are amplitude and frequency of the support excitation respectively.

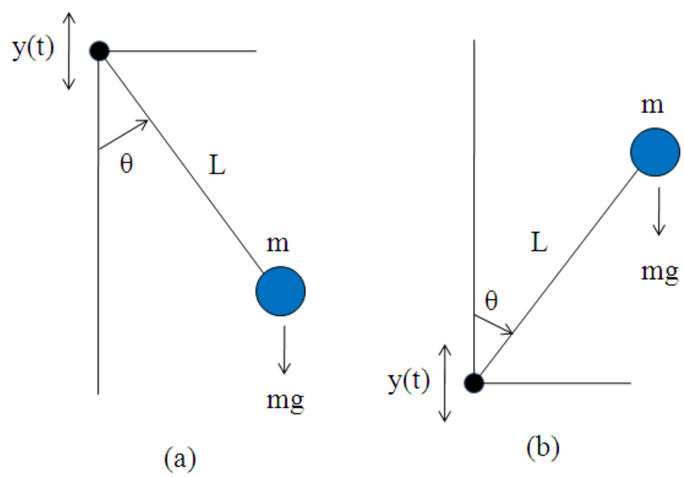


**Figure 2.1: The simple pendulum under vertical excitation at its support (a) simple pendulum (b) inverted pendulum**

According to Newton's second law of motion in the direction perpendicular to the rod of simple pendulum Figure 2.1(a), we obtain equation of motion:

$$mL^2\ddot{\theta} = -mgL\sin\theta - mgL\omega^2 A\cos(\omega t)\sin\theta \tag{2.1}$$

$$\Rightarrow \ddot{\theta} + \left(\frac{g}{L} - \frac{\omega^2 A}{L}\cos(\omega t)\right)\sin\theta = 0 \tag{2.2}$$

Similarly, for inverted pendulum we obtain equation of motion:

$$mL^2\ddot{\theta} = mgL\sin\theta - mgL\omega^2 A\cos(\omega t)\sin\theta \tag{2.3}$$

$$\Rightarrow \ddot{\theta} - \left(\frac{g}{L} - \frac{\omega^2 A}{L}\cos(\omega t)\right)\sin\theta = 0 \tag{2.4}$$

Equation (2.3) and (2.4) can be combined and written as follows

$$\ddot{\theta} \pm \left(\omega_0^2 - \frac{\omega^2 A}{L}\cos(\omega t)\right)\sin\theta = 0 \tag{2.5}$$

where $\omega_0^2 = g/L$, natural frequency of the pendulum and + sign for simple pendulum, − sign for inverted pendulum and $g$ is acceleration due to gravity. Reparametrizing Eq. (2.5) using $\tau = \omega t$, we obtain the following equation

$$\ddot{\theta} + (\delta + \varepsilon\cos(\tau))\sin\theta = 0 \tag{2.6}$$

where $\delta = \omega_0^2/\omega^2$ and $\varepsilon = A/L$. For small oscillations approximation $sin\theta \approx \theta$ holds.With this approximation Eq. (2.6) gives

$$\ddot{\theta} + (\delta + \varepsilon\cos(\tau))\theta = 0. \tag{2.7}$$

Equation (2.7) is a Mathieu equation [8] and it defines the stability of parametric oscillator. Eq. (2.7) governs the motion of simple pendulum by setting $\delta = \omega_0^2/\omega^2$ and $\varepsilon = -A/L,$ and governs inverted pendulum on setting $\delta = -\omega_0^2/\omega^2$ and $\varepsilon = A/L.$

## 2.3 Stability analysis of Mathieu equation

Mathieu equation is a second order homogenous equation with periodic coefficients. It has forest of solutions which can be stable or unstable. The objective of solving Eq. (2.7) is not to find the exact form of the solution, but to find at what combination of system parameters $(\delta, \varepsilon)$ the solution becomes unstable. The periodic solutions of Mathieu equation have either period $\pi$ or $2\pi$. These periodic solutions have transition values of $\delta$ and $\varepsilon$ from stable to unstable behaviour of the solution. Hence, a stability diagram of system parameters ($\delta$, $\varepsilon$) can be drawn from which stability of the Eq. (2.7) can be obtained. If the periodic motion at both the ends of an interval in the parameter plane possesses same period $\pi$ or $2\pi$, then the enclosed interval is characterized by unbounded/ instable motion. If the periodic motion at one end of an interval in the parameter plane possesses period $\pi$ ($2\pi$) and at the other end possesses period $2\pi$ ($\pi$), then the motion in that interval is bounded. To establish the regions of bounded and unbounded motions in the parameter plane it is required to obtain only the periodic solutions. These periodic solutions can be expressed as Fourier series expansion as follows

$$2\pi : \theta = \sum_{n=1,3,5\ldots}^{\infty} \left( a_n \cos\frac{n\tau}{2} + b_n \sin\frac{n\tau}{2} \right) \tag{2.8a}$$

$$\pi : \theta = a_0 + \sum_{n=2,4,6,\ldots}^{\infty} \left( a_n \cos\frac{n\tau}{2} + b_n \sin\frac{n\tau}{2} \right) \tag{2.8b}$$

Substituting the series Eq. (2.8) into Eq. (2.7) leads to the following sets of recursive relations for the $a_n$ and $b_n$, which are

$$\begin{cases} \left( \delta + \dfrac{\varepsilon}{2} - \dfrac{1}{4} \right) a_1 + \dfrac{\varepsilon}{2} a_3 = 0 \\ \left( \delta - \dfrac{n^2}{4} \right) a_n + \dfrac{\varepsilon}{2} \left( a_{n-2} + a_{n+2} \right) = 0 \quad n = 3, 5, \ldots \end{cases} \tag{2.9a}$$

$$\begin{cases} \left( \delta - \dfrac{\varepsilon}{2} - \dfrac{1}{4} \right) b_1 + \dfrac{\varepsilon}{2} b_3 = 0 \\ \left( \delta - \dfrac{n^2}{4} \right) b_n + \dfrac{\varepsilon}{2} \left( b_{n-2} + b_{n+2} \right) = 0 \quad n = 3, 5, \ldots \end{cases} \tag{2.9b}$$

for solution with period $2\pi$ and

$$\begin{cases} \delta a_0 + \dfrac{\varepsilon}{2} a_2 = 0 \\ \dfrac{\varepsilon}{2} a_0 + (\delta - 1) a_2 + \dfrac{\varepsilon}{2} a_4 = 0 \\ \left(\delta - \dfrac{n^2}{4}\right) a_n + \dfrac{\varepsilon}{2}\left(a_{n-2} + a_{n+2}\right) = 0 \quad n = 4, 6, \ldots \end{cases} \tag{2.10a}$$

$$\begin{cases} (\delta - 1) b_2 + \dfrac{\varepsilon}{2} b_4 = 0 \\ \left(\delta - \dfrac{n^2}{4}\right) b_n + \dfrac{\varepsilon}{2}\left(b_{n-2} + b_{n+2}\right) = 0 \quad n = 4, 6, \ldots \end{cases} \tag{2.10b}$$

for solution with period $\pi$. The system of linear homogenous Eqs. (2.9-2.10) has solutions different from zero only when the determinant composed of coefficients of system of equations is equal to zero. The obtained determinants equipped of the coefficients $a_n$ and $b_n$ are referred as Hill's determinants. By taking a finite number of terms in Eq. (2.8), the Hill determinants are given as follows:

$$\begin{vmatrix} \delta \pm \varepsilon - \frac{1}{4} & \frac{\varepsilon}{2} & 0 & 0 & \cdots & 0 \\ \frac{\varepsilon}{2} & \delta - \frac{9}{4} & \frac{\varepsilon}{2} & 0 & \cdots & 0 \\ 0 & \frac{\varepsilon}{2} & \delta - \frac{25}{4} & \frac{\varepsilon}{2} & \cdots & \cdots \\ \cdots & \cdots & \cdots & \cdots & \cdots & \cdots \\ 0 & 0 & 0 & \frac{\varepsilon}{2} & \delta - \frac{(n-2)^2}{4} & \frac{\varepsilon}{2} \\ 0 & 0 & 0 & 0 & \frac{\varepsilon}{2} & \delta - \frac{n^2}{4} \end{vmatrix} = 0 \tag{2.11}$$

where Eq. (2.9a) and Eq. (2.9b) are combined into one Hill determinant under ± sign, Eq. (2.11) is Hill determinant obtained for $2\pi$ periodic solution and $n = 3,5,\ldots$ in Eq. (2.11). Similarly Hill determinants for $\pi$ periodic solution with $n = 2, 4\ldots$ is given by

$$\begin{vmatrix} \delta & \frac{\varepsilon}{2} & 0 & 0 & \cdots & 0 \\ \varepsilon & \delta-1 & \frac{\varepsilon}{2} & 0 & \cdots & 0 \\ 0 & \frac{\varepsilon}{2} & \delta-4 & \frac{\varepsilon}{2} & \cdots & \cdots \\ \cdots & \cdots & \cdots & \cdots & \cdots & \cdots \\ 0 & 0 & 0 & \frac{\varepsilon}{2} & \delta-\frac{(n-2)^2}{4} & \frac{\varepsilon}{2} \\ 0 & 0 & 0 & 0 & \frac{\varepsilon}{2} & \delta-\frac{n^2}{4} \end{vmatrix} = 0 \qquad (2.12a)$$

and

$$\begin{vmatrix} \delta-1 & \frac{\varepsilon}{2} & 0 & 0 & \cdots & 0 \\ \frac{\varepsilon}{2} & \delta-4 & \frac{\varepsilon}{2} & 0 & \cdots & 0 \\ 0 & \frac{\varepsilon}{2} & \delta-9 & \frac{\varepsilon}{2} & \cdots & \cdots \\ \cdots & \cdots & \cdots & \cdots & \cdots & \cdots \\ 0 & 0 & 0 & \frac{\varepsilon}{2} & \delta-\frac{(n-2)^2}{4} & \frac{\varepsilon}{2} \\ 0 & 0 & 0 & 0 & \frac{\varepsilon}{2} & \delta-\frac{n^2}{4} \end{vmatrix} = 0 \qquad (2.12b)$$

The Hill determinants can be solved for $\delta$ by increasing $\varepsilon$ step wise. On plotting the obtained values of $\delta$ for the corresponding $\varepsilon$ values, a stability diagram is obtained. The stability diagram of Mathieu equation Eq. (2.7) is obtained as shown in Figure 2.2.

## 2.4 Numerical results and discussion

To check the reliability of stability diagram obtained, the response of the parametric oscillator is simulated for different system parameters lying in stability diagram. Equation (2.7) is solved using fourth order Runge-Kutta method. A pendulum of length 0.19 m is considered. Its natural frequency is $\omega_0 = (g/L)^{½} =$

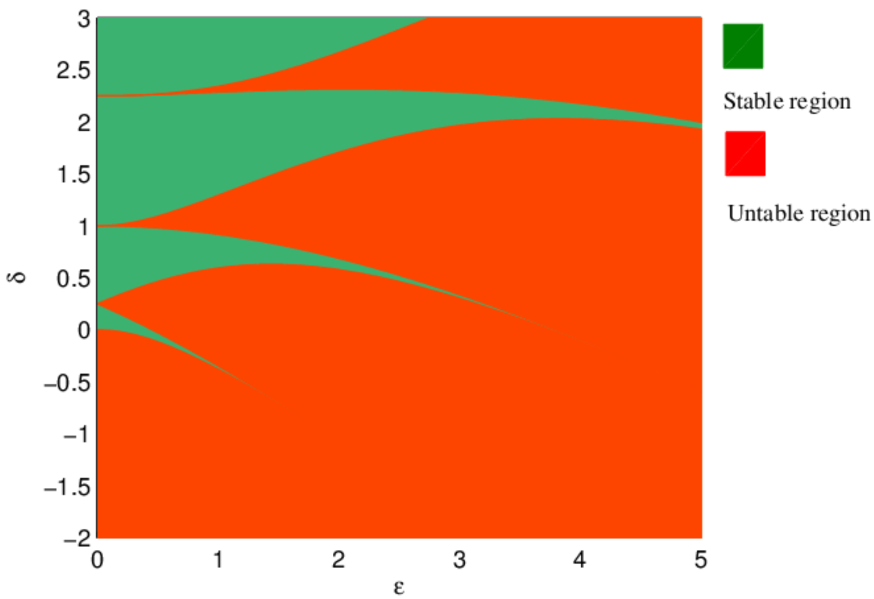


**Figure 2.2: Stability diagram of Mathieu equation (Eq. 2.7)**

7.1855 rad/s, where $g$ = 9.81 m/s$^2$. The amplitude of support excitation is considered as $A$ = 0.0133 m, which gives $\varepsilon = A/L$ = 0.07. For all the simulation cases carried out in the present chapter, same amplitude is taken and different frequencies which lie in stable and unstable region are taken. The system parameters considered are given in Table 2.1.

**Table 2.1: Support excitation frequencies for fixed amplitude lying in stable and unstable regions of stability diagram**

| S. No | Simple pendulum | | Inverted pendulum | |
|---|---|---|---|---|
| | ω (rad/s) | δ | ω(Hz) | δ |
| 1 | 15.8701 | 0.2050 | 140.9195 | 0.0026 |
| 2 | 15.6801 | 0.2100 | 145.1693 | 0.0024 |
| 3 | 15.4967 | 0.2150 | 151.4839 | 0.0022 |
| 4 | 15.3196 | 0.2200 | 185.5291 | 0.0015 |

### 2.4.1 Response of parametric oscillator

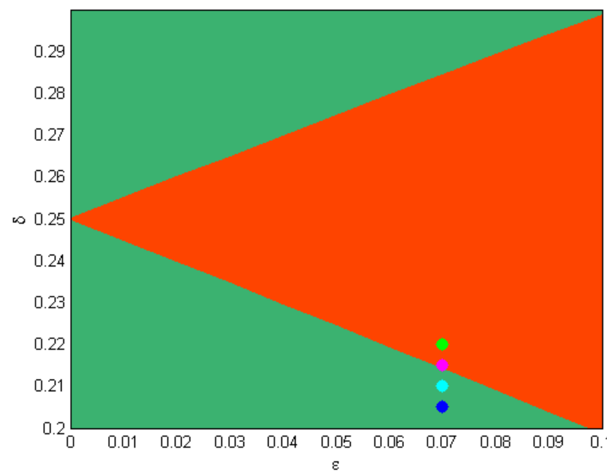


**Figure 2.3: Location of system parameters for simple pendulum**

Figure 2.3 shows the location of system parameters for pendulum under support excitation. These system parameters are given in Table 2.1. Figure 2.4 shows response of the pendulum and the respective phase plane plots for the given system parameters.

First two system parameters lie in stable region and the other two system parameters lie in unstable region. Figure 2.4 (a, c) shows the response of the pendulum for the first two system parameters and Figure 2.4 (b, d) shows the respective phase plane plots, as expected from the stability chart it is clear that, the response of the oscillator is stable or bounded for these cases. Figure 2.4 (e, g) shows the response for the system parameters lying in unstable region. The response clearly shows unstable or unbounded motion of the pendulum as expected from the stability chart. The state of the response can be clearly understood from the respective phase plane plots shown in Figure 2.4 (f, h). The response of the oscillator in unstable regions is exponentially increasing which is a peculiar characteristic is of

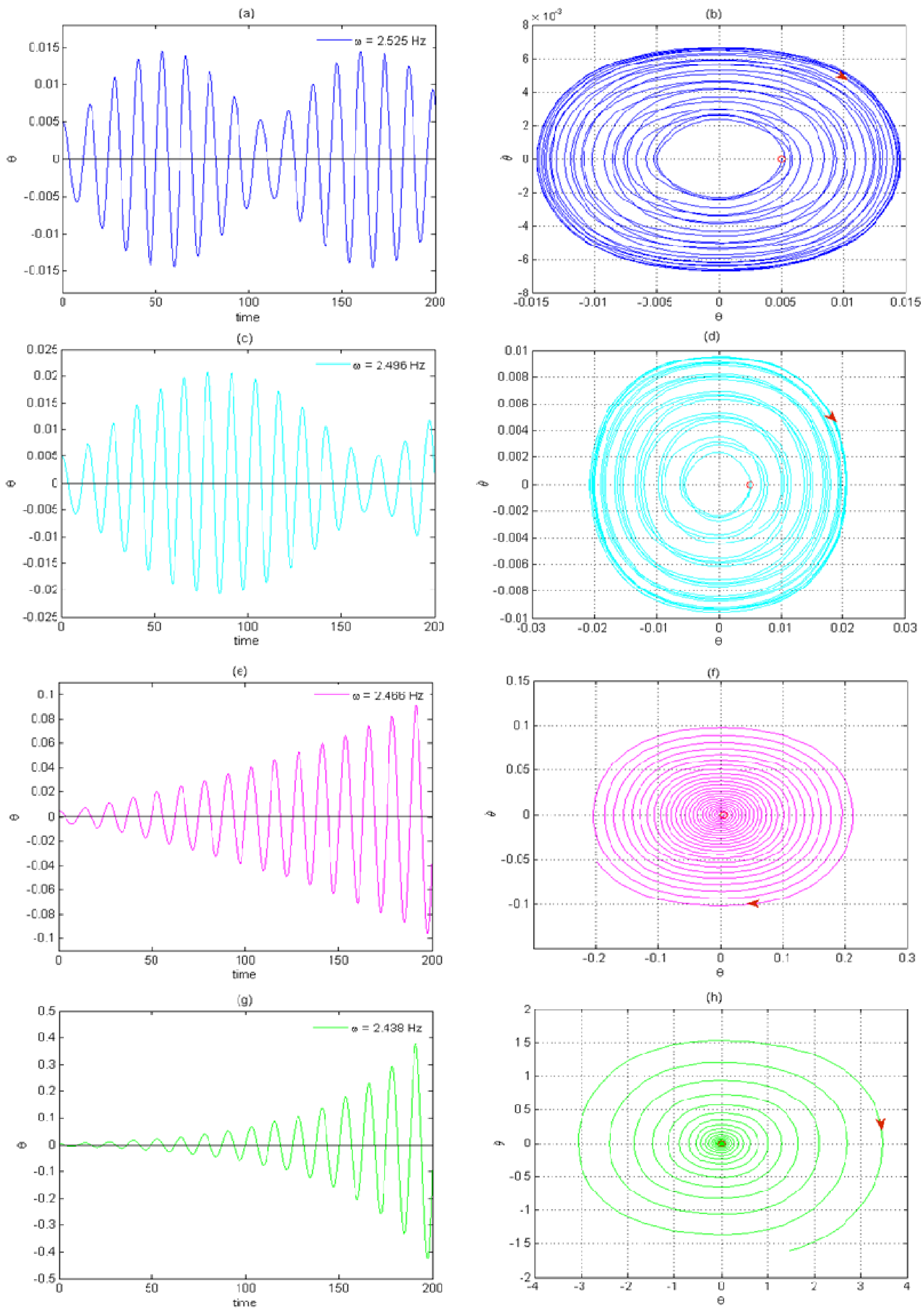


**Figure 2.4: Response of parametric oscillator for the system parameters shown in Figure 2.3**

parametric instability. The response of the pendulum is as expected from the stability diagram.

The animation of simple pendulum's response in stable region shown in Figure 2.4 (c) can be seen in the link http://youtu.be/QwSHhknz9ys. The animation of the pendulum in unstable region whose response is shown in Figure 2.4 (e) can be seen in the link http://youtu.be/L-Q6xg2KbCA.

### 2.4.2 Response of inverted pendulum

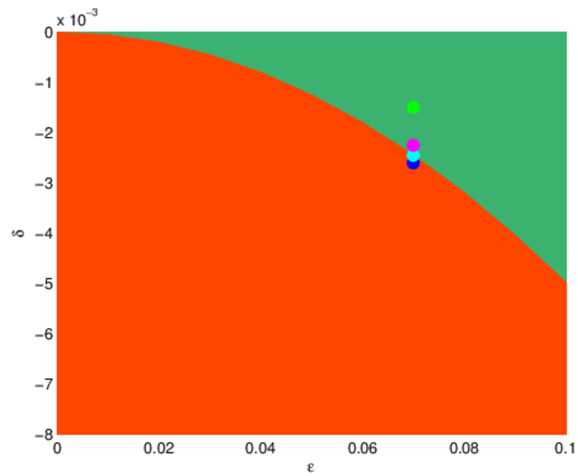


**Figure 2.5: Location of system parameters for inverted pendulum**

Figure 2.5 shows the location of system parameters for inverted pendulum under parametric excitation. These system parameters are given in Table 2.1. The response of the inverted pendulum for given parameters is shown in Figure 2.6. The parameters taken here, move from unstable region to stable region and from response of the inverted pendulum shown in Figure 2.6 it is clear that the pendulum attains stability as the system parameters move from unstable region to stable region. From this study it can be inferred that pendulum has to be excited with large frequencies to make it stable. The response of the inverted pendulum is as expected from the stability diagram. The response animation of inverted pendulum under

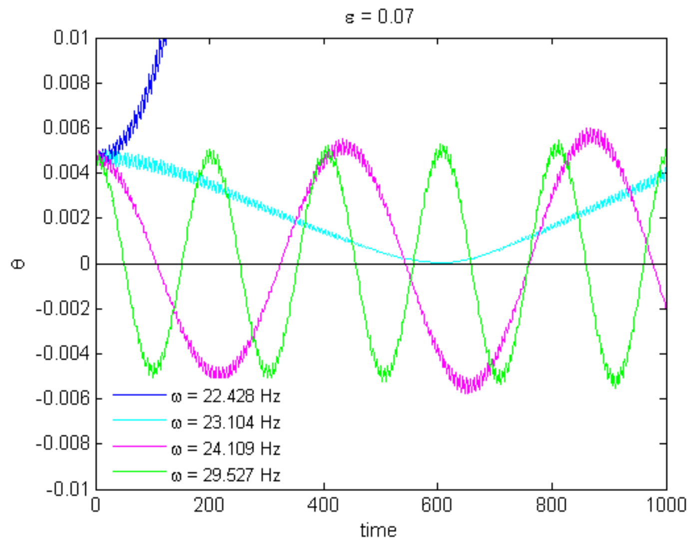


**Figure 2.6: Response of inverted pendulum for system parameters shown in Figure 2.5**

stable excitation and unstable excitation parameters can be viewed in the links http://youtu.be/GwlegJHI4vQ and http://youtu.be/ytkwtTaWOq0 respectively.

## 2.5 Summary

Present chapter discusses SDOF parametric systems. The simple pendulum and inverted pendulum serves in many ways as a pedagogical tool to understand complicated physical phenomena and mathematics involved with systems under going oscillatory motion. The governing equation for the parametric oscillator is Mathieu equation. Stability diagram is plotted using Bolotin's approach and reliability of the stability diagram is checked via simulation of response of Mathieu equation employing Runge-Kutta method. The response of the pendulum was as expected from the stability chart.

# Chapter 3

# DYNAMIC STABILITY OF SLENDER BEAMS

## 3.1 Introduction

The function of beam structure in most of the engineering applications is to carry a static load. To minimize costs, it is often desired to reduce the mass of the supporting structure as much as possible, while retaining high stiffness. Thin-walled structures or slender structures which have high stiffness to mass ratio are often used for this purpose. These structures carry static load and are prone to buckling under high loads. A static buckling analysis should be carried out to assess their static stability. In many situations, for example due to motion of the base of the structure under seismic events, a dynamic load can act on the structure in addition to the static load. This dynamic load acting on the structure can be parametric and can cause dynamic buckling or parametric instability resulting in structural damage or total collapse of the structure. Hence it is required to carry out stability analysis of the structure under parametric loadings to avoid such damages.

The governing equation for dynamic stability of elastic structures under parametric excitation is a Mathieu-Hill equation [8, 14]. The dynamic stability of mechanical systems, according to Bolotin's definition [14], represents a specific aspect of the stability of motion. Several works have been presented along the lines of Bolotin's studies [14] aiming to give quantitative description of the phenomenon. But those methods become difficult to apply on slender structures of complex shape with arbitrary boundary conditions. Thus, to analyse the stability of complex structures, numerical methods are prefered. Numerical methods like finite difference method and finite element methods can be employed to solve the Mathieu-Hill equation. Brown [33] was the first to employ the finite element method to solve the dynamic stability problem; he employed finite element method to solve dynamic stability of bars. Shastry [37-39] applied the finite element method to study the dynamic stability of cantilever columns subjected to axial loads. The finite element approach of Mathieu-Hill equation in case of shallow shells has been proposed by Basar [40], the proposed method is applicable to all types of structures. Briseghella [41] applied finite element method to investigate the stability of slender beam and a frame under vertical axial periodic excitation. T. Iwatsubo and Saigo [60, 61] employed the finite difference method to analyze the stability of columns under periodic axial loads. Most of the studies target to study the response of structure under parametric excitation alone. There are chances that along with the parametric excitation, a forcing excitation act on the structure which can set structure to resonance. Few studies exist on the investigation of stability of structures under combined parametric and forcing excitations. Lin and Shih [62] investigated earthquake response of cantilever beam under both lateral and transverse loadings. Hara [63] analyzed response of a downward hanging cantilever beam with a concentrated mass at the tip under combined lateral and transverse excitations. R. F. Fung [64] analyzed the stability of beam subjected to combined excitations using average method and method of multiple scales. Park [65] analyzed long slender marine structures under combined parametric and forcing excitations using finite element method. Chiba [66] conducted an experiment to analyze the influence of horizontal excitations on dynamic stability of a slender beam subjected simultaneous horizontal and vertical excitations. Hamed [67] studied the dynamic behavior of string-beam coupled system under combined excitations using method of multiple scales.

In the present chapter, dynamic stability of slender beam is analyzed using finite element Bolotin's approach and Hsu's method. To verify the reliability of the stability diagram, response of the beam under parametric excitation is computed by employing Newmark's method of direct time integration technique.

## 3.2 Governing equations

The continuum model considered by Bolotin for a slender column subjected to external periodic load is shown in Figure 3.1. The column is discretized using two-noded Euler beam elements with two degrees of freedom namely transverse displacement and rotation at each node as shown in Figure 3.2. Beam element neglecting axial degree of freedom (d.o.f) is used for this study. Let E be the Young's modulus, I be the moment of inertia of the beam cross sectional area. To describe the displacement at intermediate nodal points Hermite polynomial shape functions are used [68]. Referring to the beam element we can write:

Displacement function, $$u = N^T q \tag{3.1}$$

Strain, $$\varepsilon = Lu = LN^T q = B^T q \tag{3.2}$$

Stress, $$\sigma = D\varepsilon = DB^T q \tag{3.3}$$

where $N$ is a vector of shape functions, $q$ is vector of d.o.f., $L$ is curvature differential operator, $B$ is strain displacement matrix and $D$ is bending stiffness modulus. The element equation for beam according to principle of virtual work is,

$$\delta\int_{t_1}^{t_2}\left(T^e - U^e + W^e\right)dt = 0 \tag{3.4}$$

where $T^e$ is kinetic energy, $U^e$ is internal potential energy of the beam element and $W^e$ is work done on the beam element by the external periodic force *p(t)*. With the help of principle of virtual work it is possible to obtain the element mass, stiffness and geometric stiffness matrix.

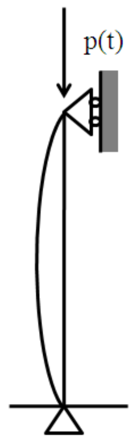


**Figure 3.1: Column subjected to axial loading**

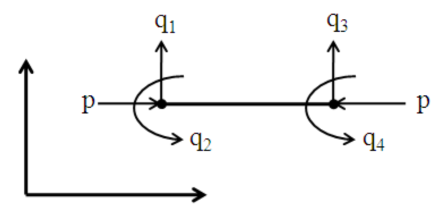


**Figure 3.2: Two noded beam element**

### 3.2.1 Element mass matrix

Elemental kinetic energy of the beam element is given by,

$$T^e = \frac{1}{2}\int_0^l \rho A \frac{\partial^2 w}{\partial t^2} \tag{3.5}$$

where $\rho$ is the mass density per unit volume, $A$ is the cross sectional area of the beam, $l$ is the element length. Substituting Eq. (3.1) in Eq. (3.5) and applying Galerkin's method results in the elemental mass matrix for the beam. Element mass matrix $M^e$ of the beam is given as,

$$M^e = \int_0^l N^T \rho A N dx \tag{3.6}$$

$$\Rightarrow M^e = \frac{\rho A l}{420}\begin{bmatrix} 156 & 22l & 54 & -13l \\ 22l & 4l^2 & 13l & -3l^2 \\ 54 & 13l & 156 & -22l \\ -13l & -3l^2 & -22l & 4l^2 \end{bmatrix} \tag{3.7}$$

### 3.2.2 Element stiffness matrix

Elemental potential energy of the beam element is given by

$$U^e = \frac{1}{2}\int_0^l \frac{\partial^2}{\partial x^2}\left(EI\frac{\partial^2 w}{\partial x^2}\right) \tag{3.8}$$

Substituting Eq. (3.1) in Eq. (3.8) and applying Galerkin's method results in the elemental stiffness matrix for the beam. Element stiffness matrix $K^e$ of the beam is given by,

$$K^e = \int_0^l B^T EIBdx \tag{3.9}$$

$$\Rightarrow K^e = \frac{EI}{l^3}\begin{bmatrix} 12 & 6l & -122 & 6l \\ 6l & 4l^2 & -6l & 2l^2 \\ -12 & -6l & 12 & -6l \\ 6l & 2l^2 & -6l & 4l^2 \end{bmatrix} \tag{3.10}$$

### 3.2.3 Element geometric stiffness matrix

The beam is subjected to external periodic transverse loading *p(t)*. The elemental work done on the beam by the external periodic force *p(t)* is given by,

$$W^e = \frac{1}{2}\int_0^l p(t)\frac{\partial^2 w}{\partial x^2}dx \tag{3.11}$$

Substituting Eq. (3.1) in Eq. (3.11) and applying Galerkin's method results in the elemental geometric stiffness matrix for the beam. Elemental geometric stiffness matrix $K_g^e$ of the beam is given by,

$$K_g^e = \int_0^l \left(\frac{\partial N}{\partial x}\right)^T \left(\frac{\partial N}{\partial x}\right)dx \tag{3.12}$$

$$\Rightarrow K_g^e = \frac{1}{30l}\begin{bmatrix} 36 & 3l & -36 & 3l \\ 3l & 4l^2 & -3l & -l^2 \\ -36 & -3l & 36 & -3L \\ 3L & -l^2 & -3l & 4l^2 \end{bmatrix} \tag{3.13}$$

### 3.2.4 Governing equation for dynamic stability

On substituting the element matrices Eq. (3.7), Eq. (3.10) and Eq. (3.13) into Eq. (3.4) of principle of virtual work and on assembling the element matrices, the following governing equation is obtained

$$M\ddot{q} + \left(K - p(t)K_g\right)q = 0 \tag{3.14}$$

The damping effects in the governing equation can be included by introducing the damping matrix [8, 14] in the form $C = \alpha M$ in the above equation, we get

$$M\ddot{q} + C\dot{q} + \left(K - p(t)K_g\right)q = 0 \tag{3.15}$$

where $M$ is mass matrix, $C$ is damping matrix, $K$ is elastic stiffness matrix, $K_g$ is geometric stiffness matrix or stability matrix, $p(t)$ is external periodic force and $q$ is vector of d.o.f. The periodic force is assumed to be of the form

$$p(t) = P_s + P_d \cos\Omega t \tag{3.16}$$

where $P_s$ is the static load component, $P_d$ is the dynamic load component and $\Omega$ is the frequency of the parametric periodic force. It can be expressed as

$$p(t) = \alpha P_{cr} + \beta P_{cr} \cos\Omega t \tag{3.17}$$

where $\alpha = P_s/P_{cr}$ and $\beta = P_d/P_{cr}$ are termed as the static and dynamic load factors respectively, $P_{cr}$ is the critical buckling load of the beam. Buckling load of the beam can be obtained numerically by solving the following eigenvalue problem

$$\left|K - \lambda K_g\right| = 0. \tag{3.18}$$

Where $\lambda$ is vector of buckling values and $P_{cr}$ is the minimum value of vector $\lambda$.

## 3.3 Stability analysis of slender beam

Stability analysis of slender beam with any arbitrary boundary conditions can be carried out using the methods discussed in Chapter 1. Bolotin's finite element approach is used here.

### 3.3.1 Finite element Bolotin's approach

Substitution of Eq. (3.16) into Eq. (3.15) leads to

$$M\ddot{q} + C\dot{q} + (K + K_{gs} + K_{gd}\cos\Omega t)q = 0 \qquad (3.19)$$

where $K_{gs} = -P_s \times Kg$, $K_{gd} = -P_d(t) \times K_g$. Eq. (3.19) is similar to Eq. (1.15). To apply Bolotin's approach the required mass, damping, stiffness and geometric stiffness matrices are formed and to obtain the stability chart Eq. (1.22) and Eq. (1.23) are solved for critical frequencies with increasing dynamic load component $P_d$. To obtain stability diagram without damping Eq. (A.1 – A.4) given in Appendix – A are solved. This approach cannot plot combination resonance regions. Combination resonance regions can be captured using Hsu's method.

### 3.3.2 Dynamic stability diagram

Using the proposed Bolotin's approach the dynamic stability of a beam simply supported at both ends is examined. A simply supported beam of length 7 m, Young's modulus $2.1\times10^{11}$ N/m$^2$, moment of inertia $2003\times10^{-8}$ m$^4$ and mass per unit length of 61.3 Kg/m is considered for analysis. The dimensions are of a HEB 200 beam. A simply supported beam is considered because the theoretical solution of this case is known and can be used for comparison. For dynamic analysis the static component of the external periodic force is taken zero i.e. $p_s = 0$. The theoretical natural frequencies and Euler buckling load for the simple beam supported at both the ends are,

$$f = \frac{k_n}{2\pi L^2}\sqrt{\frac{EI}{m}} \tag{3.20}$$

where $k_n$ = 9.87, 39.5, 88.8 for the first three modes respectively.

$$P_{cr} = \frac{\pi^2 EI}{L^2} \tag{3.21}$$

Table 3.1 gives the comparison of natural frequencies and Euler buckling load of the simply supported beam obtained using theoretical and finite element method. In the finite element analysis 10 beam elements are considered.

**Table 3.1: Natural frequencies ($s^{-1}$) and buckling load (N) for simple supported beam**

| Mode | Theory | FEM | Error % |
|---|---|---|---|
| 1 | 52.7644 | 52.7623 | 0.004 |
| 2 | 211.1645 | 211.0536 | 0.052 |
| 3 | 474.7192 | 474.9113 | -0.040 |
| **Buckling load** | 847235 | 847669 | -0.051 |

Figure 3.3 shows the region of instability, obtained from solving *2T* period eigenvalue solution, Eq. (1.22). The exact solution obtained using theoretical continuum solution [14] is also shown. From the Figure 3.3, it is clear that exact solution and FEM solution are in good match. This instability region obtained from *2T* period eigenvalue solution is called the principal instability region, and it is the most dominating and dangerous. This instability region corresponds to the first fundamental frequency.

Figure 3.4 shows the instability regions of the beam for damped and undamped case, obtained from solving *2T* and *T* eigenvalue solutions. The instability regions shown correspond to the first fundamental frequency. Also there exist infinite regions of instability corresponding to infinite modes of vibration but

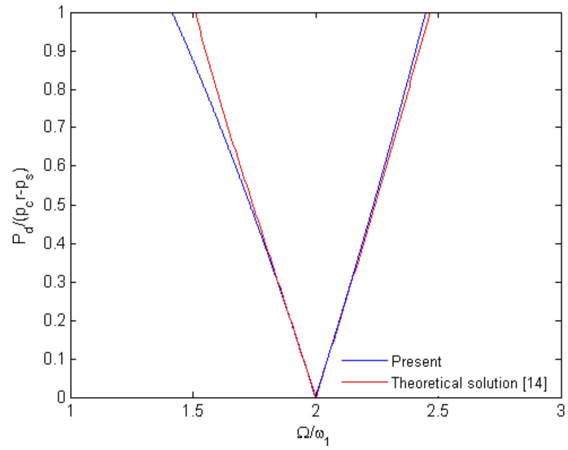


**Figure 3.3: Comparison between FEM solution and theoretical solution**

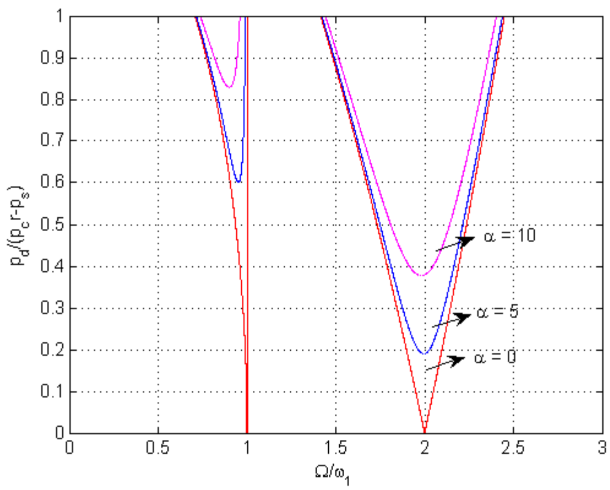


**Figure 3.4: Dynamic stability diagram for simply supported beam**

those instability regions are of least importance. The instability region obtained from the 2T period eigenvalue solution will be wider than the instability region obtained from T period eigenvalue solution. The presence of damping increases the structures chance of stability under dynamic loading. From Figure 3.4 it is clear that the instability region is reduced due to damping. There exists a critical excitation parameter, below which the system is always stable. From the stability chart, one can conclude that, when the axial loading parameters lie in the instability regions, the structure undergoes instability, i.e. the structure's response goes unbounded. Contrarily, if the loading parameters are outside the instability zones, the structure is stable.

## 3.4 Numerical results and discussion

To verify the reliability of stability chart obtained a direct numerical integration of the Mathieu equation Eq. (3.15) is carried out. To compute the response of the beam under parametric excitation, a direct time integration technique Newmark's method is employed. A time step of $\Delta t = 5\times10^{-4}$ s and $\beta = 0$; $\gamma = 0.5$ are the parameters employed for direct time integration. A damping parameter of $\alpha = 5$ is considered for numerical time integration.

The load cases examined under parametric excitation are shown in Figure 3.5 and are given in Table 3.2. A very small initial displacement of 3 mm to the translational degree of freedom is imposed to evaluate the response, without this initial displacement there won't be any response in the structure.

Figure 3.6 shows structure's response w.r.t time at time integration points A, B and C. The left side cases (a), (c) and (e) are computed without damping, where as the right hand side cases (b), (d) and (f) are computed with damping present in the structure. From Figure 3.5, it is clear that these excitation parameters lie in principal instability region and as expected the response of the beam is unbounded. Figure 3.6(a) shows gradual increase in the response, where as in Figure 3.6(b) the structure come to rest due to damping, achieving stability. Point A lies in stability region when damping is present, thus a stable response is shown. From Figures 3.6(c) – 3.6(f) parametric instability can be noted; response shows an exponential increase in time. The rate of increase of amplitude is low in presence of damping, which can be

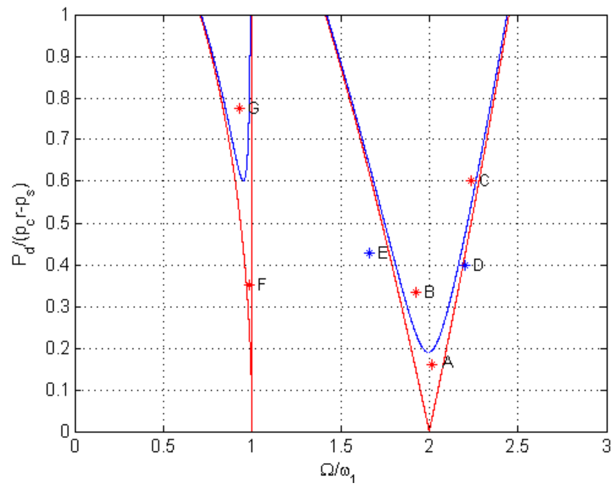


**Figure 3.5: Location of system parameters for direct time integration**

**Table 3.2: System parameters shown in Figure 3.5**

| Case | $\Omega/\omega_1$ | $P_d/P_{cr}$ |
|---|---|---|
| A | 2.0150 | 0.1594 |
| B | 1.9251 | 0.3348 |
| C | 2.2362 | 0.6009 |
| D | 2.2016 | 0.3991 |
| E | 1.6624 | 0.4284 |
| F | 0.9850 | 0.3523 |
| G | 0.9297 | 0.7763 |

seen from Figure 3.6(d), 3.6(f) when compared to Figure 3.6(c), 3.6(e). Damping can only reduce the rate of increase of amplitude and may delay occurrence of instability but have no control on final amplitude. From Figure 3.6, it can be seen that, as the loading amplitude is high, the rate of increase of amplitude is high, irrespective of presence or absence of damping. Since these points lie in unstable region, the response is unstable as expected. The response animation of the beam for the case A lying in unstable region and whose reponse is shown in Figure 3.6 (a) can be seen in the link http://youtu.be/xW065jvw_wg.

Figure 3.7 shows structure's response at points D and E with and without damping. The point D lie on the boundary curve of principal instability region and

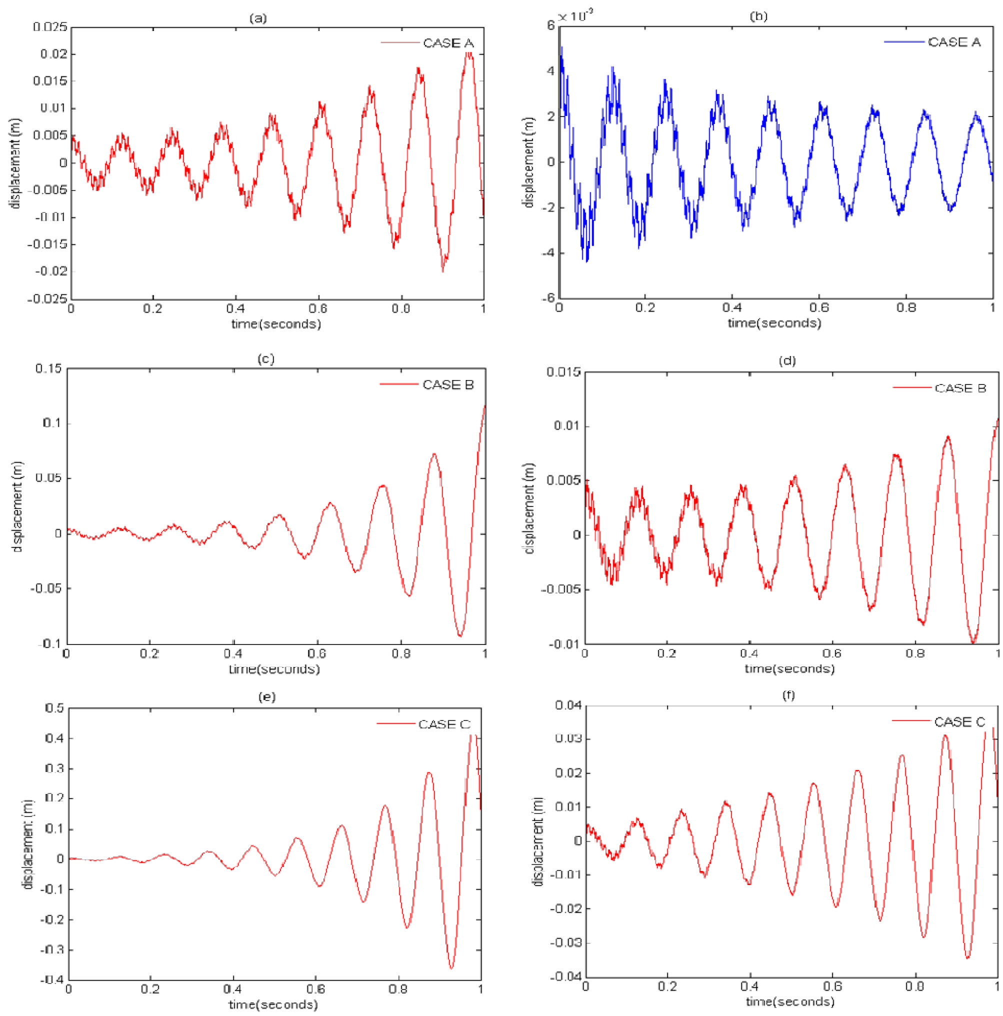


**Figure 3.6: Structure's response at points A, B and C**

the point E lies in stable region. Both the points should show a stable response and from Figure 3.7 it is evident that the response of the beam is stable. In Figure 3.7(a) the response of the beam shows a beating phenomenon; the displacement function is the product of periodic function with period T and a function of difference of two harmonic functions with limited different frequencies of vibration. The difference of the frequencies of the harmonic functions have a phase difference, thus the oscillation amplitudes add or subtract themselves showing beating phenomenon. This kind of behavior is not observed in presence of damping. As the points lie in

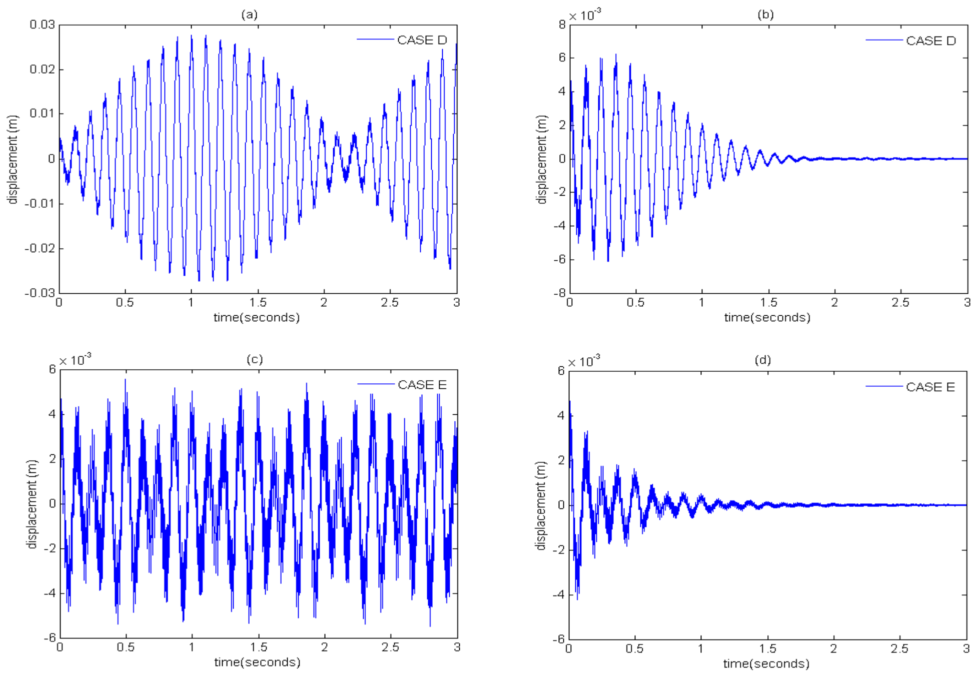


**Figure 3.7: Structure's response at points D, E**

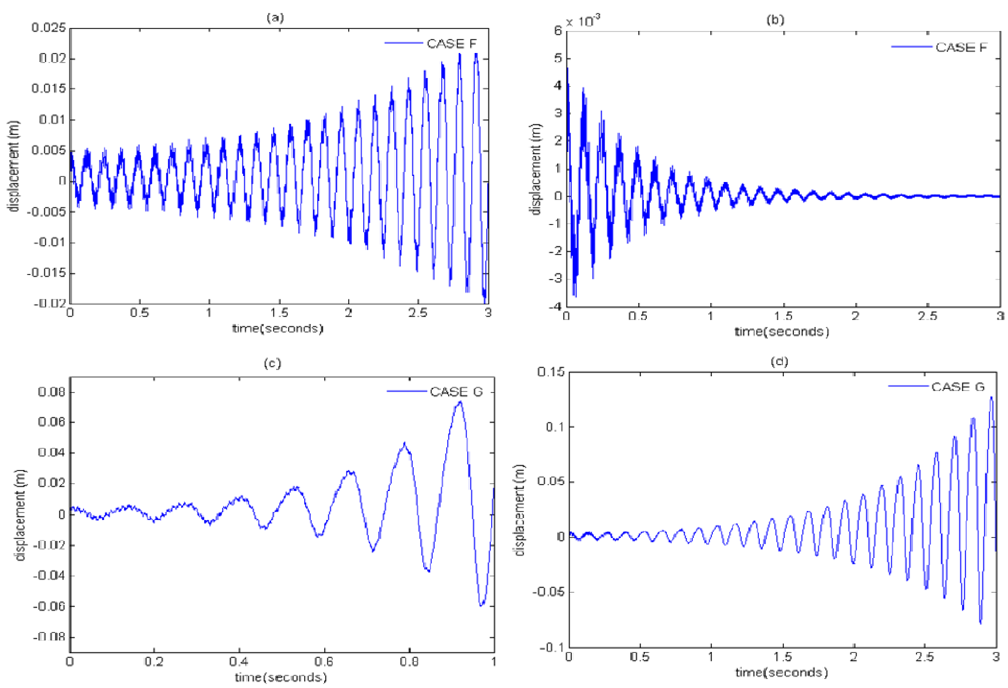


**Figure 3.8: Structure's response at points F, G**

the stable region, as expected stable response of the beam is observed. The response of the beam for the case E, which lies in stable region and whose reponse is shown in Figure 3.7 (c) can be viewed in the link http://youtu.be/mOAmeDxQq9w.

Figure 3.8 shows structure's response at points F and G with and without damping. The parameters F and G lie in the instability region bounded by boundary curves of solution with period *T*. This instability region corresponds to the beams response characterized by vibration with period equal to *T*. Figure 3.8(a) shows response at point F without damping. The time taken for the amplitude to grow is large when compared to the time taken by parameters lying in principal instability region. The parameters for F lie in stable region when damping is present and a stable response is shown in Figure 3.8(b). Figures 3.8(c), 3.8(d) shows the beams response at point G, both the responses show instability. The time taken for amplitude to grow up is large when compared to response of the beam in principal instability region. It can be seen from Figure 3.4, that as the damping increases the, instability region becomes small and vanishes.

It was discussed in Chapter 1, that Bolotin's approach cannot plot parametric combination instability regions. To plot those regions Hsu's stability criteria can be used. For the present simply supported beam, Hsu's criteria for combination resonance Eq. (1.60) were applied and it was found that no combination resonance is possible in this case of beam simply supported at both the ends.

## 3.5 Summary

Using finite element formulation of beam the dynamic stability of simply supported slender beam is investigated. The instability regions are obtained using finite element Bolotin's approach. To check the reliability of the procedure direct time integration using Newmark's method is carried out. The instability regions are checked by plotting time vs. displacement plots at different integration points. The plots show an exponential increase in displacement in the instability region and bounded solution in the stability region as estimated from the theory. This numerical procedure can be applied to any complex structure with arbitrary boundary condition under any load for which the analytical solution is difficult to use.

# Chapter 4

# DYNAMIC STABILITY OF THIN PLATES

## 4.1 Introduction

Plate is defined as a flat body whose thickness is much smaller than its other dimensions. A flat plate carries a lateral load by bending; it develops bending moments in two directions and a twisting moment. Slabs in civil engineering structures, bearing plates under columns, many parts of mechanical components are the common examples of plates. In the fields of aerospace, aeronautics, transportation etc. lighter and thin-walled structures are used because they offer better economy satisfying the functional requirements. Thus it is of great concern to study the mechanical behavior of such structures when they are subjected to a static or dynamic loading. In particular, when a plate is subjected to an out-of-plane sinusoidal loading it exhibits forced resonance and when the plate is subjected to in-plane loading it exhibits lateral instability (parametric instability) over certain regions of the system parameters. A number of researchers have investigated the dynamic stability of plates due to periodic in-plane loads. For example, Hutt and Salam [71] used the thin plate finite element model to study the dynamic instability of plates. Krajcinovic and Herrmann [72] used an integral equation technique to solve the dynamic stability problem of an isotropic rectangular plate. Tani and Nakamura [73] studied annular plates. Srinivasan and Chellapandi [74] studied the dynamic stability of thin rectangular layered plates by the finite strip method. Takahashi [75] analyzed dynamic stability of rectangular plates analytically. Chen and Yang [76] studied the dynamic stability of laminated composite plates by the finite element method. Deolasi and Datta [77] analyzed the parametric resonance of rectangular plates under non-uniform edge loading using method of multiple scales. Sassi [78-81] analyzed the behavior of plates under combined parametric and forcing excitation.

In the present chapter dynamic stability of thin plate is analyzed using finite element method. Two plate theories exist, Kirchhoff theory and Mindlin theory. In the Kirchhoff theory, transverse shear deformation is not considered and in Mindlin theory it is accounted. In the present chapter Mindlin plate theory is considered.

## 4.2 Mindlin plate theory

Plate is a flat surface having considerably large dimensions as compared to its thickness. Due to this geometry, 3D finite element analysis is not required to model plates; a 2D finite element analysis is adequate. A plate of thickness $t$ is modeled by its midsurface at a distance $t/2$ from each lateral surface. Let the $xy$ plane be the plate midsurface, so that $z=0$ defines the midsurface. The behavior of plate is idealized by a line normal to the midsurface under applied loads. In Mindlin plate theory, the straight line normal to the midsurface remains straight but not normal to the deformed midsurface after applying load. The Mindlin plate theory takes shear deformation into account. The normal gets rotated by components $\theta_x$ and $\theta y$. Thus a point not on the midsurface has the $x$-direction displacement $u$, $y$-direction displacement $v$ and $z$-direction displacement $w$. For small displacements and rotations, stresses and strains can be written as [68, 70, and 82];

Bending stresses and strains are written as

$$\sigma_b^T = \begin{bmatrix} \sigma_x & \sigma_y & \tau_{xy} \end{bmatrix} \tag{4.1}$$

$$\varepsilon_b^T = \begin{bmatrix} \varepsilon_x & \varepsilon_y & \gamma_{xy} \end{bmatrix} \tag{4.2}$$

Transverse shear stresses and strains are written as

$$\sigma_s^T = \begin{bmatrix} \tau_{xz} & \tau_{yz} \end{bmatrix} \tag{4.3}$$

$$\varepsilon_s^T = \begin{bmatrix} \gamma_{xz} & \gamma_{yz} \end{bmatrix} \tag{4.4}$$

The assumed displacement field for a plate can be written as

$$u = z\theta_x; v = z\theta_y; w = w_0 \tag{4.5}$$

For small displacements and rotations, strains can be written as [68, 70, and 82];

**4.2.1 Strains**

Bending strains are obtained as

$$\begin{aligned} \varepsilon_x &= \frac{\partial u}{\partial x} = z\frac{\partial \theta_x}{\partial x} \\ \varepsilon_y &= \frac{\partial v}{\partial y} = z\frac{\partial \theta_y}{\partial y} \\ \gamma_{xy} &= \frac{\partial u}{\partial y} + \frac{\partial v}{\partial x} = z\left(\frac{\partial \theta_y}{\partial x} + \frac{\partial \theta_x}{\partial y}\right) \end{aligned} \tag{4.6}$$

Transverse shear strains are obtained as

$$\begin{aligned} \gamma_{xz} &= \frac{\partial w}{\partial x} + \frac{\partial u}{\partial z} = \frac{\partial w}{\partial x} + \theta_x \\ \gamma_{yz} &= \frac{\partial w}{\partial y} + \frac{\partial v}{\partial z} = \frac{\partial w}{\partial y} + \theta_y \end{aligned} \tag{4.7}$$

**4.2.2 Stresses**

The linear elastic stress-strain relations in bending for a homogenous isotropic material is defined as

$$\sigma_b = D_b \varepsilon_b \tag{4.8}$$

where $D_b$ is defined as

$$D_b = \frac{E}{1-\nu^2}\begin{bmatrix} 1 & \nu & 0 \\ \nu & 1 & 0 \\ 0 & 0 & \frac{1-\nu}{2} \end{bmatrix} \tag{4.9}$$

The linear elastic stress-strain relations in transverse shear for a homogenous isotropic material is defined as

$$\sigma_s = D_s \varepsilon_s \tag{4.10}$$

where $D_s$ is defined as

$$D_s = \begin{bmatrix} G & 0 \\ 0 & G \end{bmatrix} \tag{4.11}$$

where $E$, $v$ and $G$ are Young's modulus, Poisson's ratio and shear modulus of the homogenous isotropic material respectively.

## 4.3 Finite element discretization

The generalized displacements are independently interpolated using the same shape functions as follows

$$\begin{aligned} w &= \sum_{i=1}^{n} N_i(\xi,\eta) w_i \\ \theta_x &= \sum_{i=1}^{n} N_i(\xi,\eta) \theta_{xi} \\ \theta_y &= \sum_{i=1}^{n} N_i(\xi,\eta) \theta_{yi} \end{aligned} \tag{4.12}$$

where $N_i(\xi,\eta)$ are the shape functions and $n$ is the number of nodes in the element. Strains can be defined as

$$\varepsilon_b = zB_b d^e ; \varepsilon_s = B_s d^e \tag{4.13}$$

where $B_b$ and $B_s$ are the strain-displacement matrices for bending and shear contributions and can be written from shape functions as

$$B_b = \begin{bmatrix} 0 & \frac{\partial N_1}{\partial x} & 0 & \cdots & 0 & \frac{\partial N_n}{\partial x} & 0 \\ 0 & 0 & \frac{\partial N_1}{\partial y} & \cdots & 0 & 0 & \frac{\partial N_n}{\partial y} \\ 0 & \frac{\partial N_1}{\partial y} & \frac{\partial N_1}{\partial x} & \cdots & 0 & \frac{\partial N_n}{\partial y} & \frac{\partial N_n}{\partial x} \end{bmatrix} \quad (4.14)$$

$$B_s = \begin{bmatrix} \frac{\partial N_1}{\partial x} & N_1 & 0 & \cdots & \frac{\partial N_n}{\partial x} & N_n & 0 \\ \frac{\partial N_1}{\partial y} & 0 & N_1 & \cdots & \frac{\partial N_n}{\partial y} & 0 & N_n \end{bmatrix} \quad (4.15)$$

and $d^e$ is the degrees of freedom of node

$$d^{eT} = \left\{ w_1 \quad \theta_{x1} \quad \theta_{y1} \quad \cdots \quad w_n \quad \theta_{xn} \quad \theta_{yn} \right\} \quad (4.16)$$

### 4.3.1 Element mass matrix

The kinetic energy of the Mindlin plate is given as

$$T = \frac{1}{2}\int_V \rho\left(\dot{u}^2 + \dot{v}^2 + \dot{w}^2\right) dv \quad (4.17)$$

Substituting the above defined field equations, the kinetic energy for an element can be written as

$$T^e = \frac{1}{2}\int_{\Omega^e} \rho\left(t\dot{w}^2 + \frac{t^3}{12}\dot{\theta}_x^2 + \frac{t^3}{12}\dot{\theta}_y^2\right) d\Omega^e \quad (4.18)$$

The element mass matrix is computed as

$$M^e = \int_{\Omega^e} \rho N^T I N d\Omega^e \quad (4.19)$$

where $I$ is given by

$$I = \begin{bmatrix} t & 0 & 0 \\ 0 & \frac{t^3}{12} & 0 \\ 0 & 0 & \frac{t^3}{12} \end{bmatrix} \quad (4.20)$$

If isoparametric shape functions are used, the stiffness matrix becomes

$$M^e = \int_{-1}^{+1}\int_{-1}^{+1} \rho N^T I N \left|J\right| d\xi d\eta \tag{4.21}$$

**4.3.2 Element stiffness matrix**

The strain energy of the Mindlin plate is given as

$$U = \frac{1}{2}\int_v \sigma_b^T \varepsilon_b dv + \frac{\alpha}{2}\int_v \sigma_s^T \varepsilon_s dv \tag{4.22}$$

where $\alpha$ is the shear correction factor and can be taken as 5/6. The finite element strain energy for an element can be written as

$$U^e = \frac{1}{2} d^{eT} \int_{\Omega^e}\int_z B_b^T D_b B_b dz d\Omega^e d^e + \frac{\alpha}{2} d^{eT} \int_{\Omega^e}\int_z B_s^T D_s B_s dz d\Omega^e d^e \tag{4.23}$$

The element stiffness matrix of the Mindlin plate is then obtained as

$$K^e = \frac{t^3}{12}\int_{\Omega^e} B_b^T D_b B_b d\Omega^e + \alpha t \int_{\Omega^e} B_s^T D_s B_s d\Omega^e \tag{4.24}$$

If isoparametric shape functions are used, the stiffness matrix becomes

$$K^e = \frac{t^3}{2}\int_{-1}^{+1}\int_{-1}^{+1} B_b^T D_b B_b \left|J\right| d\xi d\eta + \alpha t \int_{-1}^{+1}\int_{-1}^{+1} B_s^T D_s B_s \left|J\right| d\xi d\eta \tag{4.25}$$

where $J$ is the Jacobian matrix.

**4.3.3 Element geometric stiffness matrix**

The geometric stiffness matrix is a result of initial stress present in the structure. The strain energy for an initially stressed Mindlin plate, after neglecting terms with third and higher powers in displacement gradients is written as [83],

$$U = \frac{1}{2}\int_v \sigma_b^T \varepsilon_b dv + \frac{\alpha}{2}\int_v \sigma_s^T \varepsilon_s dv + \int_v \left(\sigma_0\right)^T \varepsilon^L dv \tag{4.26}$$

where $\sigma_0$ is initial membrane stress distribution present in the plate and

$$\varepsilon^L = \begin{bmatrix} \frac{1}{2}\left(\left(\frac{\partial u}{\partial x}\right)^2 + \left(\frac{\partial v}{\partial x}\right)^2 + \left(\frac{\partial w}{\partial x}\right)^2\right) \\ \frac{1}{2}\left(\left(\frac{\partial u}{\partial y}\right)^2 + \left(\frac{\partial v}{\partial y}\right)^2 + \left(\frac{\partial w}{\partial y}\right)^2\right) \\ \frac{\partial u}{\partial x}\frac{\partial u}{\partial y} + \frac{\partial v}{\partial x}\frac{\partial v}{\partial y} + \frac{\partial w}{\partial x}\frac{\partial w}{\partial y} \end{bmatrix} \tag{4.27}$$

On integrating over the plate thickness, the strain energy is

$$\begin{aligned} U = {} & \frac{1}{2}\int_{\Omega^e} \varepsilon_b^T D_b \varepsilon_b d\Omega^e + \frac{1}{2}\int_{\Omega^e} \varepsilon_s^T D_s \varepsilon_s d\Omega^e \\ & + \frac{1}{2}\int_{\Omega^e} \begin{bmatrix} \left(\frac{\partial w}{\partial x}\right) & \left(\frac{\partial w}{\partial y}\right) \end{bmatrix} \hat{\sigma}_0^T \begin{bmatrix} \left(\frac{\partial w}{\partial x}\right) \\ \left(\frac{\partial w}{\partial y}\right) \end{bmatrix} t d\Omega^e \\ & + \frac{1}{2}\int_{\Omega^e} \begin{bmatrix} \left(\frac{\partial \theta_x}{\partial x}\right) & \left(\frac{\partial \theta_x}{\partial y}\right) \end{bmatrix} \hat{\sigma}_0^T \begin{bmatrix} \left(\frac{\partial \theta_x}{\partial x}\right) \\ \left(\frac{\partial \theta_x}{\partial y}\right) \end{bmatrix} \frac{t^3}{12} d\Omega^e \\ & + \frac{1}{2}\int_{\Omega^e} \begin{bmatrix} \left(\frac{\partial \theta_y}{\partial x}\right) & \left(\frac{\partial \theta_y}{\partial y}\right) \end{bmatrix} \hat{\sigma}_0^T \begin{bmatrix} \left(\frac{\partial \theta_x}{\partial x}\right) \\ \left(\frac{\partial \theta_x}{\partial y}\right) \end{bmatrix} \frac{t^3}{12} d\Omega^e \end{aligned} \tag{4.28}$$

where

$$\hat{\sigma}_0 = \begin{bmatrix} \sigma_x^0 & \tau_{xy}^0 \\ \tau_{xy}^0 & \sigma_y^0 \end{bmatrix} \tag{4.29}$$

The element geometric stiffness matrix from Eq. (4.28) is obtained as

$$\begin{aligned} K_G^e = {} & t\int_{\Omega^e} G_b^T \hat{\sigma}_0 G_b d\Omega^e \\ & + \frac{t^3}{12}\int_{\Omega^e} G_{s1}^T \hat{\sigma}_0 G_{s1} d\Omega^e + \frac{t^3}{12}\int_{\Omega^e} G_{s2}^T \hat{\sigma}_0 G_{s2} d\Omega^e \end{aligned} \tag{4.30}$$

where

$$G_b = \begin{bmatrix} \frac{\partial N_1}{\partial x} & 0 & 0 & \cdots & \frac{\partial N_n}{\partial x} & 0 & 0 \\ \frac{\partial N_1}{\partial y} & 0 & 0 & \cdots & \frac{\partial N_n}{\partial y} & 0 & 0 \end{bmatrix} \tag{4.31}$$

$$G_{s1} = \begin{bmatrix} 0 & \frac{\partial N_1}{\partial x} & 0 & \cdots & 0 & \frac{\partial N_n}{\partial x} & 0 \\ 0 & \frac{\partial N_1}{\partial y} & 0 & \cdots & 0 & \frac{\partial N_n}{\partial y} & 0 \end{bmatrix} \tag{4.32}$$

$$G_{s2} = \begin{bmatrix} 0 & 0 & \frac{\partial N_1}{\partial x} & \cdots & 0 & 0 & \frac{\partial N_n}{\partial x} \\ 0 & 0 & \frac{\partial N_1}{\partial y} & \cdots & 0 & 0 & \frac{\partial N_n}{\partial y} \end{bmatrix} \tag{4.33}$$

The geometric stiffness matrix $K_G$ can be written as,

$$K_G = K_{Gb} + K_{Gs} \tag{4.44}$$

where $K_{Gb}$ is bending contribution and given by first term of Eq. (4.30) and $K_{Gs}$ is shear contribution and given by last two terms of Eq. (4.30). On using isoparametric shape functions, the geometric stiffness matrix becomes

$$\begin{aligned} K_G &= t\int_{-1}^{+1}\int_{-1}^{+1} G_b^T \sigma_0^T G_b \left|J\right| d\xi d\eta \\ &+ \frac{\mathrm{t}^3}{12}\int_{-1}^{+1}\int_{-1}^{+1} G_{s1}^T \sigma_0^T G_{s1} \left|J\right| d\xi d\eta + \frac{\mathrm{t}^3}{12}\int_{-1}^{+1}\int_{-1}^{+1} G_{s2}^T \sigma_0^T G_{s2} \left|J\right| d\xi d\eta \end{aligned} \tag{4.45}$$

The mass, stiffness and geometric stiffness matrices given by Eq. (4.21), Eq. (4.25) and Eq. (4.45) respectively are computed by numerical integration employing Gaussian integration. For thin plates, the shear contribution shall reduce and become negligible. Shear contribution is significant for thicker plates. But it should be noted that, as the bending energy is proportional to $t^3$ and shear energy proportional to $t$, the shear energy becomes dominant compared to the bending energy as the plate thickness $t$ becomes very small compared to its side length. This is called shear locking. To resolve this shear locking problem, the reduced integration technique was proposed. The remedy of shear locking is, shear term is under integrated compared to bending term i.e. bending term is integrated using the exact integration rule and shear term with reduced integration. For example, when four-noded bilinear isoparametric elements are used, the 2×2 Gauss-Legendre quadrature is used for the bending term while 1-point integration is used for the shear term. Similarly, for the nine-node biquadratic isoparametric elements the bending term is integrated using 3×3 integration order and shear term is integrated using 2×2 integration order.

## 4.4 Governing equation for dynamic stability

Application of finite elements to a plate under parametric in-plane loading yields the following equilibrium equation

$$M\ddot{q} + C\dot{q} + \left(K + P(t)K_G\right)q = 0 \qquad (4.46)$$

where *M, C, K* and $K_G$ are the global assembled mass, damping, elastic stiffness and geometric stiffness matrices respectively. All these matrices are square symmetric matrices of order *N*, where *N* is the number of degrees of freedom of the system and *q* is the nodal displacement column vector of order *N*. *P(t)* is the magnitude of the dynamic load acting on the edges of the plate. In the present analysis, a plate simply supported at all its edges and under uniform load *P(t)* on the opposite edges as shown in Figure 4.1 is considered. The matrices *M*, *K* are obtained by finite element formulation as derived in the previous section and *C* is obtained from the mass matrix by multiplying the mass matrix with proportionality constant. To calculate $K_G$, initially plane stress analysis under the uniform edge loading at the opposite edges is carried out to obtain initial stress distribution and from these initial stress distribution $K_G$ matrix is evaluated.

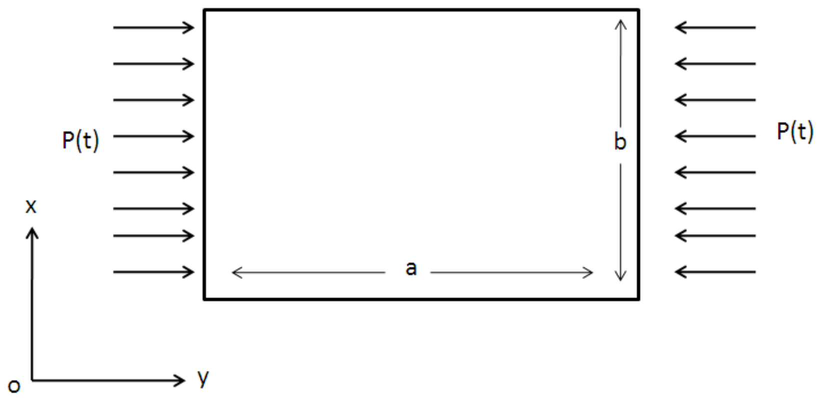


**Figure 4.1: Simply supported plate under uniform edge loading at opposite edges**

For the free vibration problem without damping, Eq. (4.46) can be reduced to

$$\left[K-\omega^2 M\right]\phi=0 \tag{4.47}$$

where $\omega$ is the natural frequency of vibration and Ø gives the normal mode of vibration of the plate. For static stability or for the buckling problem Eq. (4.46) reduces to

$$\left[K-P_{cr}K_G\right]\varphi=0 \tag{4.48}$$

where $P_{cr}$ is the buckling load and $\varphi$ is the mode shape of buckling. Both the equations Eq. (4.47) and Eq. (4.48) are eigenvalue problems. These are solved to get the fundamental natural frequencies and the critical buckling load of the plate.

If the edge in-plane loading is considered periodic in the form

$$P(t)=P_s+P_d\cos\Omega t \tag{4.49}$$

where $P_s$, $P_d$ are static and dynamic component of the parametric excitation and $\Omega$ the frequency of excitation, Eq. (4.46) reduces to

$$M\ddot{q}+C\dot{q}+\left[K+K_{Gs}+K_{Gd}\left(t\right)\right]q=0 \tag{4.50}$$

$$\Rightarrow M\ddot{q} + C\dot{q} + \left[ K_E + K_{Gd}\left(t\right) \right] q = 0 \qquad (4.51)$$

where $K_{Gs}$ is the geometric stiffness matrix corresponding to the static load component and $K_{Gd}$ is the geometric stiffness matrix corresponding to the dynamic load component and this matrix changes with respect to time. $K_E$ is the elastic stiffness matrix which is equal to sum of $K$ and $K_{Gs}$.

## 4.5 Stability analysis of thin plates

Stability analysis of thin plates with any arbitrary boundary conditions can be carried out using the methods discussed in Chapter 1. Bolotin's finite element approach and Hsu's stability criteria are used here. Bolotin's approach can give only simple parametric instability regions, while with Hsu's conditions stability regions for simple and combination resonance can be obtained.

### 4.5.1 Hsu's method

To apply Hsu's method, Eq. (4.51) is transformed into a suitable form by means of modal transformation. The global displacement matrix is assumed as

$$q = \phi\xi \qquad (4.52)$$

where $\emptyset$ is a normalized modal matrix containing the normal modes of free vibration problem,

$$M\ddot{q} + K_E q = 0 \qquad (4.53)$$

and $\xi$ is a set of normal coordinates. Substituting Eq. (4.52) into Eq. (4.51) under the parametric excitation given in Eq. (4.49) results in

$$\ddot{\xi}_m + 2\eta_m\omega_m\dot{\xi}_m + \omega_m^2\xi_m + \beta P_{cr}\cos\Omega t\sum_{n=1}^{N} d_{mn}\xi_n = 0 \qquad (4.54)$$

Eq. (4.54) is set of coupled Mathieu equations, where $m = 1, 2, \ldots N$ corresponds the mode number, $\omega_m$ is the natural frequency of $m^{th}$ mode obtained from Eq. (4.53), $\eta_m$

is the modal damping ratio, $\beta$ (= $P_d$ / $P_{cr}$) is the dynamic load factor and $d_{mn}$ are the elements of the matrix

$$D = -\phi^{-1} M^{-1} K_g \phi \tag{4.55}$$

To apply Hsu' method, stability conditions Eq. (1.60 – 1.64) are modified and can be written as [69] follows:

i. Simple resonance, $\Omega = 2\omega_j + \varepsilon\lambda \ (i=j)$

$$\left|\Omega - 2\omega_j\right| < \frac{\varepsilon}{2}\sqrt{\left(\frac{d_{jj}}{\omega_j}\right)^2 - 4\left(\frac{\eta_j}{\varepsilon}\right)^2} \tag{4.56}$$

ii. Combination resonance of sum type, $\Omega = \omega_i + \omega_j + \varepsilon\lambda \ (i \neq j)$

$$\left|\Omega - \left(\omega_i + \omega_j\right)\right| < \frac{1+\eta_{ij}}{2\sqrt{\eta_{ij}}}\frac{\varepsilon}{2}\sqrt{\frac{d_{ij}d_{ji}}{\omega_i\omega_j} - 4\eta_{ij}\left(\frac{\eta_i}{\varepsilon}\right)^2} \tag{4.57}$$

iii. Combination resonance of difference type, $\Omega = \omega_i - \omega_j + \varepsilon\lambda \ (i>j)$

$$\left|\Omega - \left(\omega_i - \omega_j\right)\right| < \frac{1+\eta_{ij}}{2\sqrt{\eta_{ij}}}\frac{\varepsilon}{2}\sqrt{-\frac{d_{ij}d_{ji}}{\omega_i\omega_j} - 4\eta_{ij}\left(\frac{\eta_i}{\varepsilon}\right)^2} \tag{4.58}$$

In the above conditions $\eta_{ij} = \eta_i/\eta_j$. In the case of simple resonance, $i = j$ and it gives always $\eta_{ij} = 1$.

### 4.5.2 Dynamic stability chart of simply supported plate under uniform edge loading

A program is written to perform all the computations described above. Plate is discretized with isoparametric four noded elements. Elements elastic stiffness and mass matrices are obtained using Gaussian reduced integration and these elements are assembled into global matrices. A plane stress analysis is performed to know the initial stress distribution under given edge loading, which is required to calculate geometric stiffness matrix. Reduced Gaussian quadrature is used for obtaining element geometric stiffness matrices and these matrices are assembled into global geometric stiffness matrix. After obtaining the global matrices, the appropriate boundary conditions are applied. The stability chart is plotted point by point using Eq. (4.56 – 4.58).

In order to check the validity of the code, the free vibration problem and buckling problem are solved to get natural frequencies and buckling load and these results are compared with the available literature. These values are expressed in the non-dimensional form defined as follows.

Non-dimensional buckling load, $$\gamma = \frac{P_{cr}a}{D} \tag{4.59}$$

Non-dimensional frequency $$\lambda = \omega b^2 \sqrt{\frac{\rho t}{D}} \tag{4.60}$$

where $a$, $b$ are the plate lengths in x- and y- directions respectively; $\rho$ is mass density of the plate material; $t$ is plate thickness. $D$ is flexural rigidity given by

$$D = \frac{Et^3}{12\left(1-\nu^2\right)} \tag{4.61}$$

where $E$ is the Young's modulus and $\nu$ is the Poisson's ratio.

**Table 4.1: Comparison of non-dimensional natural frequencies of the plate with [83]**

| a/b | $\lambda$ | | | |
|---|---|---|---|---|
| | Mode 11 | Mode 12 | Mode 21 | Mode 22 |
| 1.0 | 19.7170<br>(19.7392) | 49.2771<br>(49.3480) | 49.2771<br>(49.3480) | 78.6045<br>(78.9568) |
| | Mode 11 | Mode 21 | Mode 31 | Mode 12 |
| 2.0 | 12.3346<br>(12.3370) | 19.7531<br>(19.7392) | 32.2215<br>(32.0762) | 41.9529<br>(41.9458) |

**Table 4.2: Comparison of non-dimensional buckling load of plate with [84]**

| a/b | Present | [84] |
|---|---|---|
| 1 | 39.4312 | 39.4784 |
| 2 | 78.9353 | 78.9568 |

Table 4.1 and 4.2 shows the comparison of non-dimensional natural frequencies and buckling load for square and rectangular plate obtained using the present code and the available literature.

Figure 4.2 shows the region of principal parametric instability corresponding to first fundamental frequency, obtained from solving *2T* period eigenvalue solution in Bolotin's method, Eq. (1.22) and Hsu's stability criteria Eq. (4.56) without considering damping. From the Figure 4.3, it is clear that both the solutions are in good match.

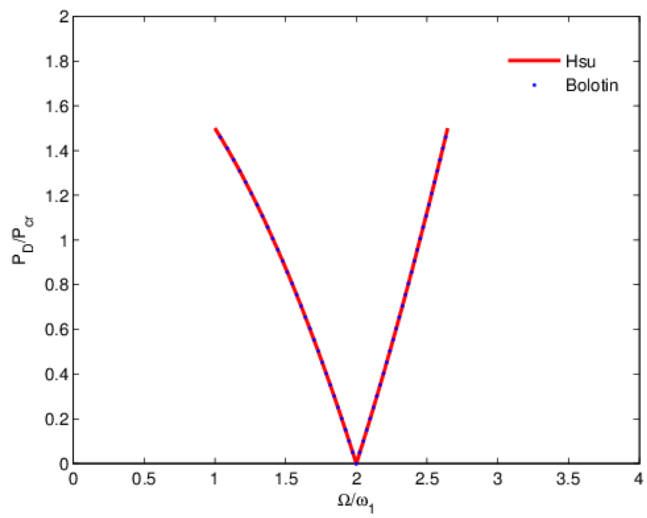


**Figure 4.2: Comparison of principal parametric instability region for plate a/b = 1**

Figure 4.3-4.4 show the complete stability chart for the plate with and without damping ($\alpha$ = 0 and $\alpha$ = 50). The stability chart shows the regions of instability of first order and second order. The first five mode shapes are considered in the stability chart. The boundaries in the chart shows the simple and sum type instability regions. It is found that, for the uniform loading on opposite edges when all the edges are simply supported no combination resonance of difference type is possible. As the load on the edges increases, the width of instability region increases.

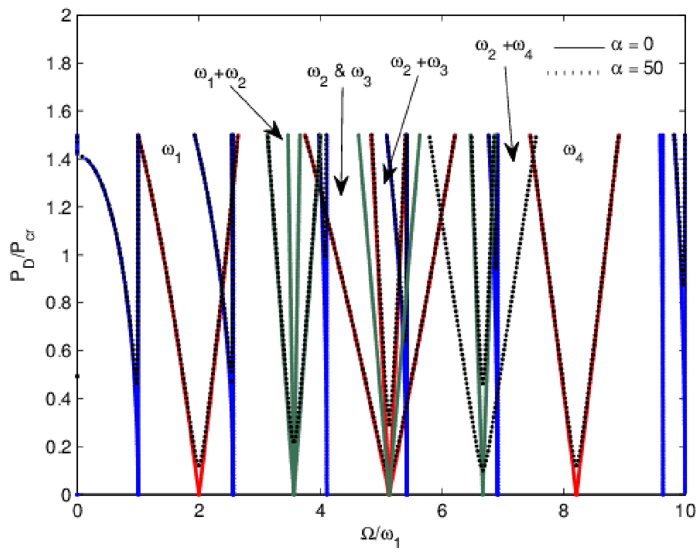


**Figure 4.3: Dynamic stability chart of simply supported plate under edge loading (*a/b*=1, $p_s$ = 0)**

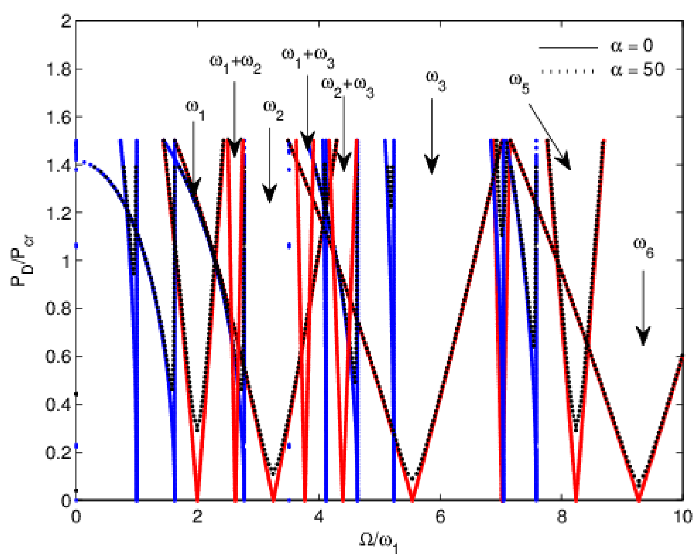


**Figure 4.4: Dynamic stability chart of simply supported plate under edge loading (*a/b*=2, $p_s$ = 0)**

It can be seen from Figures 4.3-4.4, that in the presence of damping the regions of instability gets smaller. In the presence of damping, there exists a critical dynamic load value for each instability region below which the plate cannot be dynamically unstable. The value of this dynamic load factor increase as the damping increases. The widths of combination resonance will be very small in the presence of damping. The effect of damping on the combination resonances is so high such that in few cases the combination resonance cannot occur.

### 4.5.3 Effect of static load factor on dynamic stability

Figure 4.5 shows the influence of static load on the dynamic stability of square and rectangular plate. Figure 4.5(a) shows the principal parametric instability region of square plate under different static load factor. Figure 4.5(b) shows the first three instability regions of first order without damping for three different static load factors. For square plate, as the static load $P_s$ increases, the instability region shift outwards along the frequency ratio axis and the width of instability region almost remains same. For rectangular plate, as the static load $P_s$ increases, all the instability regions shift inward along the frequency ratio axes and their width increases. This shows that as the static load increases, the rectangular plate is prone to dynamic instability.

### 4.5.4 Effect of aspect ratio on dynamic stability

From Figure 4.3 - 4.5, it can be seen that the dynamic stability behavior depends to a large extent on the plate aspect ratio. From Figure 4.3 and Figure 4.4 it is clear that for higher aspect ratio the instability regions have large width compared to less aspect ratio indicating they are more prone to dynamic instability. From Figure 4.5, it can be infered that the effect of static load factor on dynamic stability with repective to aspect ratio is also, to make the structure prone to instability. The effect of damping on simple and combination resonance characteristics is similar, irrespective of the aspect ratio of plates.

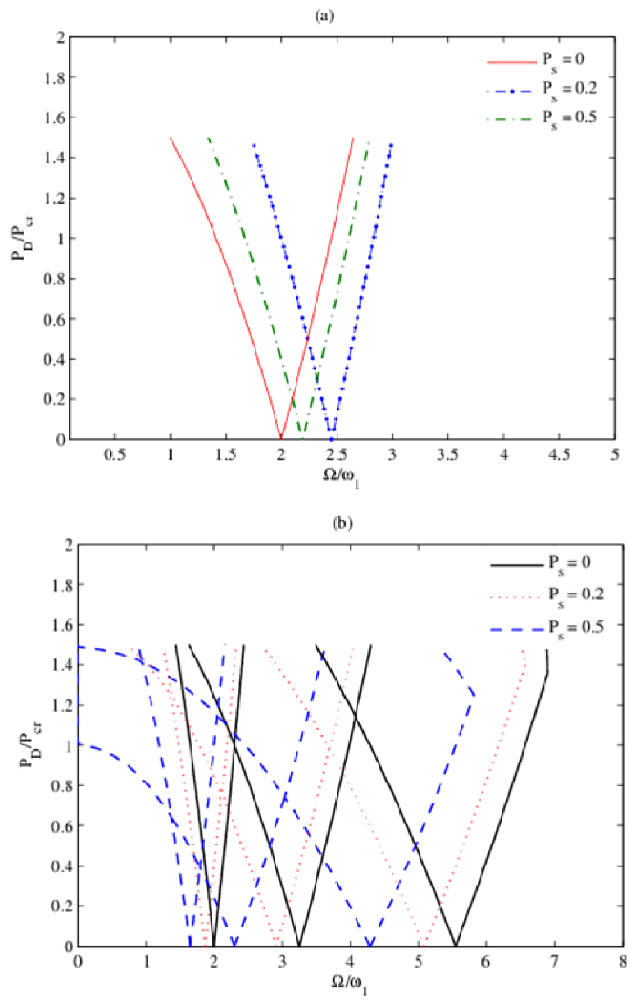


**Figure 4.5: Effect of static load factor on dynamic stability (a) a/b = 1 (b) a/b = 2**

## 4.6 Summary

The dynamic stability of simply supported thin plates under uniform edge loading is obtained using Hsu's stability criteria. The governing Mathieu-Hill equation is solved by employing finite element formulation. Mindlin plate theory is used for the formulation of global system matrices. Effects of aspect ratio, static load factor on the dynamic stability are studied. The present code developed can be used for any plate with any arbitrary boundary conditions.

# Chapter 5

# DYNAMIC STABILITY OF THIN SHELLS

## 5.1 Introduction

A shell is defined as a curved surface which develops membrane and bending stresses under external loadings. Thin-shell structures find wide applications in many branches of engineering. Examples include aircraft, space craft, cooling towers, nuclear reactors, steel silos and tanks for bulk solid and liquid storage, pressure vessels, pipelines and offshore platforms. Because of the slenderness of these structures, buckling is often the controlling failure mode. It is therefore essential that their stability behavior must be properly understood for safety and reliability. A detailed review on static buckling of thin shells can be found in [85]. The formulation of shell governing equations based on different theories can be found in [86].

If thin walled structures are subjected to pulsating excitations they may fail well before the static bifurcation load leading to dynamic instability, hence a number of studies have focused on this aspect. The dynamic stability of simply supported cylinders under periodic axial and pressure loadings has been treated by Bolotin [l4], Yao [87], and Wood and Koval [88], while that of a vertical cylinder with one end clamped and the other end free subjected to sinusoidal base motion, was studied by Vijayaraghavan and Evan-Iwanowski [89]. Nagai and Yamaki [90, 91] studied parametric oscillations in cylindrical shells using Donnell's shallow shell equations. While the reference cited above was completely based on analytical approaches, Basar [40] and Eller [92] employed finite element method for the stability analysis of shell structures under parametric excitations.

Lam [93] studied the dynamic stability of cylindrical shells under periodic axial loads using different shell theories. Paulo [94, 95] studied nonlinear oscillations under parametric excitation in cylindrical shells theoretically using Donnell shallow shell equations. Pellicano [96] studied stability of cylindrical shell connected to rigid disk.

In the present chapter the dynamic instability of thin shells under uniform periodic compressive force is investigated. Shell model is assumed to be linearly elastic, isotropic and homogenous. Finite element method is employed for dynamic stability analysis. Degenerated curved shell elements [97] are used for the formulation of finite element matrices. The next section explains in brief the formulation of degenerated shell elements.

## 5.2 Formulation of degenerated shell elements

In this section, the underlying basic ideas in the formulation of degenerated curved shell element are described in brief. Figure 5.1 shows a degenerated four-node shell element. The main assumptions made in the formulation of curved shell element degenerated from the 3D solid are,

1. Normals to the middle surface before deformation remain straight even after deformation. Same assumption is valid for thick shells as well.
2. Stress component normal to the shell mid-surface is constrained to be zero and eliminated from the constitutive equations.

Typically a nodal point of a degenerated shell element have three displacements *u, v, w* in the global directions *x, y, z* and two normal rotations $\alpha_i$ and $\beta_i$.

### 5.2.1 Element geometry

Let $\xi$, $\eta$ be the two curvilinear coordinates in the middle plane of the shell and $\zeta$ a

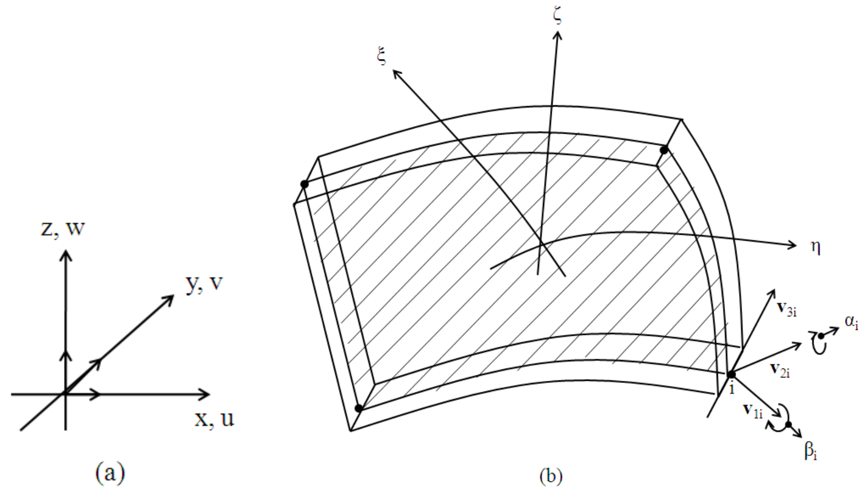


**Figure 5.1: Four node shell element (a) Global coordinate system (b) Nodal coordinate system at node *i***

linear coordinate in the thickness direction. Further $\xi$, $\eta$, $\zeta$ vary between -1 and +1 on the respective faces of the element. Global coordinates of an arbitrary point in the element can be written in terms of curvilinear coordinates in the form

$$\begin{Bmatrix} x \\ y \\ z \end{Bmatrix} = \sum N_i(\xi,\eta) \begin{Bmatrix} x_i \\ y_i \\ z_i \end{Bmatrix} + \sum N_i(\xi,\eta)\zeta \frac{t_i}{2} \mathbf{V}_{3i} \tag{5.1}$$

where $\boldsymbol{V}_{3i}$ is a vector along the thickness direction and is given by

$$\mathbf{V}_{3i} = t_i \begin{Bmatrix} l_{3i} \\ m_{3i} \\ n_{3i} \end{Bmatrix} \quad \text{where} \quad \begin{Bmatrix} l_{3i} \\ m_{3i} \\ n_{3i} \end{Bmatrix} = \frac{1}{t_i} \begin{Bmatrix} x_j - x_k \\ y_j - y_k \\ z_j - z_k \end{Bmatrix} \tag{5.2}$$

in which $l_{3i}$, $m_{3i}$ and $n_{3i}$ are the direction cosines of the midsurface normal and $t_i$ is the shell thickness at the node $i$.

Vectors $\boldsymbol{V}_{1i}$ and $\boldsymbol{V}_{2i}$ shown in Figure 5.1(b) are perpendicular to each other and to $\boldsymbol{V}_{3i}$. These vectors are used to define directions of nodal rotation degree of freedom $\alpha_i$ and $\beta_i$. Directions of $\alpha_i$ and $\beta_i$ may differ from node to node in a single element and may differ between elements at a node the elements share with each other. Before elements are assembled, each element matrices must be transformed to suit a global set of degree of freedom at structure nodes.

A vector $\boldsymbol{V_{1i}}$ can be obtained by describing it normal to both $\boldsymbol{V_{3i}}$ and the global $y$ direction by writing the cross product $\boldsymbol{V_{1i}} = \boldsymbol{j}\ X\ \boldsymbol{V_{3i}}$, where $\boldsymbol{j}$ is a unit vector in the $y$ direction. The last vector would be then $\boldsymbol{V_{2i}} = \boldsymbol{V_{3i}}\ X\ \boldsymbol{V_{1i}}$. If $\boldsymbol{j}$ and $\boldsymbol{V_{3i}}$ are parallel to each other, the above calculation fails, in that case use, $\boldsymbol{V_{2i}} = \boldsymbol{V_{3i}}\ X\ \boldsymbol{i}$ and $\boldsymbol{V_{1i}} = \boldsymbol{V_{2i}}\ X\ \boldsymbol{V_{3i}}$. We can define the matrix of direction cosine of vectors $\boldsymbol{V_{2i}}$ and $\boldsymbol{V_{3i}}$ as

$$[\mu_i] = \begin{bmatrix} -\dfrac{\mathbf{V}_{2i}}{|\mathbf{V}_{2i}|} & \dfrac{\mathbf{V}_{1i}}{|\mathbf{V}_{1i}|} \end{bmatrix} = \begin{bmatrix} -l_{2i} & l_{1i} \\ -m_{2i} & m_{1i} \\ -n_{2i} & n_{1i} \end{bmatrix} \tag{5.3}$$

**5.2.2 Displacement field**

The displacement of an arbitrary point on the midsurface of the shell element can be written as

$$\begin{Bmatrix} u \\ v \\ w \end{Bmatrix} = \sum N_i \begin{Bmatrix} u_i \\ v_i \\ w_i \end{Bmatrix} + \sum N_i \zeta \frac{t_i}{2} [\mu_i] \begin{Bmatrix} \alpha_i \\ \beta_i \end{Bmatrix} \tag{5.4}$$

**5.2.3 Strain-displacement relation**

In order to make the shell assumption of zero normal stress on the surface $\zeta$ = constant to obey, the strain components should be defined in terms of local system of axes. Thus, at any point on this surface a normal $z'$ is erected and two other orthogonal axes $x'$ and $y'$ tangent to it are considered, the significant strain components of interest are given by

$$\varepsilon' = \left\{ \varepsilon_{x'} \quad \varepsilon_{y'} \quad \gamma_{x'y'} \quad \gamma_{x'z'} \quad \gamma_{y'z'} \right\}^T = \left\{ \frac{\partial u'}{\partial x'} \quad \frac{\partial v'}{\partial y'} \quad \frac{\partial u'}{\partial y'} + \frac{\partial v'}{\partial x'} \quad \frac{\partial w'}{\partial x'} + \frac{\partial u'}{\partial z'} \quad \frac{\partial w'}{\partial y'} + \frac{\partial v'}{\partial z'} \right\}^T \tag{5.5}$$

where *u', v'* and *w'* are the displacement components in the local direction axes *x', y'* and *z'* respectively. These local derivatives are obtained from the global derivatives of the displacements *u, v* and *w*. The stress components corresponding to these strain components are defined as follows

$$\begin{aligned}\sigma' &= \begin{bmatrix}\sigma_{x'} & \sigma_{y'} & \tau_{x'y'} & \tau_{x'z'} & \tau_{y'z'}\end{bmatrix}^T \\ &= D'\varepsilon' = D'\left[B\right]\left\{d\right\}\end{aligned} \tag{5.6}$$

where *D'* is the constitute matrix of size 5×5, given by

$$D' = \frac{E}{1-\nu^2}\begin{bmatrix} 1 & \nu & 0 & 0 & 0 \\ \nu & 1 & 0 & 0 & 0 \\ 0 & 0 & \frac{1-\nu}{2} & 0 & 0 \\ 0 & 0 & 0 & \frac{(1-\nu)\alpha}{2} & 0 \\ 0 & 0 & 0 & 0 & \frac{(1-\nu)\alpha}{2} \end{bmatrix} \tag{5.7}$$

in which *E* and *v* are Young's modulus and Poisson's ratio respectively. The factor *α* included in the last two shear terms is taken as 5/6 and its purpose is to improve the shear displacement approximation.

And $$\left[B\right] = \left[B_1 \quad B_2 \quad B_3 \quad B_4\right] \tag{5.8}$$

$$\left\{d\right\} = \left\{d_1 \quad d_2 \quad d_3 \quad d_4\right\}^T \tag{5.9}$$

Where the vector $\{d_i\}$ of degrees of freedom is defined as

$$\left\{d_i\right\} = \left\{u_i \quad v_i \quad w_i \quad \alpha_i \quad \beta_i\right\} \tag{5.10}$$

And the strain displacement matrix *B* is given by

$$
\left[B_i\right]=\begin{bmatrix}
\frac{\partial N_i}{\partial x'} & 0 & 0 & -0.5\zeta t_i \frac{\partial N_i}{\partial x'} l_{2i} & 0.5\zeta t_i \frac{\partial N_i}{\partial x'} l_{1i} \\
0 & \frac{\partial N_i}{\partial y'} & 0 & -0.5\zeta t_i \frac{\partial N_i}{\partial y'} m_{2i} & 0.5\zeta t_i \frac{\partial N_i}{\partial y'} m_{1i} \\
0 & 0 & \frac{\partial N_i}{\partial z'} & -0.5\zeta t_i \frac{\partial N_i}{\partial z'} n_{2i} & 0.5\zeta t_i \frac{\partial N_i}{\partial z'} n_{2i} \\
\frac{\partial N_i}{\partial y'} & \frac{\partial N_i}{\partial x'} & 0 & -0.5\zeta t_i \left(\frac{\partial N_i}{\partial y'} l_{2i} + \frac{\partial N_i}{\partial x'} m_{2i}\right) & 0.5\zeta t_i \left(\frac{\partial N_i}{\partial y'} l_{1i} + \frac{\partial N_i}{\partial x'} m_{1i}\right) \\
0 & \frac{\partial N_i}{\partial z'} & \frac{\partial N_i}{\partial y'} & -0.5\zeta t \left(\frac{\partial N_i}{\partial z'} m_{2i} + \frac{\partial N_i}{\partial y'} n_{2i}\right) & 0.5\zeta t_i \left(\frac{\partial N_i}{\partial z'} m_{1i} + \frac{\partial N_i}{\partial y'} n_{1i}\right) \\
\frac{\partial N_i}{\partial z'} & 0 & \frac{\partial N_i}{\partial x'} & -0.5\zeta t \left(\frac{\partial N_i}{\partial x'} n_{2i} + \frac{\partial N_i}{\partial z'} l_{2i}\right) & 0.5\zeta t_i \left(\frac{\partial N_i}{\partial x'} n_{1i} + \frac{\partial N_i}{\partial z'} l_{1i}\right)
\end{bmatrix}
$$

(5.11)

### 5.2.4 Jacobian matrix

The [*B*] matrix is defined in terms of the displacement derivatives with respect to local Cartesian coordinates (*x', y', z'*). It is required to follow two sets of transformations before the element matrices are assembled with respect to the curvilinear coordinates ($\xi$, $\eta$, $\zeta$).

First, the derivatives with respect to the global (*x, y, z*) directions are obtained by using the matrix relation

$$
\begin{bmatrix}
\frac{\partial u}{\partial x} & \frac{\partial v}{\partial x} & \frac{\partial w}{\partial x} \\
\frac{\partial u}{\partial y} & \frac{\partial v}{\partial y} & \frac{\partial w}{\partial y} \\
\frac{\partial u}{\partial z} & \frac{\partial v}{\partial z} & \frac{\partial w}{\partial z}
\end{bmatrix}
=\left[J\right]^{-1}
\begin{bmatrix}
\frac{\partial u}{\partial \xi} & \frac{\partial v}{\partial \xi} & \frac{\partial w}{\partial \xi} \\
\frac{\partial u}{\partial \eta} & \frac{\partial v}{\partial \eta} & \frac{\partial w}{\partial \eta} \\
\frac{\partial u}{\partial \zeta} & \frac{\partial v}{\partial \zeta} & \frac{\partial w}{\partial \zeta}
\end{bmatrix}
\tag{5.12}
$$

where [*J*] is the Jacobian matrix and given by,

$$J = \begin{bmatrix} \frac{\partial x}{\partial \xi} & \frac{\partial y}{\partial \xi} & \frac{\partial z}{\partial \xi} \\ \frac{\partial x}{\partial \eta} & \frac{\partial y}{\partial \eta} & \frac{\partial z}{\partial \eta} \\ \frac{\partial x}{\partial \zeta} & \frac{\partial y}{\partial \zeta} & \frac{\partial z}{\partial \zeta} \end{bmatrix} \tag{5.13}$$

The derivatives $\frac{\partial u}{\partial \xi}, \frac{\partial v}{\partial \eta}, \ldots$ etc are obtained using Eq. (5.4)

Second, after establishing the direction cosines [$T_{dc}$] of local axes, the global derivatives of displacement *u, v,* and *w* are transformed to the local derivatives of the local orthogonal displacements by the transformation

$$\begin{bmatrix} \frac{\partial u'}{\partial x'} & \frac{\partial v'}{\partial x'} & \frac{\partial w'}{\partial x'} \\ \frac{\partial u'}{\partial y'} & \frac{\partial v}{\partial y'} & \frac{\partial w}{\partial y'} \\ \frac{\partial u'}{\partial z'} & \frac{\partial v'}{\partial z'} & \frac{\partial w'}{\partial z'} \end{bmatrix} = \left[T_{dc}\right]^T \begin{bmatrix} \frac{\partial u}{\partial x} & \frac{\partial v}{\partial x} & \frac{\partial w}{\partial x} \\ \frac{\partial u}{\partial y} & \frac{\partial v}{\partial y} & \frac{\partial w}{\partial y} \\ \frac{\partial u}{\partial z} & \frac{\partial v}{\partial z} & \frac{\partial w}{\partial z} \end{bmatrix} \left[T_{dc}\right] \tag{5.14}$$

The direction cosines needed in [$T_{dc}$] are the direction cosines of the vectors $\boldsymbol{V_1}$, $\boldsymbol{V_2}$ and $\boldsymbol{V_3}$.

### 5.2.5 Element stiffness matrix

The element stiffness matrix for a four noded isoparametric element is given by

$$\left[K^e\right]_{20X20} = \int_{-1}^{1}\int_{-1}^{1}\int_{-1}^{1} \left[B\right]^T_{20X6} \left[D\right]_{6X6} \left[B\right]_{6X20} \left|J\right| d\xi d\eta d\zeta \tag{5.15}$$

### 5.2.6 Element mass matrix

The element mass matrix for the four noded isoparametric element is given by

$$\left[M^e\right]_{20X20} = \int_{-1}^{1}\int_{-1}^{1}\int_{-1}^{1}\left[N\right]^T{}_{20X5}\,\rho\left[N\right]_{5X20}\left|J\right| d\xi d\eta d\zeta \tag{5.16}$$

where $\rho$ is the density of the material.

### 5.2.7 Element geometric stiffness matrix

The geometric stiffness matrix is defined based on the constant terms of Cauchy stresses as,

$$\left[K_G^e\right] = \int_{-1}^{1}\int_{-1}^{1}\int_{-1}^{1}\left[B_{NL}\right]^T{}_{20X9}\left[\hat{\sigma}_0\right]_{9X9}\left[B_{NL}\right]_{9X20}\left|J\right| d\xi d\eta d\zeta \tag{5.17}$$

where $$\left[B_{NL}\right] = \left[B_{NL}^1 \quad B_{NL}^2 \quad B_{NL}^3 \quad B_{NL}^4\right] \tag{5.18}$$

and matrix $[B^i_{NL}]$ is formed as shown below

$$\left[B_{NL}^i\right] = \begin{bmatrix}
\frac{\partial N_i}{\partial x'} & 0 & 0 & -0.5t_il_{2i}\left(\zeta\frac{\partial N_i}{\partial x'}+\frac{\partial \zeta}{\partial x}N_i\right) & -0.5t_il_{1i}\left(\zeta\frac{\partial N_i}{\partial x'}+\frac{\partial \zeta}{\partial x}N_i\right) \\
\frac{\partial N_i}{\partial y'} & 0 & 0 & -0.5t_il_{2i}\left(\zeta\frac{\partial N_i}{\partial y'}+\frac{\partial \zeta}{\partial y}N_i\right) & -0.5t_il_{1i}\left(\zeta\frac{\partial N_i}{\partial y'}+\frac{\partial \zeta}{\partial y}N_i\right) \\
\frac{\partial N_i}{\partial z'} & 0 & 0 & -0.5t_il_{2i}\left(\zeta\frac{\partial N_i}{\partial z'}+\frac{\partial \zeta}{\partial z}N_i\right) & -0.5t_il_{1i}\left(\zeta\frac{\partial N_i}{\partial z'}+\frac{\partial \zeta}{\partial z}N_i\right) \\
0 & \frac{\partial N_i}{\partial x'} & 0 & -0.5t_im_{2i}\left(\zeta\frac{\partial N_i}{\partial x'}+\frac{\partial \zeta}{\partial x}N_i\right) & -0.5t_im_{1i}\left(\zeta\frac{\partial N_i}{\partial x'}+\frac{\partial \zeta}{\partial x}N_i\right) \\
0 & \frac{\partial N_i}{\partial y'} & 0 & -0.5t_im_{2i}\left(\zeta\frac{\partial N_i}{\partial y'}+\frac{\partial \zeta}{\partial y}N_i\right) & -0.5t_im_{1i}\left(\zeta\frac{\partial N_i}{\partial y'}+\frac{\partial \zeta}{\partial y}N_i\right) \\
0 & \frac{\partial N_i}{\partial z'} & 0 & -0.5t_im_{2i}\left(\zeta\frac{\partial N_i}{\partial z'}+\frac{\partial \zeta}{\partial z}N_i\right) & -0.5t_im_{1i}\left(\zeta\frac{\partial N_i}{\partial z'}+\frac{\partial \zeta}{\partial z}N_i\right) \\
0 & 0 & \frac{\partial N_i}{\partial x'} & -0.5t_in_{2i}\left(\zeta\frac{\partial N_i}{\partial x'}+\frac{\partial \zeta}{\partial x}N_i\right) & -0.5t_in_{1i}\left(\zeta\frac{\partial N_i}{\partial x'}+\frac{\partial \zeta}{\partial x}N_i\right) \\
0 & 0 & \frac{\partial N_i}{\partial y'} & -0.5t_in_{2i}\left(\zeta\frac{\partial N_i}{\partial y'}+\frac{\partial \zeta}{\partial y}N_i\right) & -0.5t_in_{1i}\left(\zeta\frac{\partial N_i}{\partial y'}+\frac{\partial \zeta}{\partial y}N_i\right) \\
0 & 0 & \frac{\partial N_i}{\partial z'} & -0.5t_in_{2i}\left(\zeta\frac{\partial N_i}{\partial z'}+\frac{\partial \zeta}{\partial z}N_i\right) & -0.5t_in_{1i}\left(\zeta\frac{\partial N_i}{\partial z'}+\frac{\partial \zeta}{\partial z}N_i\right)
\end{bmatrix} \tag{5.19}$$

The Cauchy stress tensor $\left[\hat{\sigma}_0\right]$ is defined as follows

$$\left[\hat{\sigma}_0\right]=\begin{bmatrix}\hat{S}_0 & 0 & 0\\ 0 & \hat{S}_0 & 0\\ 0 & 0 & \hat{S}_0\end{bmatrix} \tag{5.20}$$

with the components

$$\hat{S}_0=\begin{bmatrix}\hat{\sigma}^0_{xx} & \hat{\sigma}^0_{xy} & \hat{\sigma}^0_{xz}\\ \hat{\sigma}^0_{yx} & \hat{\sigma}^0_{yy} & \hat{\sigma}^0_{yz}\\ \hat{\sigma}^0_{zx} & \hat{\sigma}^0_{zy} & 0\end{bmatrix} \tag{5.21}$$

The stiffness, mass and geometric stiffness matrices given by Eq. (5.15), Eq. (5.16) and Eq. (5.17) respectively are computed by numerical integration employing Gaussian integration. Like plate element, thin shell also has shear locking problem, to reduce this problem reduced integration technique is carried out.

## 5.3 Governing equation for stability

Application of finite elements to a thin shell under parametric loading yields the following equilibrium equation

$$M\ddot{q}+C\dot{q}+\left(K+P\left(t\right)K_G\right)q=0 \tag{5.22}$$

where *M, C, K* and $K_G$ are the global assembled mass, damping, elastic stiffness and geometric stiffness matrices respectively. All these matrices are square symmetric matrices of order *N*, the number of degrees of freedom of the system and *q* is the nodal displacement column vector of order *N*. For the dynamic stability analysis a thin cylindrical shell under axial periodic compressive force *p(t)* is considered. A perfect thin-walled circular cylindrical shell of radius *R*, length *L* and thickness *t* made of an elastic, homogenous and isotropic material with Young's modulus *E*, Poisson ratio *v* and mass per unit area *ρ* is considered for stability analysis. The cylindrical shell is clamped at the bottom and at the top surface a uniform periodic compressive force is applied as shown in Figure 5.2. The matrices $M$, $K$ are obtained by finite element formulation as derived in the previous section and $C$ is obtained from the mass matrix by multiplying the mass matrix with proportionality constant. To calculate $K_G$ initially, plane stress analysis under the uniform compressive edge loading is carried out to obtain initial stress distribution and from these initial stress distribution $K_G$ matrix is evaluated.

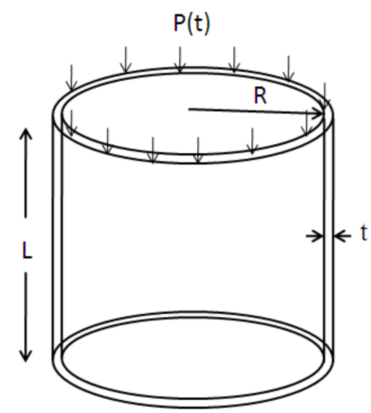


**Figure 5.2: Cylindrical shell under uniform periodic compressive force**

## 5.4 Free vibration of cylindrical shell

The natural frequencies and free vibrational modes of a circular cylindrical shell can be obtained by solving the eigenvalue problem

$$\left[K - \omega^2 M\right]\phi = 0 \tag{5.23}$$

where $\omega$ is the natural frequency of vibration and Ø gives the normal modes of vibration of the shell. The vibrational modes of a circular cylindrical shell can be classified as the cos $\theta$-type modes for which there is a single cosine wave of deflection in the circumferential direction, and as the cos $n\theta$ -type modes for which the deflection of the shell involves a number of circumferential waves higher than 1. These circumferential cos $n\theta$-type modes can be further denoted as beam-type modes because the shell behaves like a vertical cantilever beam across the length. Figure 5.3 shows the vertical nodal patterns and circumferential modes for a circular cylindrical shell.

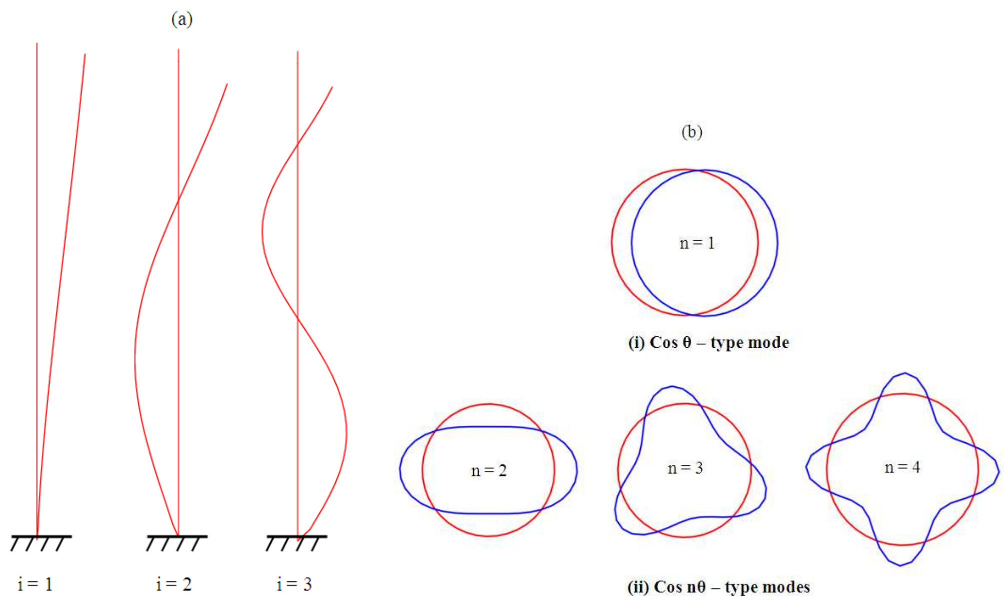


**Figure 5.3: Circular cylindrical shell vibrational modes (a) Vertical nodal patterns (b) Circumferential nodal patterns**

## 5.5 Dynamic stability of cylindrical shell

Using the modal transformation Eq. (5.22) can be transformed into the following form [31]

$$\ddot{\xi}_{in} + 2\eta_{in}\omega_{in}\dot{\xi}_{in} + \omega_{in}^{2}\xi_{in} + \varepsilon\cos\Omega t\sum_{n=1}^{N} d_{ijmn}\xi_{in} = 0 \qquad (5.24)$$

where $\varepsilon$ is a small parameter, *i, j* corresponds to frequency number of beam type and *m, n* corresponds to circumferential mode number. The stability of Eq. (5.24) can be carried out using Hsu's stability criteria as given in section 4.5 of chapter 4. Two different cylindrical tanks i.e. a tall tank and a broad tank are taken for dynamic stability studies. The geometrical data for the tall and broad cylindrical shells used for the analysis are given in Table 3.1.

**Table 5.1: Geometric and material data of the cylindrical shells**

| | Shell data | Tall shell | Broad shell |
|---|---|---|---|
| $R$ | Radius | 7.32 m | 18.130 m |
| $L$ | Length | 21.96 m | 12.20 m |
| $t$ | Thickness | 0.0254 m | 0.0254 m |
| $E$ | Young's modulus | 206.7 GPa | 206.7 GPa |
| $v$ | Poisson ratio | 0.3 | 0.3 |
| $\rho$ | Shell mass density | $7.84\times10^3$ Kg/m$^3$ | $7.84\times10^3$ Kg/m$^3$ |

A program is written to obtain the required matrices of shells. Shell is discretized with isoparametric four noded elements. Elements elastic stiffness, geometric stiffness and mass matrices are obtained using Gaussian reduced integration and these elements are assembled into global matrices. After obtaining the global matrices, the appropriate boundary conditions are applied. A free vibration problem is solved and the global matrices are converted into the form given in Eq. (5.24) using the modal transformations and then stability chart is plotted using Hsu's criteria given in Eq. (4.56 – 4.58).

### 5.5.1 Dynamic stability of tall and broad cylindrical shell

Table 5.2 shows the first ten cos $n\theta$-type modes of first and second beam mode frequencies obtained for tall and broad shell. Figure 5.4 shows the mode shapes for the frequencies given in Table 5.2 for a tall tank. Figure 5.5 and Figure 5.6 shows the stability chart of tall and broad circular cylindrical shells obtained using Hsu's conditions respectively. The stability chart is limited to 30 Hz along the frequency axis. The stability charts have regions of simple resonance and combination resonance of sum type. A damping parameter of 0.01 is considered for all the modes for both the shells. To plot the stability charts first ten cos $n\theta$-type

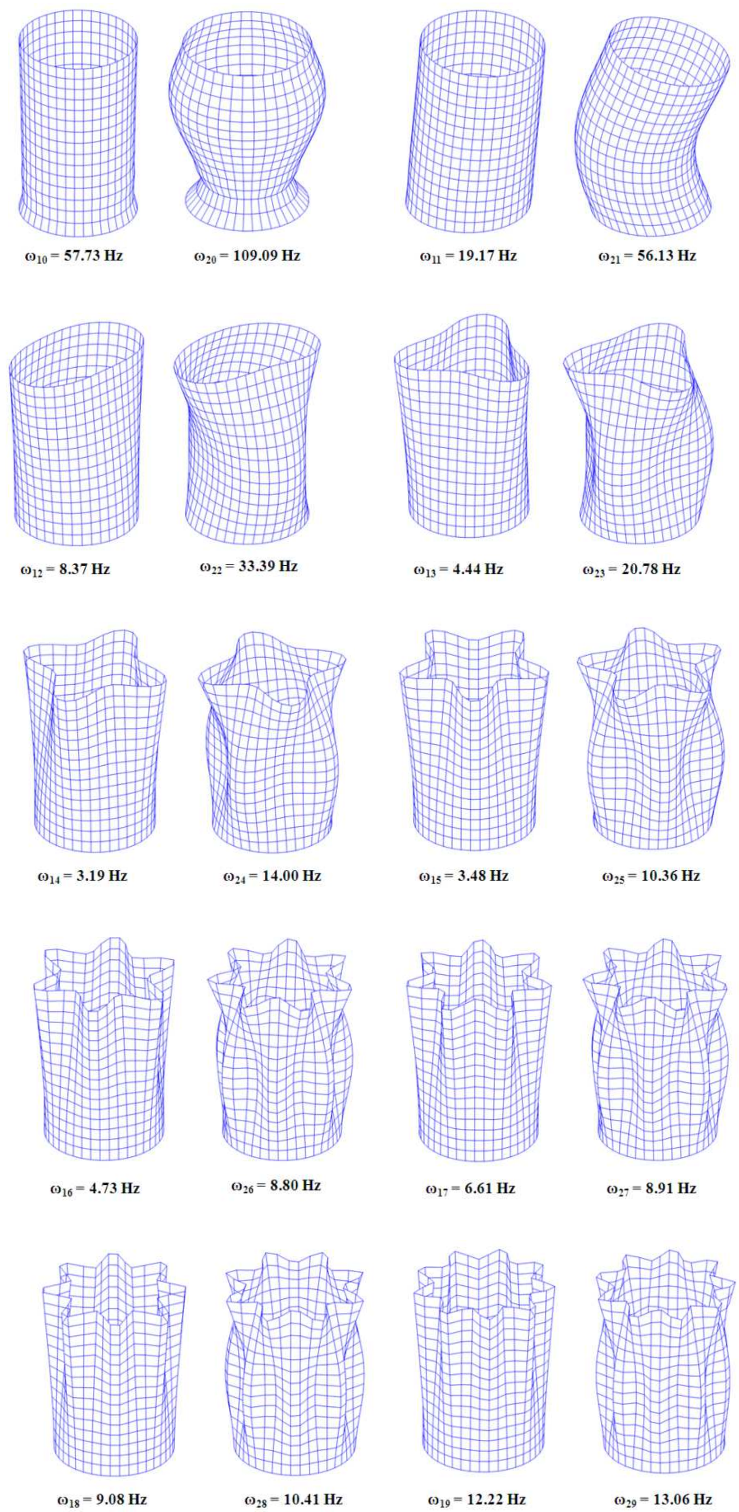


**Figure 5.4: Mode shapes of tall tank**

modes of first and second beam mode are taken. Three types of resonance regions are observed. Simple resonance regions for each first two axial modes of cos $n\theta$-type modes and combination resonance of sum type between the first two axial modes of respective cos $n\theta$-type modes. It can be observed from the stability charts that tall shell is more prone to dynamic buckling under compressive force because there are many instable regions compared to broad shell and the instability regions are wider compared to instability regions of broad shell. Combination resonance regions of difference types are not observed in this case.

**Table 5.2: Natural frequencies of tall and broad shell**

| | Tall shell Frequency (Hz) axial mode | | broad shell Frequency (Hz) axial mode | |
|---|---|---|---|---|
| | $i = 1$ | $i = 2$ | $i = 1$ | $i = 2$ |
| n | $\omega_{1n}$ | $\omega_{2n}$ | $\omega_{1n}$ | $\omega_{2n}$ |
| 0 | 57.73 | 109.09 | 44.67 | 44.36 |
| 1 | 19.17 | 56.13 | 34.02 | 43.84 |
| 2 | 8.37 | 33.39 | 23.52 | 41.46 |
| 3 | 4.44 | 20.78 | 16.74 | 37.42 |
| 4 | 3.19 | 14.00 | 12.33 | 32.62 |
| 5 | 3.48 | 10.36 | 9.37 | 28.01 |
| 6 | 4.73 | 8.80 | 7.32 | 24.04 |
| 7 | 6.61 | 8.91 | 5.90 | 18.15 |
| 8 | 9.08 | 10.41 | 4.91 | 18.15 |
| 9 | 12.22 | 13.06 | 4.26 | 16.04 |
| 10 | 12.35 | 21.29 | 3.91 | 12.99 |

## 5.6 Summary

The dynamic stability of bottom clamped cylindrical shells under uniform periodic compressive force is obtained using Hsu's stability criteria. The governing Mathieu-Hill equation is obtained by employing finite element formulation. 3D degenerated four noded shell elements are used for the formulation of global system matrices. For the considered tall tank and broad tank, it was found that tall shell is more prone to dynamic instability compared to broad shell.

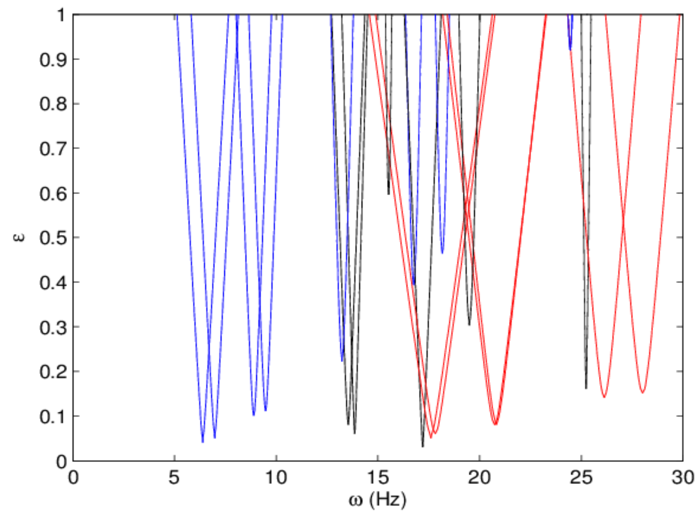


**Figure 5.5: Stability chart of a tall shell under axial periodic compressive force**

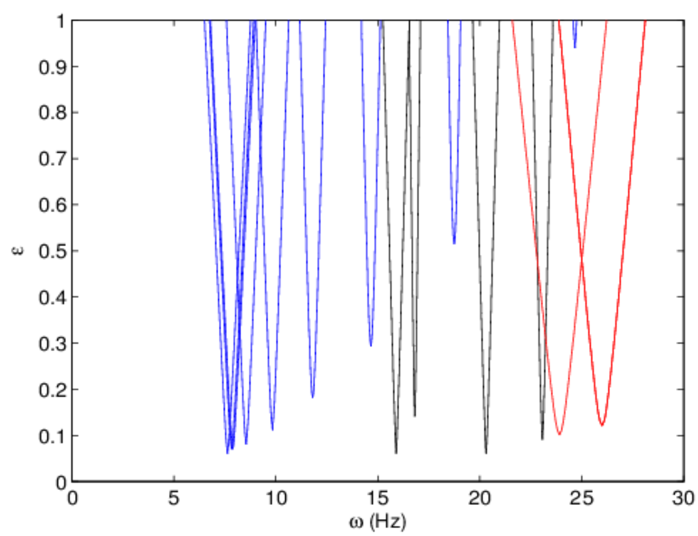


**Figure 5.6: Stability chart of a broad shell under periodic axial compressive force**

# Chapter 6

# DYNAMIC STABILITY OF PLANE FREE-SURFACE OF LIQUID

## 6.1 Introduction

The motion of an unrestrained free surface of the liquid, due to external excitation in the liquid filled container is known as sloshing. Sloshing is likely to be seen in liquid free surface experiencing disturbances in the presence of gravity. At equilibrium, the free surface of the liquid is static, when the container is perturbed; an oscillation is set up in the free surface. The phenomenon of liquid sloshing occurs in a variety of engineering applications such as sloshing in liquid propellant launch vehicles, liquid oscillation in large storage tanks by earthquake, sloshing in the pool type nuclear reactors, nuclear fuel storage tanks under earthquake and the water flow on the deck of ship. Such liquid motion is potentially dangerous problem to engineering structures and environment leading to failure of engineering structures and unexpected instability. Thus, understanding the dynamic behaviour of liquid free surface is essential. As a result the problem of sloshing has attracted many researchers and engineers motivating to understand the complex behaviour of sloshing and to design the structures to withstand its effects.

Liquid sloshing can be stimulated by a variety of container excitations. The container excitation can be horizontal, vertical or rotational. Under horizontal excitations the liquid free surface experiences normal sloshing; the sloshing frequency will be equal to excitation frequency. When the external excitation frequency is equal to fundamental slosh frequency, the free surface undergoes resonance. Extensive research has been done on sloshing response under pure horizontal excitations. When the liquid filled container is subjected to vertical excitations, for some combinations of amplitude and frequency of the external excitation the free surface undergoes unbounded motion leading to parametric instability and for few other combinations the free surface shows a bounded response.

Abundant research is available on sloshing under horizontal and the literature is vast with wide varieties of numerical methods, analytical solutions and experiments. The linear theory of sloshing and its applications concerned to aerospace were discussed extensively by Abramson [98]. Abramson covered the aspects of sloshing in various shaped containers both analytically and experimentally. A wide variety of analytical and numerical solutions are available in the literature for linear slosh dynamics in rigid and elastic containers namely Haroun [99], Aslam [100], Mitra et al. [101], Morand and Ohayon [102], Miles [103], Abramson [104], Bauer [105], Zienkiewicz and Bettes [106], Liu and David [107], Muller [108], Cho et al. [109]. Similar to vast literature on sloshing in linear domain, there are equally numerous references on sloshing in non-linear domain namely Flatinsen [110, 111], Nakayama and Washizu [112], Ortiz and Barhorst [113], Wu and Taylor [114 – 116], Chen et al. [117], Turnbull et al. [118], Frandsen [119], Cho et al. [120], Wang and Khoo [121], Sriram et al. [122], Biswal et al. [123], Kanok-Nukulchai [124]. Ibrahim et al. [125] gives an excellent review of sloshing phenomenon with extensive number of references available in literature.

In all the references cited above except Wu et al. [116] and Frandsen [119] the concentration was on sloshing under pure horizontal excitation. Fluid free-surface undergoes parametric resonance under vertical excitations which is important for study of ship motion and for dynamic stability of fluid in fluid-filled shells. The problem of liquid response under vertical excitations was first studied experimentally by Faraday [1], reporting that the frequency of the liquid vibrations on free surface is half of the external excitation frequency. The sloshing waves generated under vertical excitation are sometimes referred as Faraday waves. Rayleigh [5, 6] analyzed the Faradays study and confirmed Faraday's observations. Matthiessen [4] conducted experiments and reported that the fluid free surface vibrations are synchronous to the external excitation. The discrepancy between Faraday's observations and Matthiessen's observations were explained mathematically by Benjamin and Ursell [7]. Benjamin and Ursell [5] investigated the stability of fluid under vertical excitations theoretically. They considered linearized inviscid potential flow model with surface tension. They concluded that the response of the plane free surface of fluid under vertical excitation is governed by Mathieu equation. The solution of Mathieu equation [8] may be stable, periodic or unstable depending on the system parameters. The problem of sloshing under vertical excitation in various geometric shapes of the container has been studied by various researchers. For example, Dodge [126], Miles [127] have studied the liquid surface oscillations under vertical excitation in cylindrical tanks. Khandelwal [128] have studied the parametric instability in rectangular tanks. The problem of parametric oscillations in liquid free surface was also discussed by Miles and Henderson [129], in their review paper and by Perlin and Schultz [130] and Jiang et al. [131]. Frandsen [119, 132] analyzed the problem numerically and theoretically, considering fully non linear inviscid potential flow equations. Wu [116] applied finite element method for solving sloshing 2D and 3D sloshing problems. Wu discussed the sloshing response under vertical excitations in rectangular tanks. De-

Zhi Ning [133] applied boundary element method to study the liquid sloshing in rectangular containers under coupled horizontal and vertical excitation.

In the present paper the sloshing response under vertical excitations in liquid filled tanks is taken up. First, the stability of plane free surface of liquid in tanks is obtained from the linearized equations and the sloshing response of fluid is numerically simulated for various frequencies and amplitude of the external excitation, using finite element method under pure vertical excitations. Then the numerical work is extended to explore the sloshing behaviour of tanks under coupled horizontal and vertical excitations.

## 6.2 Governing equations

Consider a rectangular tank fixed in Cartesian coordinate system *Oxz*, which is moving with respective to inertial Cartesian coordinate system $O_0x_0z_0$. The origins of this system are at the left end of the tank wall at the free surface and pointing upwards in *z* direction. These two Cartesian systems coincide when the tank is at rest. Figure 6.1 shows the tank in the moving Cartesian coordinate system *Oxz* along with the prescribed boundary conditions. Let the displacements of the tank be governed by the directions of axes as,

$$X = \left[ x_t\left(t\right), z_t\left(t\right) \right] \tag{6.1}$$

Fluid is assumed to be inviscid, incompressible and irrotational. Therefore the fluid motion is governed by Laplace's equation with the unknown as velocity potential $\phi$,

$$\nabla^2 \phi = 0 \tag{6.2}$$

The fluid obeys Neumann boundary conditions at the walls of the container and Dirichlet boundary condition at the liquid free surface. In the moving coordinate

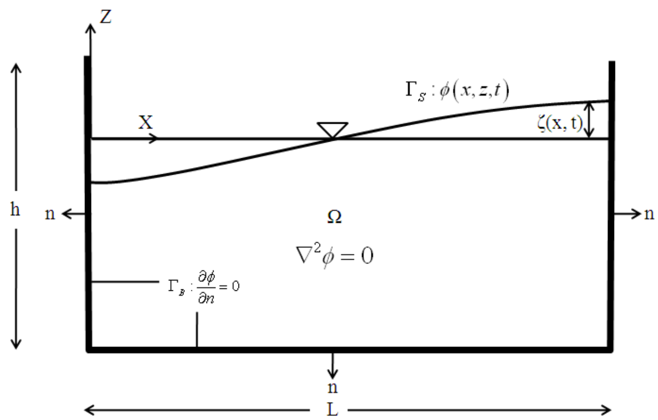


**Figure 6.1: Sloshing wave tank in moving coordinate system**

system the velocity component of the fluid normal to the walls is zero. Hence, on the bottom and on the walls of the tank ($\Gamma_B$) we have,

$$\left.\frac{\partial \phi}{\partial n}\right|_{x=0,L} = 0; \left.\frac{\partial \phi}{\partial n}\right|_{z=-h} = 0 \tag{6.3}$$

On the free surface ($\Gamma_s$) dynamic and kinematic conditions hold, they are given as,

$$\left.\frac{\partial \phi}{\partial t}\right|_{z=\zeta} + \frac{1}{2}\nabla\phi.\nabla\phi + \left(g + z_t''\right)\zeta + x x_t'' = 0 \tag{6.4}$$

$$\frac{\partial \zeta}{\partial t} + \frac{\partial \phi}{\partial x}\frac{\partial \zeta}{\partial x} - \frac{\partial \phi}{\partial z} = 0 \tag{6.5}$$

Where $\zeta$ is the free surface elevation measured vertically above still water level, $x_t''$ and $z_t''$ are the horizontal and vertical accelerations of the tank, and $g$ is the acceleration due to gravity.

Equations (6.1) - (6.5) give the complete behaviour of non-linear sloshing in fluids under base excitation of the tank. The position of the fluid free surface is not known a priori, to solve the problem, the fluid is assumed to be at rest with some initial perturbation on the free surface. Thus the initial conditions for the free surface in the moving Cartesian system at $t = 0$ and $z = 0$ can be written as,

$$\phi(x,0,0) = -x\frac{dx_t}{dt} - z\frac{dz_t}{dt} \tag{6.6}$$

$$\zeta(x,0) = 0 \quad \text{for horizontal excitation} \tag{6.7}$$

$$\zeta(x,0) = \zeta_0 \text{ for vertical excitation} \tag{6.8}$$

Where $\zeta_0$ is the initial elevation of the free surface. It should be noted that it is not possible to attain the initial boundary condition Eq. (6.8) maintaining Eq. (6.6), in real, it is a non-physical condition. This condition is used in case of vertical excitations alone, because in this excitation some initial perturbation is needed without which there won't be any oscillation in the liquid free surface.

## 6.3 Governing equation for dynamic stability of free -surface

In this section the governing equation for dynamic stability of free-surface of liquid under vertical excitation is derived. The general solution for Laplace equation in the rectangular domain satisfying the given rigid boundary conditions can be written as

$$\phi = \sum_{n=0}^{\infty} \frac{\cosh\left(k_n\left(z+h\right)\right)}{\cosh\left(k_n h\right)} \cos\left(k_n x\right) F_n\left(t\right) \tag{6.9}$$

$$\zeta = \sum_{n=0}^{\infty} \cos\left(k_n x\right) z_n\left(t\right) \tag{6.10}$$

where $k_n = n\pi/L$ is the wave number for mode number $n$. $F_n(t)$, $Z_n(t)$ are the time evolution functions of the respective $n^{\text{th}}$ mode and can be calculated by substituting the general solution Eq. (6.9) and Eq. (6.10) in the linear free-surface boundary conditions obtained from Eq. (6.4) and Eq. (6.5). The linearized free-surface boundary conditions are

$$\left.\frac{\partial\phi}{\partial t}\right|_{z=\zeta} + \left(g + z_t''\right)\zeta = 0 \tag{6.11}$$

$$\frac{\partial \zeta}{\partial t} - \frac{\partial \phi}{\partial z} = 0 \tag{6.12}$$

On substituting Eq. (6.9) and Eq. (6.10) in Eq. (6.11), Eq. (6.12) leads to

$$\frac{dF_n(t)}{dt} + \left(g + z_t''\right) z_n(t) = 0 \tag{6.13}$$

$$\frac{dz_n(t)}{dt} - k_n \tanh\left(k_n h\right) F_n(t) = 0 \tag{6.14}$$

On substituting Eq. (6.13) in Eq. (6.14) and arranging terms gives

$$\frac{d^2 z_n(t)}{dt^2} + \omega_n^2 \left(1 + \frac{z_t''}{g}\right) z_n(t) = 0 \tag{6.15}$$

where

$$\omega_n = \sqrt{g k_n \tanh\left(k_n h\right)} \tag{6.16}$$

Eq. (6.16) gives the linear slosh frequencies. If the tank is assumed to be subjected to harmonic vertical excitation alone given by

$$z_t(t) = a_v \cos\left(\omega_v t\right) \tag{6.17}$$

Eq. (6.15) reduces to

$$\frac{d^2 z_n(T)}{dT^2} + \Omega_n^2 \left(1 - k_v \cos\left(2T\right)\right) z_n(T) = 0 \tag{6.18}$$

where $T = ½\ \omega_v t$, $\Omega_n = \omega_n/\omega_v$ and $k_v = a_v \omega_v^2/g$. Eq. (6.18) is a Mathieu's equation. The stability and instability of the free-surface is guided by Eq. (6.18).

## 6.4 Dynamic stability chart for free-surface of liquid

Stability chart of Mathieu equation Eq. (6.18) is plotted using harmonic balance method [14, 22] and following the Bolotin's method as discussed in Chapter 1. The Hills determinants obtained are discussed in Appendix-B. The stability chart obtained for dynamic stability of liquid free-surface is as shown in Figure 6.2.

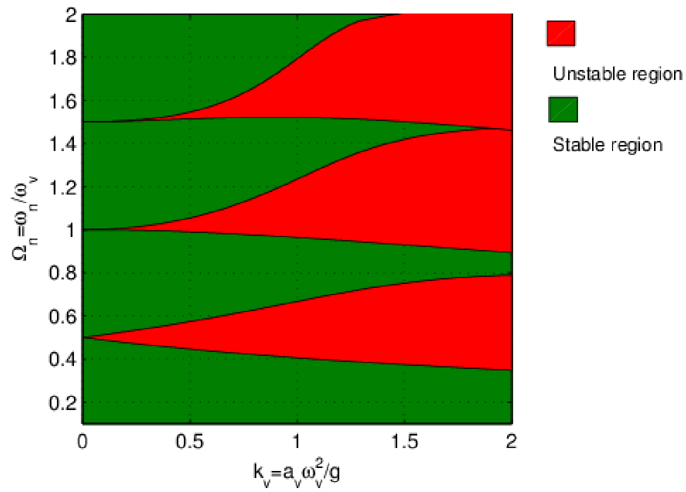


**Figure 6.2: Stability chart for dynamic stability of free-surface under vertical excitations**

## 6.5 Numerical simulation of sloshing waves

To validate the stability chart obtained, the sloshing response under vertical excitation is simulated based on numerical techniques. A finite element based numerical formulation for non-linear sloshing response of fluids under pure horizontal, pure vertical and combined excitations is developed. A finite element numerical approach based on mixed Eulerian-Lagrangian scheme is adopted. The free surface nodes behave like Lagrangian particles and interior nodes behave like Eulerian particles. For this formulation, the free-surface kinematic and boundary conditions Eq. (6.4) and Eq. (6.5) respectively are modified and written in Lagrangian form as [134] follows

$$\left.\frac{d\phi}{dt}\right|_{z=\zeta}=\frac{1}{2}\nabla\phi.\nabla\phi-\left(g+z_t''\right)\zeta-xx_t'' \tag{6.19}$$

$$\frac{dx}{dt}=\frac{\partial\phi}{\partial x};\frac{dz}{dt}=\frac{\partial\phi}{\partial z} \tag{6.20}$$

In order to solve this nonlinear sloshing problem, time interval $t$ is divided into finite number of time steps, $t_n = n\Delta t$ ($n$ = 0, 1, 2, 3…..), at a particular time step

($n$ = 0), the initial boundary conditions Eqs. (6.6) - (6.8) are known, using these initial conditions along with the boundary condition Eq. (6.3), Laplace equation, Eq. (6.2) is solved to get velocity potential $\varnothing$. Further velocity $v$ is evaluated from the velocity potential $\varnothing$ using patch recovery technique by Zienkiewicz [135]. Using these evaluated velocities the kinematic and dynamic free surface boundary conditions, Eqs. (6.19) - (6.20) are time integrated using Runge-Kutta method and the position of free surface is updated to get the free surface position for the next time step ($n$ = 1). In this manner the sloshing response is numerically simulated.

## 6.6 Numerical procedure

### 6.6.1 Finite element formulation

The solution of the non-linear sloshing boundary value problem is obtained using finite element method. The entire liquid domain is discretized by using four noded isoparametric quadrilateral elements. A typical mesh structure is shown in Figure 6.3. By introducing the finite element shape functions the liquid velocity potential can be approximated as

$$\phi(x,z) = \sum_{j=1}^{n} N_j(x,z)\phi_j \qquad (6.21)$$

where $N_j$ is the shape function, $n$ is the number of nodes in the element and $\phi_j$ is nodal velocity potential. The potential on the free surface at a particular time step is obtained from the free surface boundary condition (like at $t$= 0, Eq. (6.6)). It is needed to calculate the velocity potential for the interior nodes. Applying Galerkin weighted residual method to the Laplace equation along with the Neumann boundary conditions and taking the free surface nodes where the potential is known to the right hand side will lead to the following system of finite element equation,

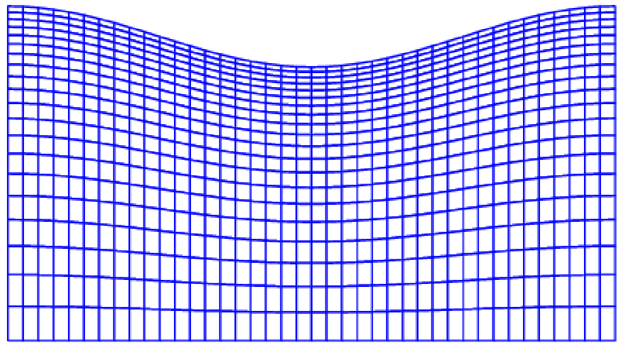

**Figure 6.3: Finite element discretization of liquid domain**

$$\int_{\Omega} \nabla N_i \sum_{j=1}^{m} \phi_j \nabla N_j \, d\Omega \Big|_{i, i \notin \Gamma_S} = -\int_{\Omega} \nabla N_i \sum_{j=1}^{m} \phi_j \nabla N_j \, d\Omega \Big|_{j \in \Gamma_S, i \notin \Gamma_S} \quad (6.22)$$

Where *m* is the total number of nodes in the liquid domain.

**6.6.2 Velocity recovery**

To track the free-surface Eq. (6.19) and Eq. (6.20) need velocities, which can be computed from the calculated potential using

$$\overline{v} = \nabla N_j . \phi_j \quad (6.23)$$

The velocities calculated using Eq. (6.23) are the velocities at the Gauss integration points and they do not possess inter element continuity and have low accuracy at nodes and element boundaries. Utmost care was taken to calculate the velocities; a small error in the velocity recovery will affect the accuracy of free surface updating or tracking and gets accumulated with time and leads to underestimation of the solution. In order to derive a smoothed and continuous velocity, patch recovery technique by Zienkiewicz [135] is applied. In patch recovery technique, the continuous velocity field is obtained by considering the linear interpolation of the velocities at the Gauss integration points,

$$\hat{v} = a_1 + a_2 \xi + a_3 \eta + a_4 \xi \eta \quad (6.24)$$

where $\hat{v}$ is any velocity component ($\hat{v}_x$ or $\hat{v}_y$), $\xi$, $\eta$ are the Gauss locations and $a_1$, $a_2$, $a_3$, $a_4$ are unknowns which need to be evaluated. To evaluate these unknowns, a least square fit is considered between $\hat{v}$ and $\overline{v}$ as given below

$$F(a) = \sum_{i=1}^{4} \left[ \hat{v}(\xi_i, \eta_i) - \overline{v}(\xi_i, \eta_i) \right]^2 \qquad (6.25)$$

where $i$ is the 2x2 order Gauss integration points. Then, the four unknown coefficients are determined from four simultaneous equations obtained from

$$\frac{\partial F(a)}{\partial a_k} = 0; \quad where\ k = 1,2,3,4 \qquad (6.26)$$

Substituting these calculated $a_k$'s in Eq. (6.24) gives the velocity values for individual elements and these are averaged for the common nodes. Finally, a smoothed velocity field which is inter element-continuous is constructed by interpolating the finite element shape functions used in Eq. (6.21) and nodal averaged velocities. The global continuous velocity field is given as,

$$v = N.\hat{v} \qquad (6.27)$$

where $v$ is velocity component ($v_x$ or $v_y$).

### 6.6.3 Numerical time integration and free-surface tracking

After calculating the velocity at a time step $t$, we need to calculate the position of free surface from Eq. (6.20) and determine the potential on the free surface using Eq. (6.19) for the next time step $t+\Delta t$. As a result, the liquid mesh and the boundary condition required for the next-time step are established. This is done using a finite difference numerical procedure. The numerical time integration scheme plays a major role in any time marching problem. The fourth-order Runge-Kutta method using explicit time integration is carried out in the present work. The nodal coordinates of the free surface and the associated velocity potential at a current time step *i*, are known and can be represented in a single variable as,

$$s_i = \left(x_i, z_i, \phi_i\right) \tag{6.28}$$

where

$$\begin{aligned} x_i &= \left(x_1, x_2, \ldots, x_{NX+1}\right)_i \\ z_i &= \left(z_1, z_2, \ldots, z_{NX+1}\right)_i \\ \phi_i &= \left(\phi_1, \phi_2, \ldots, \phi_{NX+1}\right)_i \end{aligned} \tag{6.29}$$

where *NX* is number of segments along the free-surface. Similarly the time derivative can be written as

$$\frac{Ds_i}{Dt} = F\left(t_i, s_i\right) = F_i. \tag{6.30}$$

The free-surface position and associated velocity potential at the next time step *i+1* can be expressed as

$$s_{i+1} = s_i + \frac{s_1}{6} + \frac{s_2}{3} + \frac{s_3}{3} + \frac{s_4}{6} \tag{6.31}$$

where

$$\begin{aligned} s_1 &= \Delta t F\left(t_i, s_i\right) \\ s_2 &= \Delta t F\left(t_i + \frac{\nabla t}{2}, s_i + \frac{s_1}{2}\right) \\ s_3 &= \Delta t F\left(t_i + \frac{\nabla t}{2}, s_i + \frac{s_2}{2}\right) \\ s_4 &= \Delta t F\left(t_i + \nabla t, s_i + s_3\right) \end{aligned} \tag{6.32}$$

After obtaining the new positions and potential of the free surface, the liquid domain is re-meshed based on these obtained new coordinate positions.

### 6.6.4 Regridding algorithm

At the beginning of the numerical simulation, the free surface nodes are uniformly distributed along the $x$-direction with zero surface elevation. As the time proceeds the free surface nodes are spaced unequally and cluster into a steep gradient leading to numerical instability. This problem occurs for a long time simulation; to avoid this instability, an automatic regridding condition using cubic spline is employed when the movement of the nodes is 75% more or less than the initial grid spacing. For the regridding, first the free surface length $L_f$ is obtained. Then the free surface is divided into $NX$ segments with the identical arc length. The coordinates of node is denoted as ($x_l$, $y_l$ ) ($l=1,2,\ldots,NX+1$) and let the arc length between two successive points $l$ and $l+1$ be $S_l$. Being a uniform regridding, $S_l$ can be expressed as

$$S_l = \frac{lL_f}{NX} \tag{6.33}$$

The coordinates of the nodes ($x_l$, $y_l$) is a function of the arc length $S_l$,

$$\left(x_l, y_l\right) = f\left(S_l\right) \tag{6.34}$$

The cubic spline interpolation is used to calculate the coordinates ($x_l$, $y_l$) and the velocity potential on the new uniform free-surface is also obtained in a similar fashion.

### 6.6.5 Complete algorithm for nonlinear sloshing

Including all the steps above, the algorithm for numerical simulation of nonlinear sloshing is as shown in Figure 6.4.

## 6.7 Numerical results and discussion

Numerical simulations are carried out with the above discussed numerical formulation to explore the behaviour of sloshing under pure vertical and combined harmonic excitations of the tank. First the natural slosh frequencies are calculated followed by sloshing response.

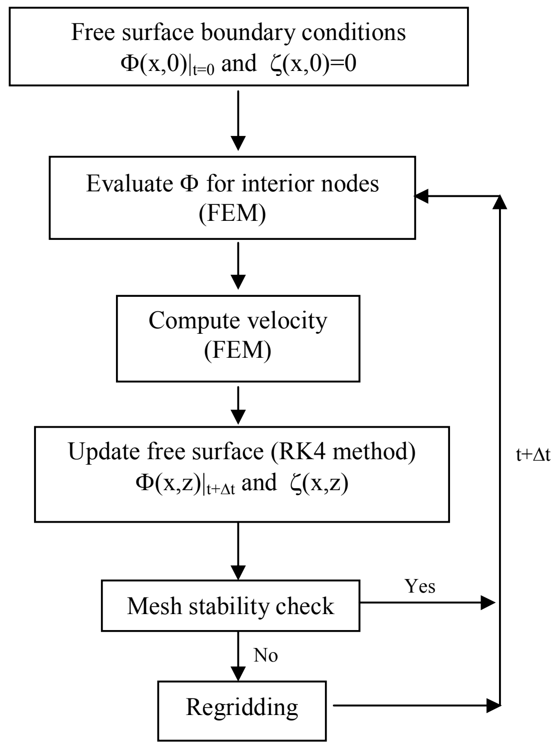


**Figure 6.4: Numerical procedure for nonlinear sloshing simulation**

### 6.7.1 Free vibration analysis

To validate the code for stiffness matrix formulation, a free vibration problem is solved first. A mass matrix as given in Eq. (6.35) for the free surface of the liquid is formed:

$$M = \frac{1}{g}\int_{\Gamma_s} N^T N d\Gamma_s \tag{6.35}$$

If $\omega_n$ denotes the $n^{th}$ natural slosh frequency of the coupled system and $\{\Psi_n\}$ the corresponding mode shape, the free vibration problem to be solved is

$$\left(K - \omega_n^2 M\right)\{\Psi_n\} \tag{6.36}$$

The natural slosh frequencies obtained from Eq. (6.36) are compared with the analytical formula obtained in Eq. (6.16).

### 6.7.2 Verification problems

Following the above numerical formulation, a code is developed. The developed code can deal with Eigen sloshing analysis and the sloshing response can be obtained for any excitation of the tank with frequency and amplitude of the excitation as variable. Also the liquid depth, width of the tank and the number of elements on the free-surface and in the fluid domain are taken as variables. First, the developed code is validated; sloshing response is simulated for horizontal forced excitation of the tank. The horizontal forced excitation is assumed to be harmonic as

$$x_h(t) = a_h \sin(\omega_h t) \tag{6.37}$$

where $a_h$ is the amplitude and $\omega_h$ is the frequency of forcing excitation. Two simulation cases are considered which are given in Table 6.1. The two cases taken by previous investigators are for the comparison purpose with the existing reference solutions: case 1 by Nakayama and Washizu [112] and case 2 by Frandsen [119]. The natural slosh frequencies calculated for the cases considered are shown in Table 6.2. Natural Slosh frequencies obtained numerically are compared with analytical solution Eq. (6.16) in Table 6.2 and are in good match.

**Table 6.1: Simulation cases for verification problem**

| case | Tank Geometry | | Excitation | |
|---|---|---|---|---|
| | Tank width (m) | Liquid depth (m) | Amplitude (m) | Frequency (rad/s) |
| 1 | 0.9 | 0.6 | 0.002 | 5.5 |
| 2 | 2 | 1. | 0.0097 | 3.7607 |

**Table 6.2: Slosh frequencies (rad/s) compared with analytical solution for verification problems**

| Mode | Case 1 | | Case 2 | |
|---|---|---|---|---|
| No. | FEM | Theory | FEM | Theory |
| 1 | 5.7658 | 5.7637 | 3.7607 | 3.7594 |
| 2 | 8.2809 | 8.2738 | 5.5456 | 5.5411 |
| 3 | 10.1530 | 10.1355 | 6.8092 | 6.7986 |

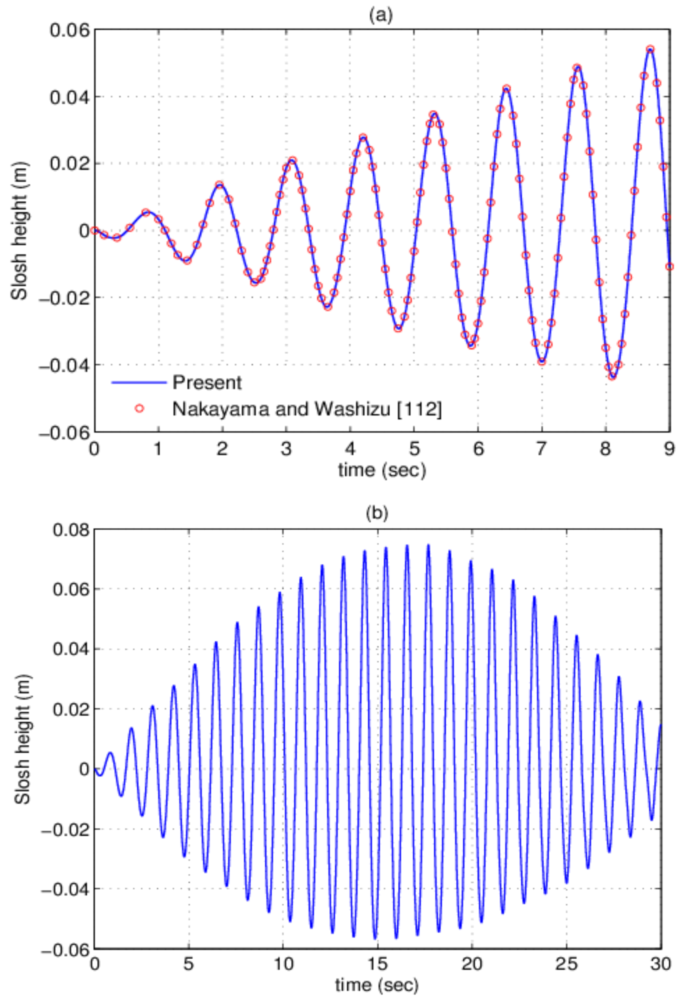


**Figure 6.5: Time history response of the free-surface elevation (case 1) (a) comparison with Nakayama and Washizu [112] (b) extension to t = 30 s**

Figure 6.5(a) shows the comparison of time history of sloshing response at right of the wall with the solution by Nakayama and Washizu [112] that has been frequently used as a reference solution in comparative numerical experiments. For this simulation, 20 nodes along the free-surface and 10 nodes along the height and a time step of 0.001 s are used. It can be observed that the numerical solution by the proposed method is in good agreement with the reference solution. In view of the fundamental sloshing frequency $\omega_1$ = 5.76077 rad/s, the excitation frequency $\omega_h$ is taken as $\omega_h$ = 0.9547 $\omega_1$. Figure 6.5(b) presents the time history response of free surface elevations at right wall that is extended to 30 s. From the plot, we see that the free surface elevation reaches the peak level and then its magnitude gradually decreases after that.

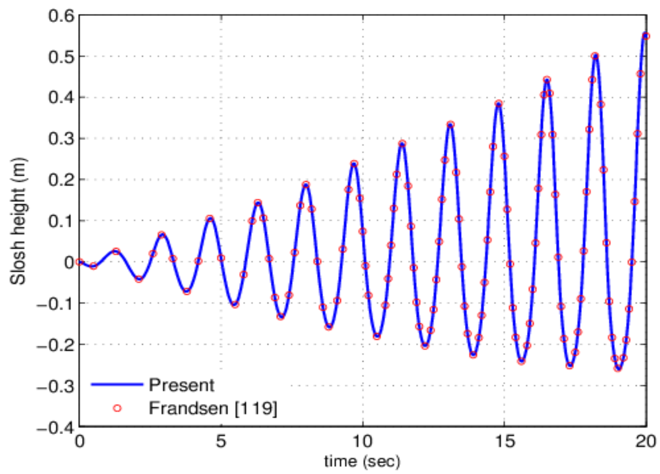


**Figure 6.6: Free-surface elevation at the left wall for case 2 compared with Frandsen [119]**

Figure 6.6 shows the free-surface elevation at the left wall for case 2 compared with numerical result of Frandsen [119]. For this simulation, 40 nodes along the free-surface, 20 nodes along the depth and a time step of 0.001 s are taken. As the fundamental slosh frequency, $\omega_1$ = 3.7607 rad/s and excitation frequency, $\omega_h$ = 3.7607 are equal, this case is a resonance case; with the amplitude of excitation considered is large. For the present case the sloshing response shows nonlinearity. As expected in resonance, the sloshing response increases with time and as the forcing excitation is large eventually, as the amplitude increases, the non-linear effects begin to play a considerable role leading to higher peaks and smaller troughs in the surface elevation. From the Figure 6.6 it can be seen that the present numerical solution is in an excellent agreement with the reference solution considered. Check the link http://www.youtube.com/watch?v=LlwUOWMmVtc for the sloshing response animation in this resonance case.

**6.7.3 Sloshing response under pure vertical excitation**

In this section, sloshing response of free-surface under vertical harmonic excitation is carried out. The tank is subjected to forced harmonic vertical motion given in Eq. (6.17). For only pure vertical excitation to exist $x_t''$ is assumed zero. Eq. (6.17) gives excitation velocity as $-a_v\omega_v sin(\omega_v t)$, which leads to a zero free surface velocity potential as initial condition from Eq. (6.6). As far as the free-surface is at rest, no motion can be generated by the vertical excitation. Thus to simulate the sloshing response under vertical excitation the initial conditions play an important role, there should be some initial perturbation on the free-surface for slosh response. The initial conditions can be prescribed as

$$\phi(x,0,0)=0 \tag{6.38}$$

$$\zeta(x,0)=a\cos(k_n x) \tag{6.39}$$

where $a$ is the initial wave profile and $x$ is the horizontal distance from the origin. The measure of non-linearity depends on the adopted initial condition, $\varepsilon = a\omega_n^2/g$ [119].

The sloshing response is simulated for various cases inside and outside the regions of parametric resonance; six different cases are considered and are marked on the stability chart shown in Figure 6.7. The parameters for the cases shown in Figure 6.7 are given in Table 6.3. The test cases considered are similar to the test

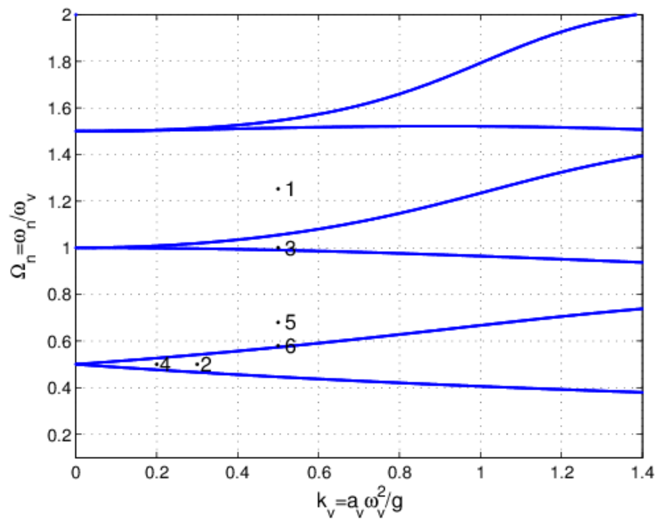


**Figure 6.7: Stability chart for sloshing response under vertical excitations with test cases (Value are shown in Table 6.3)**

**Table 6.3: Excitation parameters for the test cases shown in Figure 6.7**

| Case | $\Omega_n$ | $k_v$ | $\omega_v$ | $a_v\omega_v^2$ |
|---|---|---|---|---|
| 1 | 1.253 | 0.5 | $0.7981\omega_1$ | 0.5g |
| 2 | 0.5 | 0.3 | $2\omega_1$ | 0.3g |
| 3 | 1.0 | 0.5 | $\omega_1$ | 0.5g |
| 4 | 0.5 | 0.2 | $2\omega_3$ | 0.2g |
| 5 | 0.6 | 0.5 | $1.66\omega_1$ | 0.5g |
| 6 | 0.55 | 0.5 | $1.8182\omega_1$ | 0.5g |

**Table 6.4: Slosh frequencies compared with analytical solution**

| Mode No. | Present (rad/s) | Theory (rad/s) | Error % |
|---|---|---|---|
| 1 | 3.7607 | 3.7594 | 0.0353 |
| 2 | 5.5456 | 5.5411 | 0.0801 |
| 3 | 6.8092 | 6.7986 | 0.1553 |
| 4 | 7.8715 | 7.8510 | 0.2620 |
| 5 | 8.8126 | 8.7777 | 0.3983 |

cases by Frandsen [119]; to make comparison. In the present numerical simulations, the tank is assumed to be rigid with aspect ratio (*h/L*) of 0.5; *h* is depth of fluid, *L* is length of the tank and 40 nodes along the x-direction and 20 nodes along the z-direction are taken and a time step of 0.001 s is adopted. Table 6.4 shows the slosh

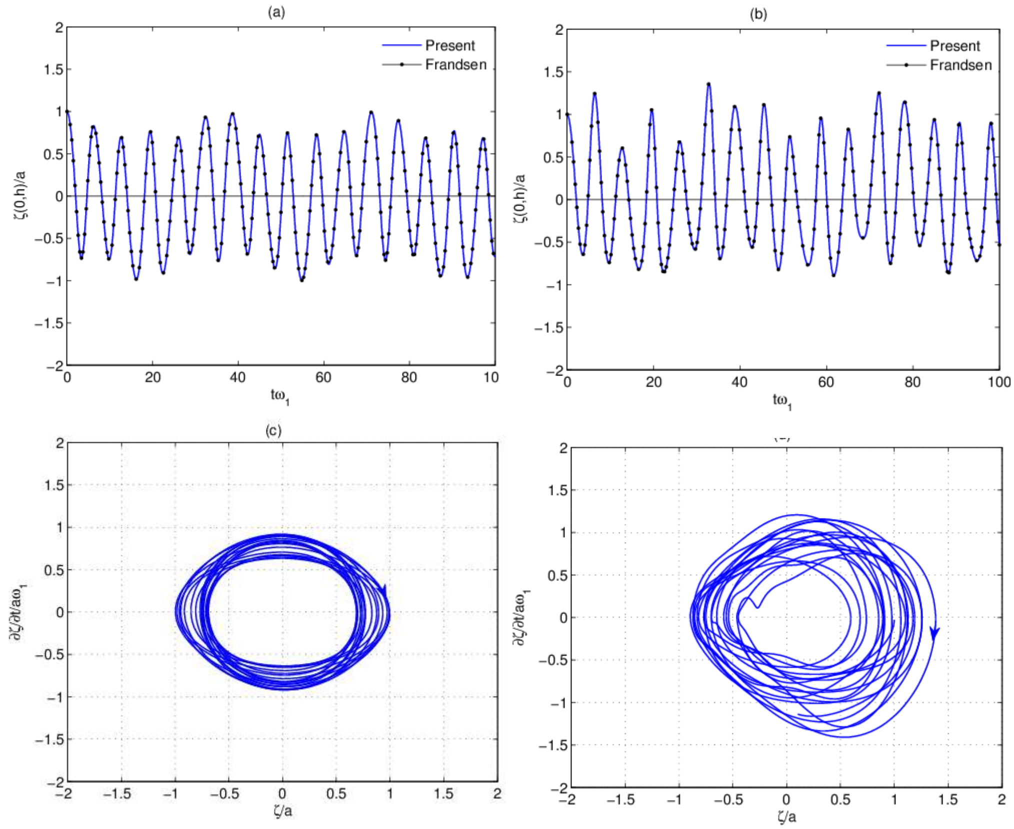


**Figure 6.8: Free-surface elevation at the left wall in the stable region (test case 1) $\Omega_1$ = 1.253, $k_v$ = 0.5 for (a) $\varepsilon$ = 0.0014 (b) $\varepsilon$ = 0.288 and the respective phase-plane plots**

frequencies in rad/s obtained for the present tank using finite element method and the above analytical formula Eq. (6.16).

The first test case is in stable region, with frequency ratio $\Omega_1$ = 1.253, and forcing amplitude $k_v$ = 0.5; test case 1 as shown in Figure 6.7. The slosh response at the left wall of the tank for low ($\varepsilon$ = 0.0014) and high ($\varepsilon$ = 0.288) wave steepness are shown in Figure 6.8(a) and 6.8(b) respectively. Figure 6.8(c) and 6.8(d) shows the respective phase-plane plots for the small and steep wave cases. The time histories of the free-surface elevation are non-dimensionalised. The slosh response obtained with the present simulation is compared with numerical results of Frandsen [119]. Both the results are in excellent agreement. The slosh response for low steep waves is symmetric i.e. amplitudes of peak and troughs are equal, where as for high steep waves the response is asymmetric showing different amplitudes for peaks and troughs. This is an indication of non-linear response. This non-linear behaviour can be noticed from the respective phase-plane plots. The phase-plane plot of slosh response with low wave steepness shown in Figure 6.8(c) has a closed orbit displaying a linear behavior, where as the phase-plane plot of slosh response with high wave steepness have non-repeatable, non-closed orbits displaying a non-linear characteristic.

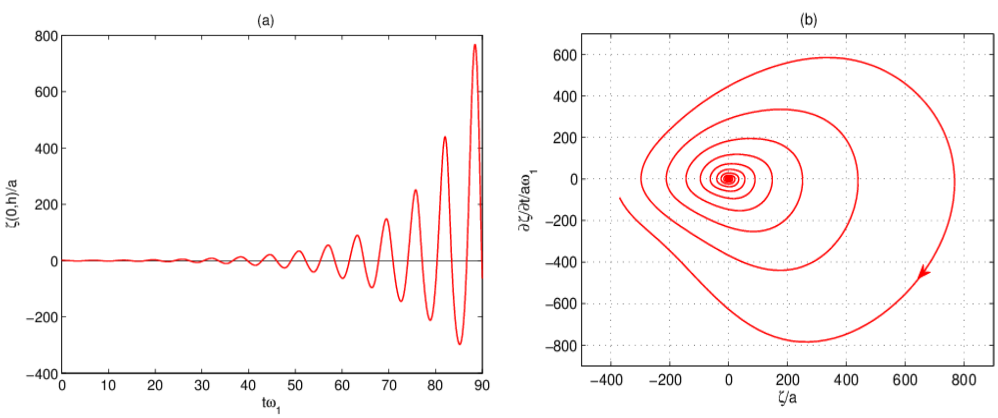


**Figure 6.9: Free-surface elevation at the left wall in the unstable region (test case 2) for $\Omega_1$ = 0.5, $k_v$ = 0.5, $\varepsilon$ = 0.0014 and the respective phase plane plot**

The second test case lies in the unstable region, with frequency ratio $\Omega_1 = 0.5$, and forcing amplitude $k_v = 0.3$; test case 2 as shown in Figure 6.7. Figure 6.9(a) shows the free surface elevation at the left wall of the tank for a low wave steepness of $\varepsilon = 0.0014$. As the excitation parameters lie in unstable region, an unbounded response is expected; the slosh response plot displays the expected behaviour. Figure 6.9(b) shows the corresponding phase-plane diagram. The phase-plane plot and the response plot clearly show that the nonlinear effects are predominant. A moving mesh generated at different time steps in this instable region for parametric

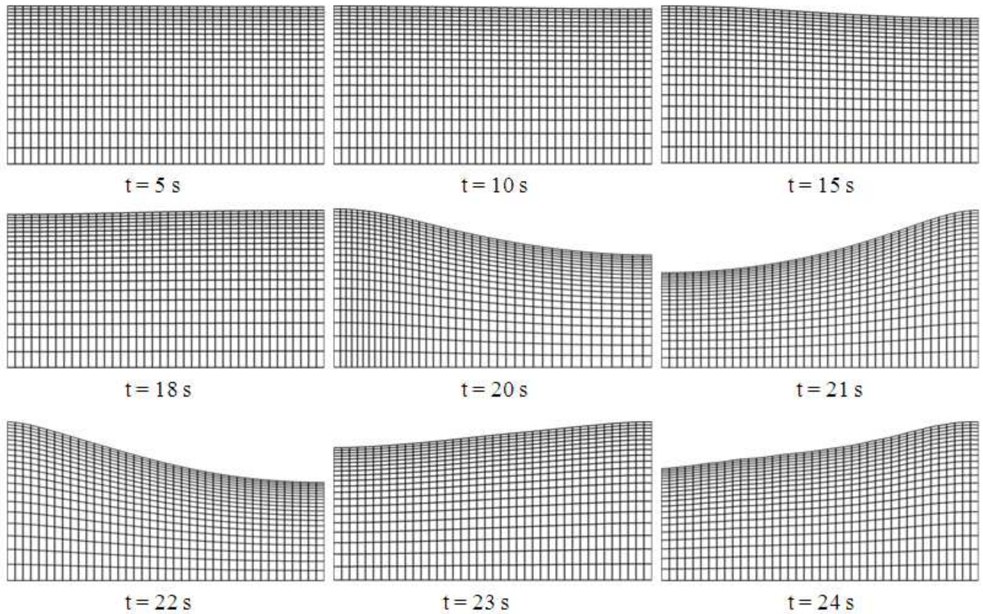


**Figure 6.10: Moving mesh generated at different time steps in parametric resonance**

resonance is shown in Figure 6.10. The response of free surface of fluid in this case showing parametric instability can be seen in the link [http://youtu.be/VTsA0I7Ry4s](http://youtu.be/VTsA0I7Ry4s).

Figure 6.11 also shows the slosh response time histories in unstable regions. A low wave steepness parameter of $\varepsilon = 0.0014$ is considered. Figure 6.11(a) shows the slosh response time history for frequency ratio $\Omega_1 = 1.0$, forcing amplitude $k_v = 0.5$; test case 3 as shown in Figure 6.7. This case corresponds to instability in first sloshing mode lying in the second instability region. According to the theory, the effect of parametric resonance gradually reduces as we move to the higher regions of instability. As expected, the amplitudes do not grow rapidly in this instability region compared to first instability region response shown in Figure 6.9(a). First the amplitude of the slosh response starts growing exponentially in a resonance mode and then after certain time the response reduces gradually. As the amplitude

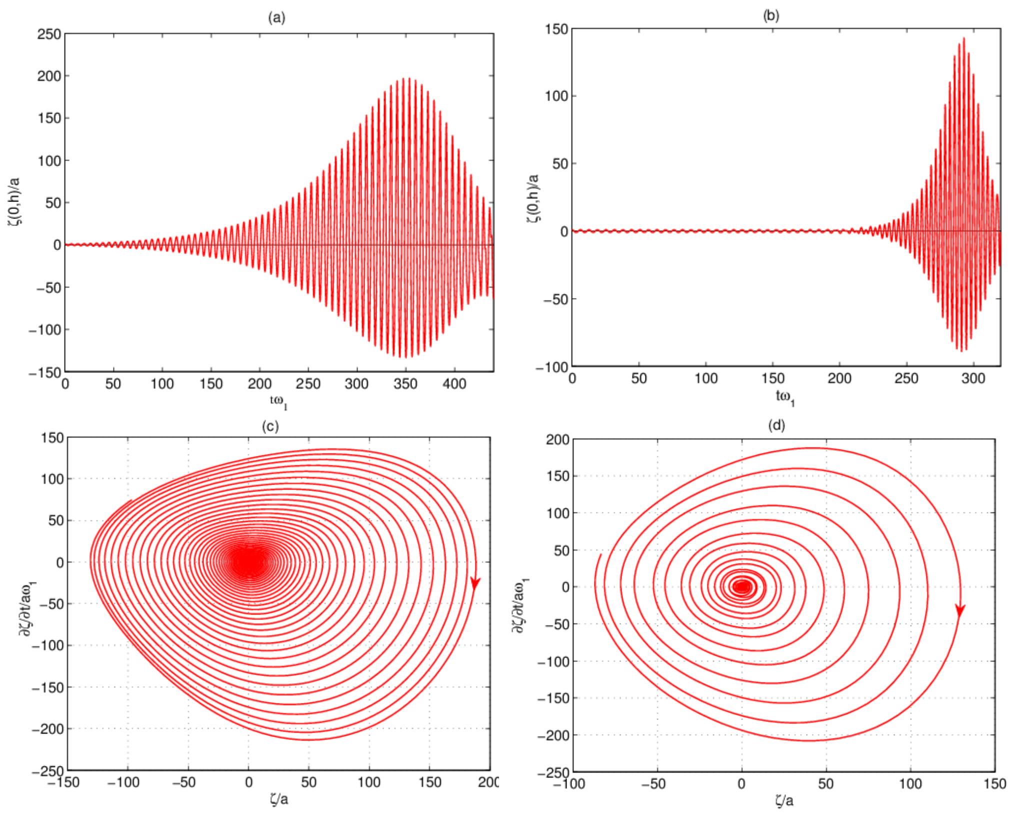


**Figure 6.11: Free-surface elevation at the left wall in the unstable regions with ε = 0.0014 (a) $\Omega_1$ = 1.0, $k_v$ = 0.5 (test case 3) (b) $\Omega_3$ = 0.5, $k_v$ = 0.4 (test case 4) and respective phase-plane plots**

increases the natural frequency of the system changes and creates low frequency amplitude oscillations leading to decrease in amplitudes of response. This behaviour is called detuning effect; under parametric excitation of frequency close to twice the natural frequency of a certain mode, the free-surface oscillates exhibiting the shape of that mode. As the excitation amplitude increases, the natural frequency changes and the input energy can excite the other neighbour modes. If the excited neighbour nodes are stable, the increase in the amplitude will be suppressed leading to detuning effect. This detuning effect can be captured only in non-linear systems. In case of linear systems [7], the response will be always increasing; this detuning effect cannot be captured. The present finite element non-linear numerical model can capture this detuning effect effectively. Figure 6.11(c) shows the respective phase-plane plot. Figure 6.11(b) shows the slosh response at left wall of tank for frequency ratio $\boldsymbol{\Omega}_3 = 0.5$, forcing amplitude $k_v = 0.2$; test case 4 as shown in Figure 6.7. This case corresponds to instability in second sloshing mode lying in the first instability region. As the instability is in second mode, the amplitudes do not grow rapidly when compared to instability in the first mode, Figure 6.9(a). After certain time, the amplitude comes down showing the detuning effect. In this case, the free-surface oscillates exhibiting the third slosh mode and as the amplitude increases, the input parametric excitation excites the first sloshing mode, which is stable and the amplitudes fall down. Figure 6.11(d) shows the respective phase plane plot. The phase-plane plots for the responses display a linear behaviour for the system. Figure 6.12 shows the moving mesh generated for the response shown in Figure 6.11(b) at various time steps. The animation of liquid free-surface sloshing for detuing effect shown in Figure 6.11 (b) can be viewed in the link http://youtu.be/ylRHuxKt3rw.

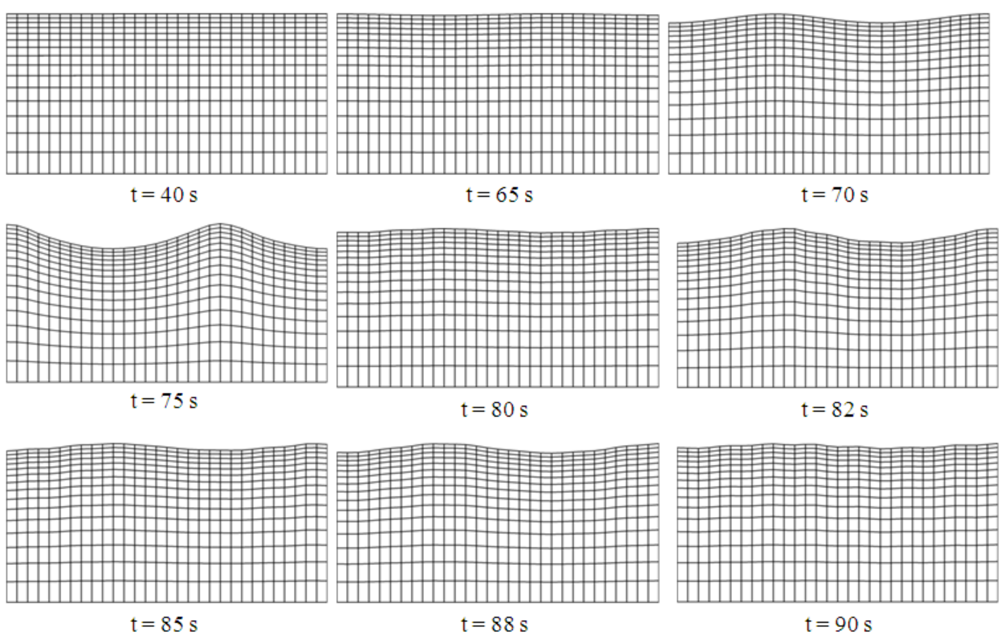


**Figure 6.12: mesh generated at different time steps in unstable region displaying detuning effect**

Figure 6.13 shows the slosh response for the test case 5 as shown in Figure 6.7, with frequency ratio $\Omega_1$ = 0.6, forcing amplitude $k_v$ = 0.5. This point lies in the stable region but very close to instability region. Figure 6.13(a) shows the slosh response for low wave steepness parameter, $\varepsilon$ = 0.0014 and Figure 6.13(b) shows the slosh response for high wave steepness parameter, $\varepsilon$ = 0.288. As expected the point is in the stable region and the slosh response is stable.

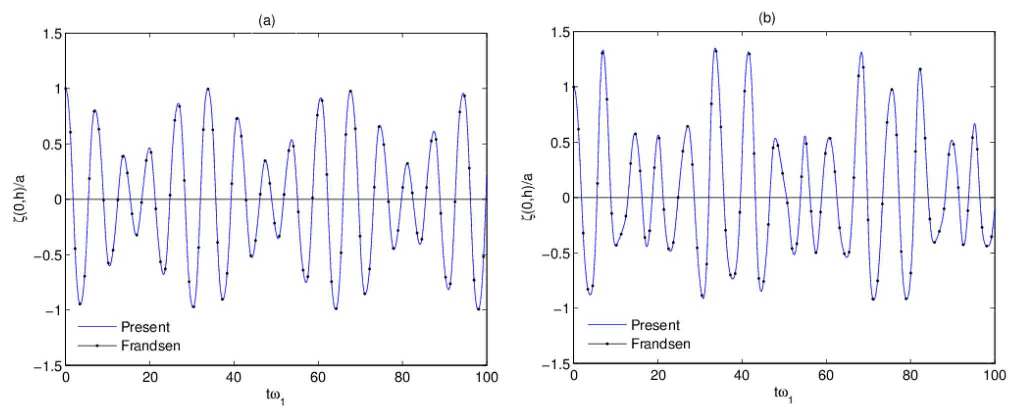


**Figure 6.13: Free-surface elevation at the left wall in the stable region (test case 5) for $\Omega_1$ = 0.55, $k_v$ = 0.5 (a) $\varepsilon$ = 0.0014 (b) $\varepsilon$ = 0.288**

Figure 6.14 shows the slosh response for test case 6 with frequency ratio $\Omega_1$ = 0.55, forcing amplitude $k_v$ = 0.5 lying in the unstable region as shown in Figure 6.7. A low steepness parameter $\varepsilon$ = 0.0014 is taken. As the point lies in the unstable region, the response is also unstable as expected. The low steepness response is sufficient to demonstrate to show the rapid increase in the amplitudes.

### 6.7.4 Sloshing response under coupled horizontal and vertical excitations

In this section the sloshing response when the tank is subjected to combined horizontal and vertical excitations is considered. Both the excitations are considered harmonic as prescribed by Eq. (6.37) and Eq. (6.17) for horizontal and vertical excitations respectively. The initial conditions required for this simulation are

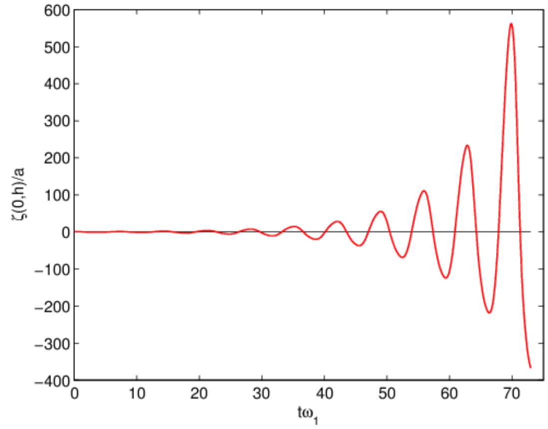


**Figure 6.14: Free-surface elevation at the left wall in unstable region (test case 6) for $\Omega_1$ = 0.55, $k_v$ = 0.5, $\varepsilon$ = 0.0014**

$$\phi(x,0,0)=0 \tag{6.40}$$

$$\zeta(x,0)=0 \tag{6.41}$$

No initial perturbation is required as needed in case of pure vertical excitation; the horizontal harmonic excitation creates the perturbation needed for slosh response under vertical excitations. The governing equation for the dynamic stability of free surface under pure vertical excitation (Eq. 6.18) differs in the case of combined excitations; a forcing term appears on the right side due to horizontal excitation. Eq. (6.18) under combined excitation of tank can be written as

$$\frac{d^2 z_n(T)}{dT^2}+\Omega_n^2\left(1-k_v\cos(2T)\right)z_n(T)=x_t''(T) \tag{6.42}$$

Eq. (6.42) is a non-homogenous Mathieu Hill equation. It should be noted that the stability chart of the Mathieu- Hill equation is independent of the term on right hand side. The stability chart shown in Figure 6.2 is still valid, but the response of the free-surface is affected by the presence of horizontal loading. This horizontal term can produce resonance, which is recognized by the linear growth of amplitude in time. It is known that, under pure horizontal excitation when external excitation frequency is equal to fundamental sloshing frequency the free-surface undergoes resonance. In case of pure horizontal motion, system has only one resonance frequency; but under combined motion, it is found that the system has infinite resonance frequencies. When the horizontal excitation frequency $\omega_h$ is close to fundamental slosh frequency and when sum or difference of horizontal and vertical frequencies $\omega_h$, $\omega_v$ is closer to fundamental slosh frequency, system undergoes resonance. This resonance is characterized by linear growth in the amplitude if the vertical excitation parameters are in stable region. If the vertical excitation parameters are in unstable region, system grows exponentially in time. Figure 6.15-6.17 shows the slosh response for three main resonant frequencies of the horizontal motion ($\omega_h/\omega_1$ = 0.98, 0.18, 1.78) under vertical excitation lying in a stable region with $\mathbf{\Omega}_1$ = 1.253, $k_v$ = 0.5 test case 1 as shown in Figure 6.7 for small and large amplitudes of the horizontal excitation.

Figure 6.15 shows the slosh response for the strongest of the resonant frequencies for low and high horizontal forcing amplitude. The horizontal forcing frequency is closer to the first slosh natural frequency ($\omega_h/\omega_1$ = 0.98). Figure 6.16 and Figure 6.17 shows the slosh response for coupled frequencies ($\omega_h \pm \omega_v$) closer to first slosh natural frequency. It can be observed from figures that the sloshing response is high in main resonant frequencies compared to secondary resonances. Influence of vertical excitation with horizontal excitation is that, if the vertical excitations parameters are in stable region and the horizontal frequency or coupled frequencies are closer to sloshing natural frequency, resonance takes place, which is characterized by linear increase in the response.

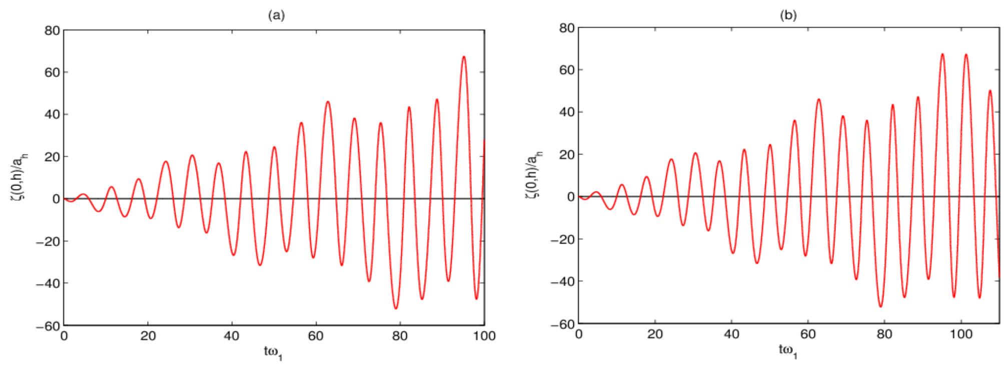


**Figure 6.15: Free-surface elevation at the left wall for the main resonance with horizontal excitation, $\omega_h/\omega_1$ = 0.98 and vertical excitation, $\omega_1/\omega_v$ = 1.253, $a_v\omega_v^2 = 0.5g$ (a) $a_h\omega_h^2 = 0.0014g$ (b) $a_h\omega_h^2 = 0.0069g$**

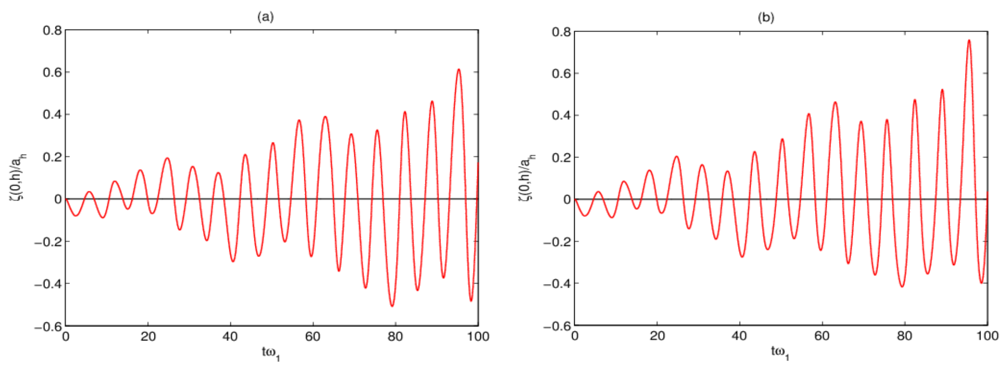


**Figure 6.16: Free-surface elevation at the left wall for the first resonance with horizontal excitation, $\omega_h/\omega_1$ = 0.18 and vertical excitation, $\omega_1/\omega_v$ = 1.253, $a_v\omega_v^2 = 0.5g$ (a) $a_h\omega_h^2$ = 4.85*10-5$g$ (b) $a_h\omega_h^2 = 0.0194g$**

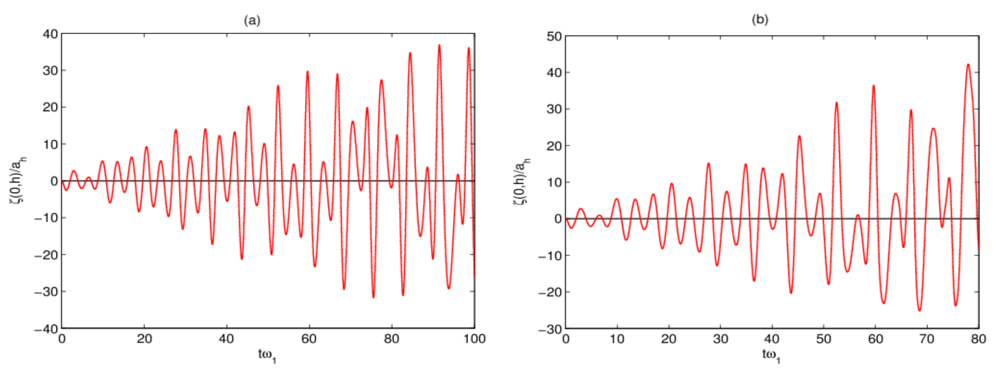


**Figure 6.17: Free-surface elevation at the left wall for the second resonance with horizontal excitation, $\omega_h/\omega_1$ = 1.78 and vertical excitation, $\omega_1/\omega_v$ = 1.253, $a_v\omega_v^2 = 0.5g$ (a) $a_h\omega_h^2 = 0.0046g$ (b) $a_h\omega_h^2 = 0.0228g$**

Figure 6.18-6.19 shows the slosh response in the unstable regions for small horizontal forcing amplitude. The vertical excitation parameters lie in unstable regions and a small horizontal forcing amplitude $a_h$ = 0.001m with a forcing frequency $\omega_h/\omega_1 = 0.18$ is considered. The difference between the present simulation and simulations carried out in section 6.7.3 is that, in the present case tank is moved horizontally with small forcing amplitude. This horizontal forcing creates necessary initial perturbation required for vertical slosh response. Figure 6.18(a) and Figure 6.18(b) shows the slosh response at the left wall of the tank and respective phase-plane plot in the unstable region, with frequency $\omega_1/\omega_v = 0.5$, with a forcing amplitude of 0.3$g$; test case 2 as shown in Figure 6.7. This corresponds to the

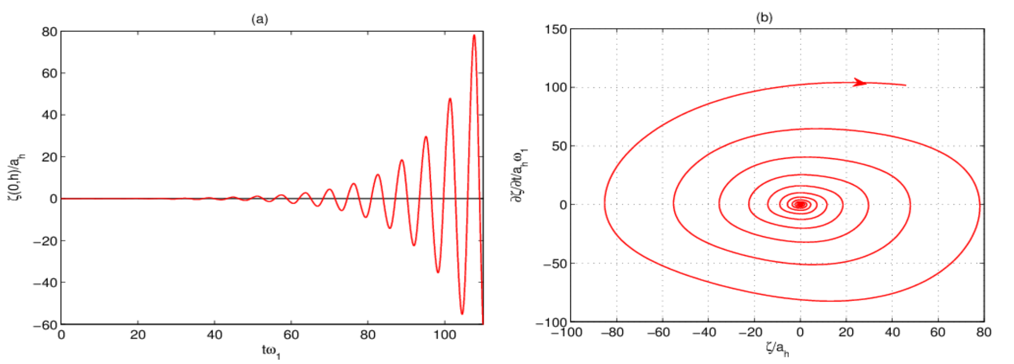


**Figure 6.18: Free-surface elevation at the left wall and corresponding phase-plane plot in the unstable region; $\omega_1/\omega_v = 0.5$, $a_v\omega_v^2 = 0.3g$ (test case 2 in Figure 6.7) with small horizontal excitation force, $\omega_h/\omega_1 = 0.18$, $a_h = 0.001$m**

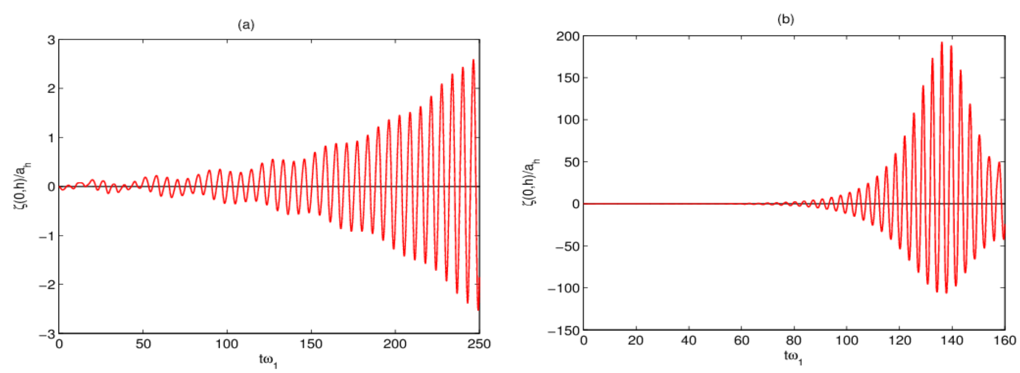


**Figure 6.19: Free-surface elevation at the left wall in unstable regions with small horizontal excitation force, $\omega_h/\omega_1 = 0.18$, $a_h = 0.001$m; (a) $\omega_1/\omega_v = 1$, $a_v\omega_v^2 = 0.5g$ (test case 3 in Figure 6.7) (b) $\omega_3/\omega_v = 0.5$, $a_v\omega_v^2 = 0.2g$ (test case 4 in Figure 6.7)**

instability of the first mode in the first instability region. The sloshing response of the combined forced tank motion, compared with response in Figure 6.9, illustrates that the small horizontal forcing excitation delays the occurrence of instability in the free-surface. Figure 6.19(a) shows the slosh response, with frequency $\omega_1/\omega_v = 1$, with a forcing amplitude of 0.5$g$; test case 3 as shown in Figure 6.7. This corresponds to the instability of the first mode in the second instability region, thus shows a less strong parametric resonance compared with response in Figure 6.18. Figure 6.19(b) shows the slosh response, with frequency $\omega_3/\omega_v = 0.5$, with a forcing amplitude of 0.2$g$; test case 4 as shown in Figure 6.7. This corresponds to the instability of the third mode in the first instability region and a stable first mode; the response grows up exponentially with time leading to an increase in frequency, which in turn excites the first stable mode and the exponential growth is suppressed. This detuning effect is nicely captured in the Figure 6.19(b).

Figure 6.20-6.21 shows the slosh response under combined excitations for the off-resonance cases when the vertical excitation parameters are in stable region. The vertical excitation has a frequency $\omega_1/\omega_v = 1.253$, and amplitude of 0.5$g$ (test case 1 in Figure 6.7). Figure 6.20(a) and Figure 6.20(b) shows the slosh response at the left wall for horizontal excitation frequency $\omega_h/\omega_1 = 0.7$ for small ($a_h\omega_h^2 = 0.0036g$) and large ($a_h\omega_h^2 = 0.036g$) forcing amplitude respectively. Figure 6.21(a) and Figure 6.21(b) shows slosh response at the left wall for horizontal excitation frequency $\omega_h/\omega_1$=1.3, for small ($a_h\omega_h^2$=0.0036$g$) and large ($a_h\omega_h^2$=0.072$g$) forcing amplitude.

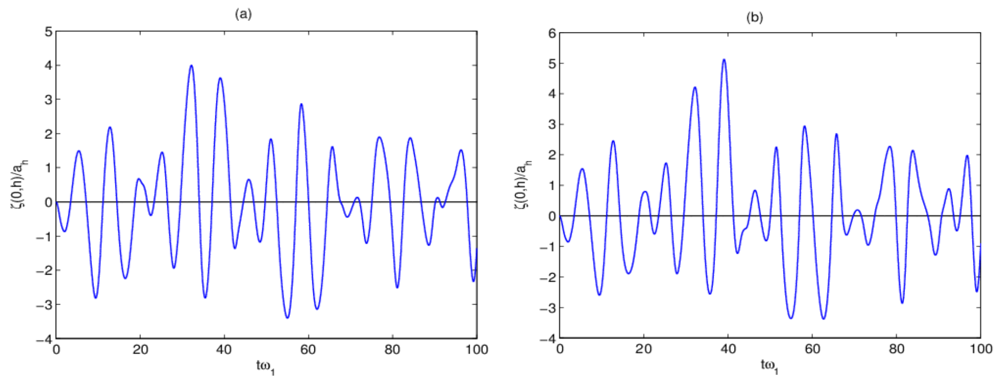


**Figure 6.20: Free-surface elevation at the left wall in stable region $\omega_1/\omega_v$ = 1.253, $a_v\omega_v^2$ = 0.5$g$ (test case in Figure 6.7), with horizontal excitation frequency, $\omega_h/\omega_1$ = 0.7 (a) $a_h\omega_h^2$ = 0.0036$g$ (b) $a_h\omega_h^2$ = 0.036$g$**

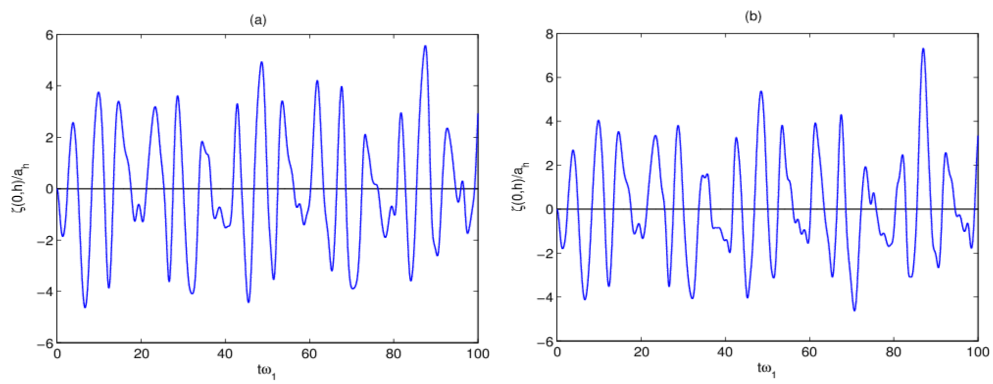


**Figure 6.21: Free-surface elevation at the left wall in stable region $\omega_1/\omega_v$ = 1.253, $a_v\omega_v^2$ = 0.5$g$ (test case 1 in Figure 6.7), with horizontal excitation frequency, $\omega_h/\omega_1$ = 1.3 (a) $a_h\omega_h^2$ = 0.0036$g$ (b) $a_h\omega_h^2$ = 0.072$g$**

## 6.8 Experimental study on dynamic stability of free-surface of fluid

### 6.8.1 Shake table experiment

Shake table test was conducted in Structural Mechanics Laboratory (SML), Indira Gandhi Centre for Atomic Research (IGCAR), Kalpakkam to analyse the slosh response in stability and instability regions of the stability chart. A rectangular tank of dimensions 1.2 x 1 x1 m filled with water to a height of 0.6 m is considered. Depth of the fluid is chosen 0.6 m to maintain an aspect ratio ($h/L$) of 0.5. Rectangular tank made of carbon steel with one side having acrylic glass window is used to perform the experiment. Acrylic glass is used in one side of the tank so as to enable visualization of the slosh waves during excitation. The details of the shake table: The shaker table is of size 3 mX3 m and has a pay load capacity of 10 ton. It has six actuators, which enable the table to move in all the six degrees of freedom (3 translations and 3 rotations). Three actuators are dedicated for the movement in two horizontal direction (x and y axes) and three actuators are for the movement in vertical direction (z axis). The actuators are driven by hydraulic power and precisely controlled by the servo-valves to produce the simultaneous and independent motions with six degrees of freedom. The shaker table can be displaced to ±100 mm. Its maximum velocity is 0.3 m/s. The maximum acceleration of shaker table is 0.3$g$ in horizontal direction and 1$g$ in vertical direction. The shaker table can be operated in 0.1 – 100 Hz frequency range. Shaker table can be excited with a sine sweep, saw tooth, ramp and random excitations. A dedicated data acquisition system with 64 channels is used for capturing the slosh response under vertical excitation. The displacement of the free surface is captured by Infrared (IR) sensors placed at the top of the tank as shown in Figure 6.22. Tiny white colored thermocol beads are placed on the free-surface, IR sensor transmits the infrared signal which senses the movement of these thermocol beads. IR sensor has a receiver and a transmitter. The transmitter will produce a signal, and the receiver receives the reflected signal, the time difference between transmitting a signal pulse and receiving signal pulse gives the slosh height. For the signal pulse to reflect thermocol beads are placed on the free-surface. This time difference generates a pulse, which will be sent to data acquisition system, where the signal pulse is amplified, calibrated. A schematic diagram of shake table test is shown in Figure 6.23.

Figure 6.22: Rectangular tank placed on shake table with IR sensors at the top

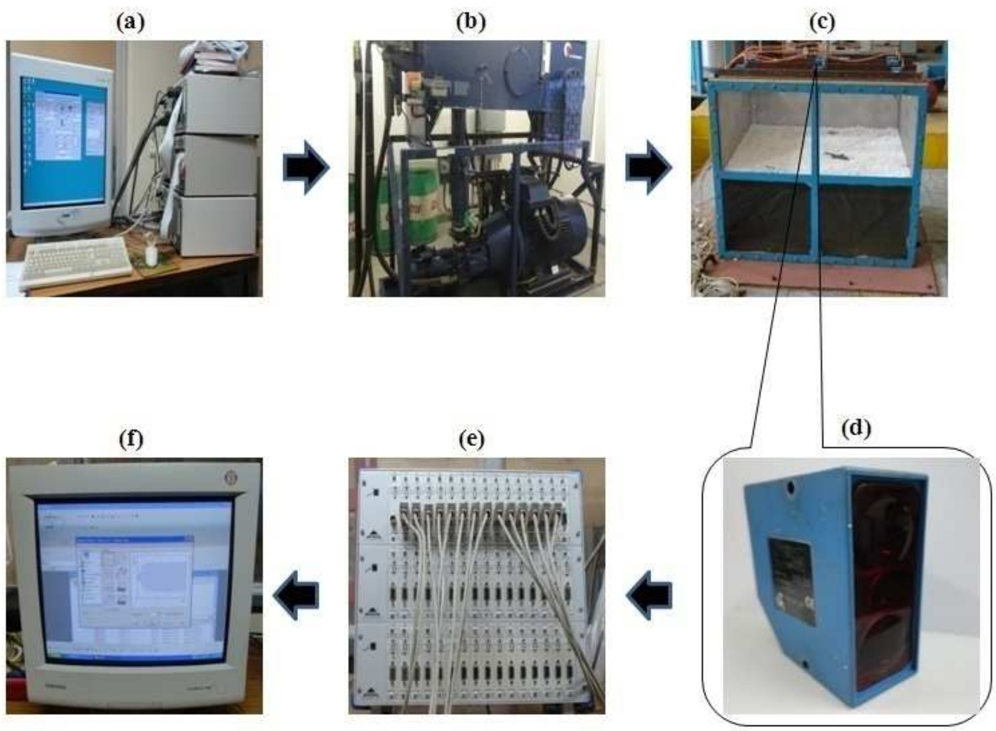


Figure 6.23: Schematic of shake table experiment carried out for dynamic stability of free-surface (a) Controlling system (b) Hydraulic pump (c) Fluid filled tank on shake table (d) IR sensor (e) Data acquisition system (f) Output display system

### 6.8.2 Free vibration analysis

A sine sweep test was conducted first to calculate the slosh natural frequencies. To calculate the sloshing natural frequencies, liquid filled container is excited sinusoidally with varying frequencies along the *X*-direction and *Y*-direction independently. Exciting the container along certain direction sinusoidally with varying frequencies is called a sine sweep. When the excitation frequency equals the natural slosh frequency resonance takes place and one can observe that the free-surface oscillates with high amplitudes or slosh elevations. These slosh elevations are recorded with respective time with the help of the IR sensor placed at the top. The data from IR sensor gives time vs. slosh elevation data, which signifies a signal data. The plot of Fourier spectrum of this signal data gives natural frequencies of the system. The Fourier amplitude spectrum of the signal data will have peaks, these peak values are the slosh natural frequencies. Table 6.5 shows the first three natural frequencies along *X* and *Y* direction obtained in experiment and compared with frequencies obtained from analytical formula Eq. (6.16) and finite element model.

**Table 6.5: Free-surface natural frequencies**

| Mode ($f_{mn}$) | Experiment (Hz) | Analytical (Hz) | FEM (Hz) |
|---|---|---|---|
| $f_{10}$ | 0.7324 | 0.7724 | 0.7726 |
| $f_{01}$ | 0.8544 | 0.8634 | 0.8636 |
| $f_{20}$ | 1.0986 | 1.1385 | 1.1393 |
| $f_{02}$ | 1.3567 | 1.2489 | 1.2497 |
| $f_{30}$ | 1.4648 | 1.3969 | 1.3988 |
| $f_{03}$ | 1.7089 | 1.5303 | 1.5324 |

### 6.8.3 Slosh response under vertical excitation

The container is excited vertically with various frequencies and amplitudes selected from the stability chart which lie in stable and unstable regions. To obtain- the response under vertical excitation, the free-surface requires some initial perturbation. To create some perturbation on the free-surface, the container is excited horizontally with a frequency of 0.5 Hz and amplitude of 0.5 mm for the first 10 seconds and then the container is excited vertically. The focus was on the principal parametric instability region, which is most dominating and catastrophic. Principal parametric resonance region corresponds to instability at a frequency equal to twice the fundamental natural frequency.

Figure 6.24 shows the slosh response of free-surface for excitation parameters lying in stable and unstable regions respectively. Figure 6.24(a) shows the response of the free-surface when the external excitation frequency is 0.8 times of the fundamental slosh frequency, amplitude 0.2*g*, these system parameters lie in stable region, as expected bounded / stable response is obtained. Figure 6.24(b) shows the response of the free-surface when the external excitation frequency is twice the fundamental slosh frequency with amplitude of 0.2*g*, these system parameters lie in unstable region, and as expected the free-surface is unstable and shows unbounded response. Figure 6.24(b) shows the exponential increase in the amplitude of the free-surface wave, which is a peculiar behaviour of parametric instability. Figure 6.25 shows the snapshots of the experiment at various time steps, for the response shown in Figure 6.24(a), when the free-surface is stable. Figure 6.26 shows the snapshots of the experiment at various time steps, for the response shown in Figure 6.24(b), when the free-surface is unstable. Figure 6.25 displays a bounded response of the free-surface. The video of this case can be seen in the http://youtu.be/L1LADAPVKG4. Figure 6.26 displays an unbounded response of the free-surface. The video of this case can be seen in the http://youtu.be/4ft_jd5dkvQ.

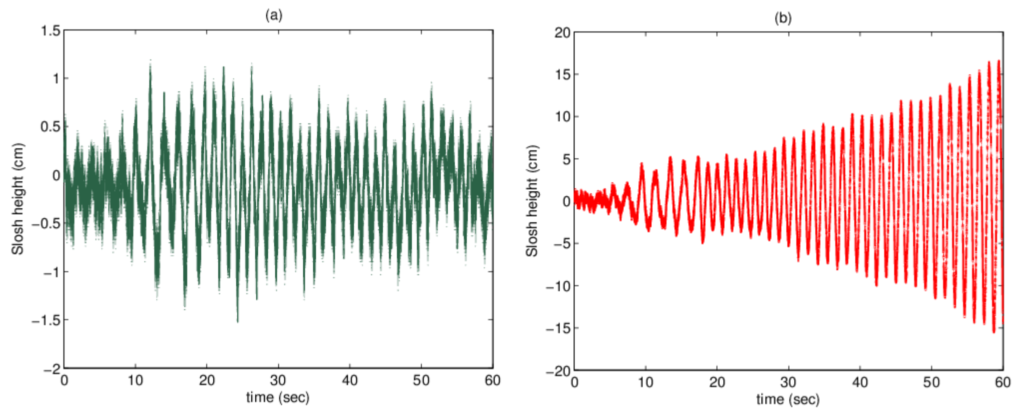


**Figure 6.24: (a) Stable response, $\omega_v = 0.8f_{10}$, $a_v = 0.2g$ (b) Unstable response, $\omega_v = 2f_{10}$, av = 0.2$g$**

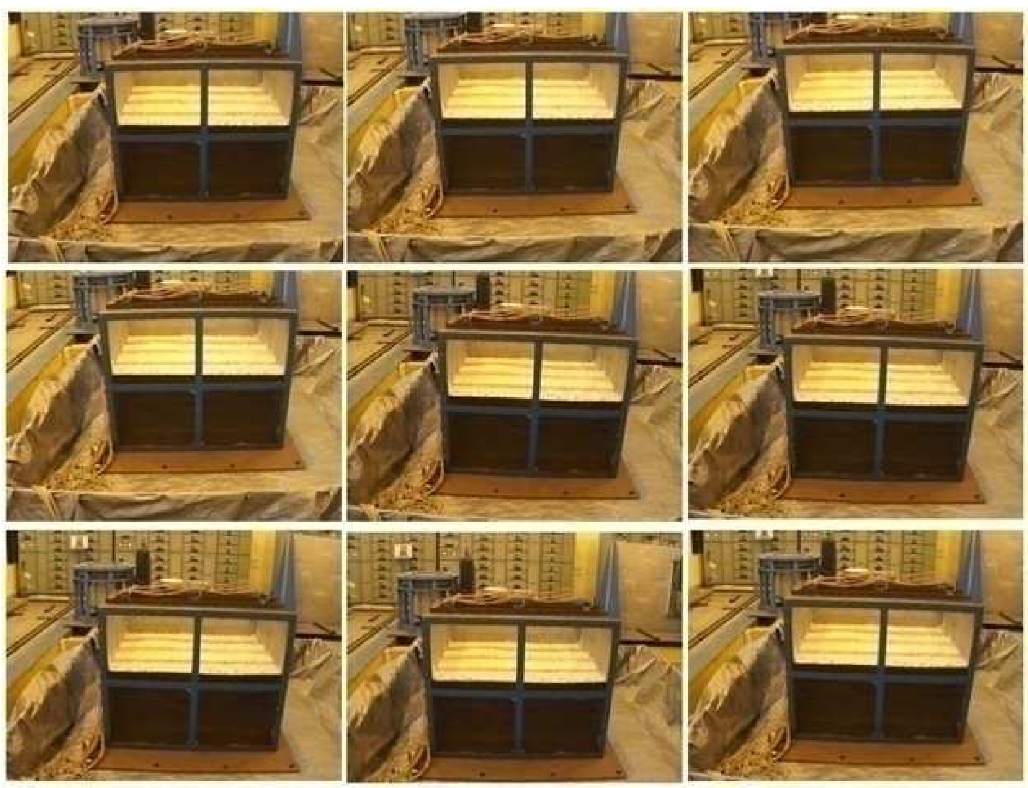

**Figure 6.25: Snapshots of free-surface at different time steps showing stable response as shown in Figure 6.24(a)**

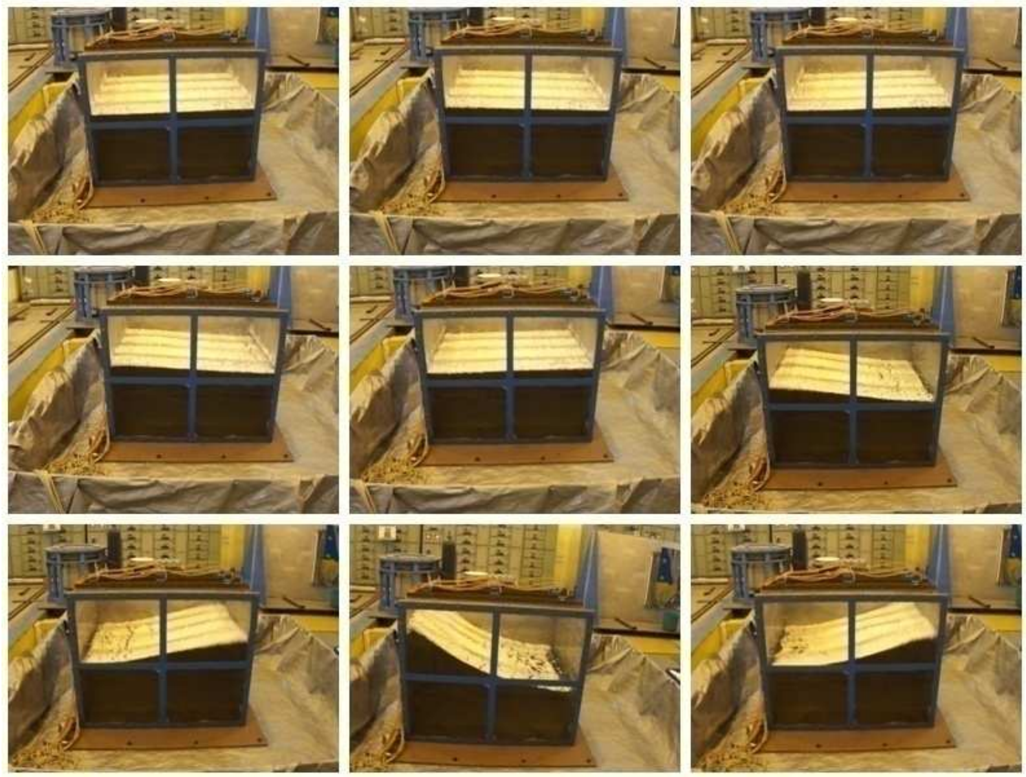

**Figure 6.26: Snapshots of free-surface at different time steps displaying parametric instability as shown in Figure 6.24(b)**

### 6.8.4 Validity of stability chart

The liquid filled container was excited with various frequencies ranging from $0.5f_{10}$ to $2.5f_{10}$ for fixed amplitude ranging from $0.1g$ to $1g$ picking the frequencies from the stability chart lying in the principal parametric instability region to validate the stability chart obtained. The focus was on the principal parametric instability region because it is the most dominating and catastrophic. For these different excitation parameters the response of the fluid free-surface is checked, the excitation parameters for which free-surface response is unbounded or bounded are noted and a chart is plotted. Figure 6.27 shows the experimental test points for which the free-surface response is stable and unstable. Figure 6.27 also shows the theoretical boundary curve separating the stable and unstable region. Figure 6.27 indicates that the predicted boundaries of the instability region agree closely with the experiment.

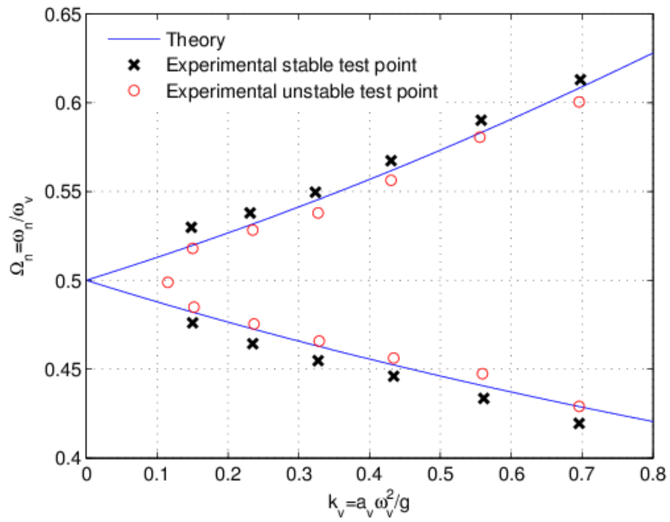


**Figure 6.27: Comparison of theoretical and experimental stable and unstable regions**

## 6.9 Summary

Stability of free-surface sloshing response of liquid in 2-D fixed and forced tanks is investigated numerically considering fully non-linear equations. The stability of the free-surface is obtained theoretically. A fully non-linear finite element numerical model has been developed based on potential flow theory to simulate the sloshing response. Free-surface sloshing response is simulated under regular harmonic base excitations for small and steep waves as defined by Frandsen. The slosh response is simulated for horizontal, vertical and combined base excitations of the tank. An experiment on shake table is carried out to validate the stability chart obtained. It is found that numerical and experimental results are in good agreement with the stability chart obtained theoretically.

# Chapter 7

# DYANMIC STABILITY OF THIN SHELLS FILLED WITH LIQUID

## 7.1 Introduction

Thin cylindrical shells are used extensively in several branches of engineering especially in civil, off-shore, nuclear, petrochemical, mechanical, marine and aerospace engineering. These cylindrical shells are utilized as a containment vessels or tanks for the storage of liquids. This is mainly due to the important role played by these shells as efficient load carrying members, particularly axial and lateral loads. Under dynamic loadings like seismic excitations, these thin-walled cylindrical shells experience axial compressive loads and exhibit highly nonlinear behaviour and lose stability there by failing at load levels very much less than the material's ultimate strength. The inertial coupling between fluid motion (sloshing) and shell wall motions may affect significantly the dynamic behaviour and stability of fluid filled shells. When a thin cylindrical storage tank is subjected to vertical excitations, axisymmetric dynamic liquid loads act on the shell wall resulting in large amplitude vibrations with circumferential wave numbers equal to or larger than one. The frequencies of these vibrations will be half the frequency of the excitation force and this type of vibration can be explained as parametric resonance. Hence, in order to utilize the thin cylindrical shells effectively without failing under dynamic loads, it is important to study the dynamic behaviour of shells under dynamic excitations.

In 1960, Bublik and Merkulov [136] analyzed the dynamic stability of a simply supported cylindrical tank under axial excitations theoretically and showed that the problem is governed by Hill's equation. Kana and Craig [137, 138] considered a cantilever cylindrical shell completely filled with liquid and analyzed the stability of the shell theoretically and experimentally. Vijayaraghavan and Evan-Iwanowski [139] investigated the parametric instability of thin cylindrical shells subjected to in-plane longitudinal inertia loading arising from sinusoidal base excitation analytically and experimentally. Shkenev [140] and Pavlovskii and Filin [141, 142] analyzed dynamic stability of an elastic shell filled with ideal liquid theoretically. Tani [143] studied the dynamic stability of truncated conical shells under periodic axial load theoretically. Yamaki and Nagai [144] investigated dynamic stability of cylindrical shells under periodic shearing forces theoretically. Haroun [145] and Veletsos [146] studied the axisymmetric response of a cylindrical tank subjected to vertical excitation theoretically by making few simplified assumptions. Chiba and Tani [147 – 152] studied the dynamic stability of liquid filled cylindrical shells under horizontal and vertical excitations experimentally and theoretically. Chiba and Tani carried out experimental studies with polyester test cylinders and their studies were at high frequency range (200-900 Hz) whereas the normal seismic loadings are of frequency range 1-30 Hz. The studies on investigation of dynamic buckling in the seismic frequency range were carried out by Uras and Liu [153 – 159]. Uras and Liu investigated the dynamic stability of liquid-filled shells with fluid-structure interaction theoretically through Galerkin finite element discretization procedure under the seismic loadings. Kochupillai and Ganesan [160, 161] studied the parametric instability in flexible pipes conveying fluid under time-periodic flow fluctuations of fluid numerically using finite element method. Goncalves and Silva [162 – 164] analyzed dynamic instability of circular cylindrical shells under static and harmonic axial loadings theoretically using Poincare maps and Lyapunov exponents. A detailed review of linear and non-linear shell vibrations, including fluid-shell interaction, can be found in a book by Amabili [165].

In all the references cited so far, the dynamic stability studies in fluid-filled cylindrical shells were carried out either theoretically or experimentally. Theoretical studies are possible for simple geometries with simple boundary conditions. If the geometry of the shell or the boundary conditions are complex, theoretical solution goes complex and may be even impossible for some situations. It is possible to apply numerical methods like finite element method for such cases. In the present chapter the dynamic stability of fluid-filled cylindrical shells is investigated numerically using finite element method. Both the thin shell and fluid are discretized using finite element method. Hsu's stability criteria are applied to study the dynamic stability.

## 7.2 Governing equations

The liquid-shell system under consideration is shown in Figure 7.1; it is a ground-supported circular thin-walled cylindrical shell of radius $R$, height $L$ and thickness $h$, with the wall connected to rigid base. The tank is partly filled with an inviscid, compressible liquid of mass density $\rho_f$ to a height $H$. $E$, $\upsilon$, $\rho_s$ are the structures Young's modulus, poisons ratio and density respectively.

### 7.2.1 Fluid field equations

The linearized governing equation for the inviscid, compressible, irrotational fluid domain in terms of pressure variable is the wave equation given as follows in the frequency domain

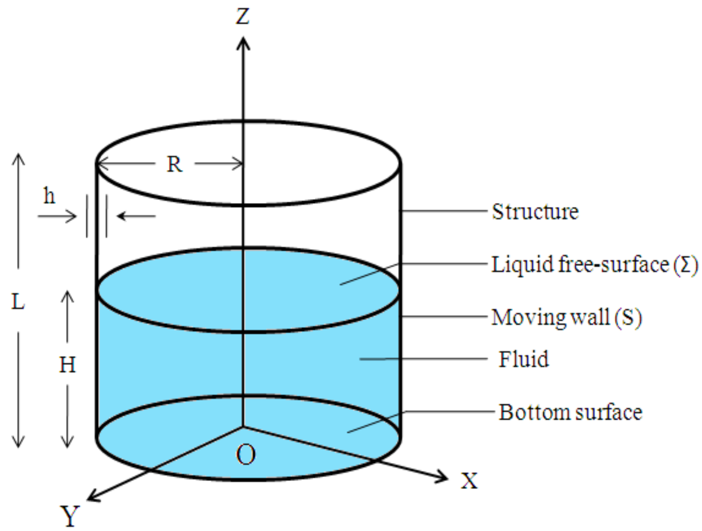


**Figure 7.1: Fluid-filled cylindrical shell and its boundary conditions**

$$\frac{1}{\rho_f}\frac{\partial^2 p}{\partial x_i^2}+\frac{1}{\rho_f}\frac{\omega^2}{c^2}\,p=0 \text{ in } V_f \tag{7.1}$$

where $V_f$ is the fluid volume, $c$ is the acoustic wave propagation velocity in fluid, $p$ is the dynamic pressure field. To the volume equation of fluid various boundary conditions are associated, as shown in Figure 7.1.

#### 7.2.1.1 Moving wall boundary condition (*S*)

$$\frac{1}{\rho_f}n_i.\frac{\partial p}{\partial x_i}-\omega^2 n_i.u_i=\overline{\gamma}_i\left(t\right).n_i \tag{7.2}$$

where $n_i$ is unit vector normal to the boundary, $u_i$ is the displacement vector of the moving wall of the thin shell and $\overline{\gamma}_i\left(t\right)$ is the dynamic load acting on the system.

#### 7.2.1.2 Free surface in gravitational field (*Σ*)

In the gravitational field $g$, the dynamic pressure on the free surface is related to the normal displacement $Z$ of fluid, by the equation

$$p=\rho_f gz \tag{7.3}$$

$$\frac{1}{\rho_f} n_i . \frac{\partial p}{\partial x_i} - \omega^2 z = -\overline{\gamma}_i \left( t \right) . n_i \tag{7.4}$$

Fixed pressure on the free surface

$$p = p_s \tag{7.5}$$

### 7.2.2 Structural filed equations

Let $u$ be the structure displacement, $\varepsilon(u)$ be the strain and $\sigma(u)$ be the stress fields of the thin-walled structure. The structure is described using an elastic shell model. The structure is assumed to have an elastic, linear, isotropic behaviour. The kinetic and potential energies of the structure are given by,

$$T\left( t \right) = \frac{1}{2} \int_{V_m} \rho_s \left( \frac{\partial u}{\partial t} \right)^2 dv \tag{7.6}$$

$$U\left( t \right) = \frac{1}{2} \int_{V_m} \sigma\left( u \right) \varepsilon\left( u \right) dv \tag{7.7}$$

The governing equation for structure in frequency domain is given by,

$$\rho_s \omega^2 u_i + \frac{\partial \sigma_{ij}\left( u \right)}{\partial x_{ij}} + F_i = 0 \text{ in } V_m \tag{7.8}$$

with boundary condition:

$$\sigma_{ij}\left( u \right) . n_j = -p n_j \text{ on } S \tag{7.9}$$

$F_i$ corresponds to volume forces of the structure.

### 7.2.3 Fluid-structure coupling

Coupling between the fluid and structure is done by the boundary conditions Eq. (7.2) and Eq. (7.9). Equation (7.2) expresses the continuity of the normal displacement component of the structure. On $S$, the structure acts on the fluid through an imposed displacement in the normal direction at the fluid boundary.

Equation (7.9) expresses the continuity of the normal component of the stress tensor at the fluid-structure interface. On *S*, the fluid acts on the structure through imposed pressure that creates a structure loading in the normal direction at the structure boundary.

## 7.3 Numerical treatment of the coupled problem

### 7.3.1 Variational formulation of the coupled problem

To obtain the numerical approximation of the coupled problem, finite element method is employed. A start of employing finite element method is to use a variational formulation approach. The variational formulation of the structure for any virtual displacement field $\delta u$ satisfying the required boundary conditions is written as:

$$\int_{V_m} \sigma_{ij}\left(u\right)\varepsilon_{ij}\left(u\right)dv - \omega^2 \int_{V_m} \rho_s u.\delta u dv - \int_{V_m} F_i \delta u dv - \int_S pn.\delta u ds = 0 \tag{7.10}$$

The variational formulation of the fluid for any virtual pressure field $\delta p$ is written as:

$$\begin{aligned} &\int_{V_f} \frac{1}{\rho_f}\frac{\partial p}{\partial x_i}\frac{\partial \delta p}{\partial x_i} dv - \omega^2 \int_{V_f} \frac{1}{\rho_f c^2} p\delta p dv - \omega^2 \int_s u.n \\ &\qquad - \int_{\Sigma} z\delta p ds + \int_{S+\Sigma} \overline{\gamma}_i\left(t\right).n_i \delta p ds = 0 \end{aligned} \tag{7.11}$$

The sloshing of the free surface is governed by Eq. (7.3), the corresponding variational formulation with any virtual normal displacement $\delta z$ can be written as:

$$\int_{\Sigma} \rho_f g z \delta z ds - \int_{\Sigma} p\delta z = 0 \tag{7.12}$$

### 7.3.2 Finite element discretization

To the above variational formulations equations, setting a suitable shape functions for each variable and spatially discretizing using finite elements gives mass, stiffness, load and fluid-structure interaction matrices [72, 80] for the structure and fluid as follows:

Structure:

$$\int_{V_m} \rho_s u.\delta u dv \to \delta U^T M_s U \tag{7.13}$$

$$\int_{V_m} \sigma_{ij}\left(u\right)\varepsilon_{ij}\left(u\right) dv \to \delta U^T K_s U \tag{7.14}$$

$$\int_{V_m} F_i \delta u dv \to F_s \tag{7.15}$$

Fluid:

$$\int_{V_f} \frac{1}{\rho_f c^2} p\delta p dv \to \delta p^T M_f p \tag{7.16}$$

$$\int_{V_f} \frac{1}{\rho_f} \frac{\partial p}{\partial x_i} \frac{\partial \delta p}{\partial x_i} dv \to \delta p^T K_f p \tag{7.17}$$

$$\int_{s+\Sigma} \overline{\gamma}_i\left(t\right).n_i \delta p ds \to F_f \tag{7.18}$$

Free surface of fluid:

$$\int_{\Sigma} \rho_f g z \delta z ds \to \delta z^T K_{\Sigma} z \tag{7.19}$$

Fluid-structure interaction:

$$\int_{S} pn.\delta u ds \to \delta U^T R_{fs} p \tag{7.20}$$

$$\int_{S} u.n\delta p ds \to \delta p^T R_{fs}^T U \tag{7.21}$$

$$\int_{\Sigma} z\delta p ds \to \delta p^T R_{sz} z \tag{7.22}$$

$$\int_{\Sigma} p\delta z \to \delta z^T R_{sz}^T p \tag{7.23}$$

In the above equations the suffix *s* stand for structure and *f* stand for fluid. Finite element discretization leads to the following coupled equations:

$$-\omega^2 M_s U + K_s U - R_{fs} p = F_s \tag{7.24}$$

$$-\omega^2 M_f p + K_f p - \omega^2 R_{fs}^T U - \omega^2 R_{sz} z = F_f \tag{7.25}$$

$$K_\Sigma z - R_{sz}^T p = 0 \tag{7.26}$$

The above dynamic equations of the coupled liquid-elastic shell system can be combined to obtain complete fluid-structure dynamic interaction matrix equation as follows:

$$\begin{bmatrix} K_s & -R_{fs} & 0 \\ 0 & K_f & 0 \\ 0 & -R_{sz}^T & K_\Sigma \end{bmatrix}\begin{bmatrix} U \\ p \\ z \end{bmatrix} - \omega^2 \begin{bmatrix} M_s & 0 & 0 \\ R_{fs}^T & M_f & R_{sz} \\ 0 & 0 & 0 \end{bmatrix}\begin{bmatrix} U \\ p \\ z \end{bmatrix} = \begin{bmatrix} F_s \\ F_f \\ 0 \end{bmatrix} \tag{7.27}$$

The above matrix eq. (7.27) is non-symmetric and extraction of eigenvalues and eigenvectors become extremely difficult. Although the eigenvalues and eigenvectors can be computed using available non-symmetric algorithms [166], they require lots of computational time. From that point of view, the non-symmetric matrix equations are converted to symmetric form. Several methods have been proposed to convert the non-symmetric coupled problem to symmetric coupled problem. In some formulations [167], the matrices are forced to take symmetrical forms by including some additional unknowns.

A new variable $\pi$ is introduced, such as:

$$\pi = -\frac{p}{\omega^2} \tag{7.28}$$

Thus the coupled problem is formulated with the unknowns as (*u, p, z,* $\pi$), where the structure has displacement, *u* as unknown and the fluid has pressure, *p*, normal free surface displacement, $z$ and $\pi$ as the unknowns. Equation (7.28) can be written as follows, using the fluid stiffness matrix, $K_f$:

$$K_f p + \omega^2 K_f \pi = 0 \tag{7.29}$$

Combining Eq. (7.29) with Eq. (7.27) gives the following system of coupled equations:

$$\begin{bmatrix} K_s & 0 & 0 & 0 \\ 0 & K_f & 0 & 0 \\ 0 & 0 & 0 & 0 \\ 0 & 0 & 0 & K_\Sigma \end{bmatrix} \begin{bmatrix} U \\ p \\ \pi \\ z \end{bmatrix} - \omega^2 \begin{bmatrix} M_s & 0 & -R_{fs} & 0 \\ 0 & 0 & -K_f & 0 \\ -R_{fs}^T & -K_f^T & -M_f & R_{sz} \\ 0 & 0 & -R_{sz}^T & 0 \end{bmatrix} \begin{bmatrix} U \\ p \\ \pi \\ z \end{bmatrix} = \begin{bmatrix} F_m \\ 0 \\ F_f \\ 0 \end{bmatrix} \tag{7.30}$$

The above matrix equation is in symmetric form and could be easily solved. The system of equation is in the general form of a usual structural system equation $K-\omega^2 M=F$, the usual numerical methods used for dynamic analysis of structure systems can be applied without any change to the coupled fluid-structure system of equations.

From the above coupled fluid-structure equations, when the equation of motion for the structure with fluid-structure interaction is considered the mass matrix gets an additional term called added mass matrix denoted by $M_{Add}$. A portion of the liquid vibrates with the tank; this portion called as impulsive mass and is characterized by the added mass. The fluid structure interaction in the frequency domain is described by the following eigenvalue problem:

$$-\omega^2 \left[ M_s + M_{Add} \right] U + K_s U = 0 \tag{7.31}$$

where

$$M_{Add} = R_{fs} M_f^{-1} R_{fs}^T \tag{7.32}$$

The added mass matrix $M_{Add}$ is positive definite. Due the added mass, the eigenfrequencies of the structure with fluid are lower than the eigenfrequencies of the structure without fluid.

## 7.4 Governing equation for dynamic stability analysis of liquid-filled shells

Thus the governing equation for dynamic stability of liquid-filled shells under vertical seismic excitations can be written as

$$M\ddot{U} + KU + K_G\left(t\right)U = 0 \tag{7.33}$$

where $M, K, K_G$ is the mass matrix (including added mass of the fluid), the stiffness matrix and the time dependent geometrical stiffness matrix. $U$ is the generalized displacement vector. The formulations of these matrices are shown in Chapter 6. Eq. (7.33) can be transformed to the following equation using natural vibration mode shapes as per the mode superposition technique

$$\ddot{u} + \left(K^{(0)} + K\left(t\right)\right)u = 0 \tag{7.34}$$

By applying the transformation, the total mass matrix is normalized to the identity matrix and stiffness matrix is reduced to a diagonal matrix $K^{(0)}$ of natural frequencies $\omega_{in}^2$ where $i$ for axial mode number and $n$ stand for circumferential mode number and $u$ is the generalized displacement in transformed coordinates. The time dependent geometric stiffness matrix $K(t)$ varies periodically with time and can be expanded as Fourier series as follows

$$K\left(t\right) = \sum_{s=1,2,\ldots}^{S} \left(D^{(s)}\cos\left(s\omega t\right) + E^{(s)}\sin\left(s\omega t\right)\right) \tag{7.35}$$

By adding a diagonal damping matrix C, whose components are given by

$$c_{in} = 2\xi\omega_{in} \tag{7.36}$$

where $\xi$ is the damping ratio and the coupling of each mode is assumed to be negligible, the governing equation of motion for dynamic stability analysis takes the form

$$\ddot{u} + C\dot{u} + K^{(0)}u + \sum_{s=1}^{S}\left(D^{(s)}\cos\left(s\omega t\right) + E^{(s)}\sin\left(s\omega t\right)\right)u = 0 \qquad (7.37)$$

In seismic analysis, the response of the fluid-structure system is dominated by only a few modes, with this assumption Eq. (7.37) can be simplified to

$$\ddot{u} + C\dot{u} + K^{(0)}u + \varepsilon Du\cos\omega t = 0 \qquad (7.38)$$

where $\omega$ and $\varepsilon$ represent a typical dominant frequency and the normalized amplitude of the seismic excitation respectively. The above equation in the component form can be written as follows

$$\ddot{u}_j + 2\xi\omega_{jn}\dot{u} + \omega_{jn}^2 u + \varepsilon\sum_j d_{ij}\cos\omega t = 0 \qquad (7.39)$$

Eq. (7.39) is a set of coupled Mathieu equations. The stability of Eq. (7.39) can be sought from the methods discussed in Chapter 1.

## 7.5 Dynamic stability analysis

For a given dimensions and physical properties of the shell and liquid, Eq. (7.39) shows the solution growing indefinitely with time under certain combinations of $\varepsilon$ and $\omega$. The dynamic stability Eq. (7.39) is obtained using Hsu's stability criteria. According to Hsu's results, the instability boundaries are given by the following equations [148]

$$\frac{\omega}{\omega_{ij}} = 1 \pm \bar{\theta}_{ij} \qquad (7.40)$$

$$\omega_{ij} = \omega_{in} + \omega_{jn}, \quad \bar{\theta}_{ij} = \sqrt{\frac{\varepsilon^2 d_{ij} d_{ji}}{16\omega_{in}^2\omega_{jn}^2} - \xi^2} \qquad (7.41)$$

In the above stability conditions, $\omega_{ij}$ and $\overline{\theta}_{ij}$ correspond to the central frequency and the relative width parameter of the instability region respectively. The instability regions obtained using Eq. (7.40 – 7.41) are the combination resonance instability regions of sum type. In addition, Eq. (7.39) has parametric instability regions when the excitation frequency $\omega$ is almost twice the natural frequency $\omega_{in}$. The boundaries of this instability region is obtained by putting $i=j$ in Eq. (7.40) and Eq. (7.41).

## 7.6 Numerical results and discussion

The dynamic stability of fluid filled shells is studied for two different cases; a tall tank and a broad tank. The geometrical data for the tall and broad storage tank used in this chapter are given in Table 7.1. Both the tanks are assumed to be filled with water to 75% of height. The dimensions of the tank are same as the dimensions of tanks taken in Chapter 5. Density of water is taken as 1000 kg/m$^3$. Before analyzing the dynamic stability of shells, it is needed to know the natural frequencies of the fluid-structure system. A free-vibration analysis is carried out in the next section.

### 7.6.1 Free vibration analysis of fluid-structure system

The natural frequencies and mode shapes of the fluid-structure system can be obtained by solving the eigenvalue problem given in Eq. (7.30). The complete analysis of the dynamic stability of fluid-structure system is carried out in CAST3M [168], an object oriented finite element software package. The validity of CAST3M for fluid-structure interaction problems can be referred in [169-171]. The vibrational modes of a circular cylindrical shell filled with fluid can be classified as

**Table 7.1: Geometric and material data of the cylindrical shells**

| Shell data | | Tall shell | Broad shell |
|---|---|---|---|
| $R$ | Radius | 7.32 m | 18.130 m |
| $L$ | Length | 21.96 m | 12.20 m |
| $t$ | Thickness | 0.0254 m | 0.0254 m |
| $E$ | Young's modulus | 206.7 GPa | 206.7 GPa |
| $v$ | Poisson ratio | 0.3 | 0.3 |
| $\rho$ | Shell mass density | $7.84*10^3$ Kg/m$^3$ | $7.84*10^3$ Kg/m$^3$ |

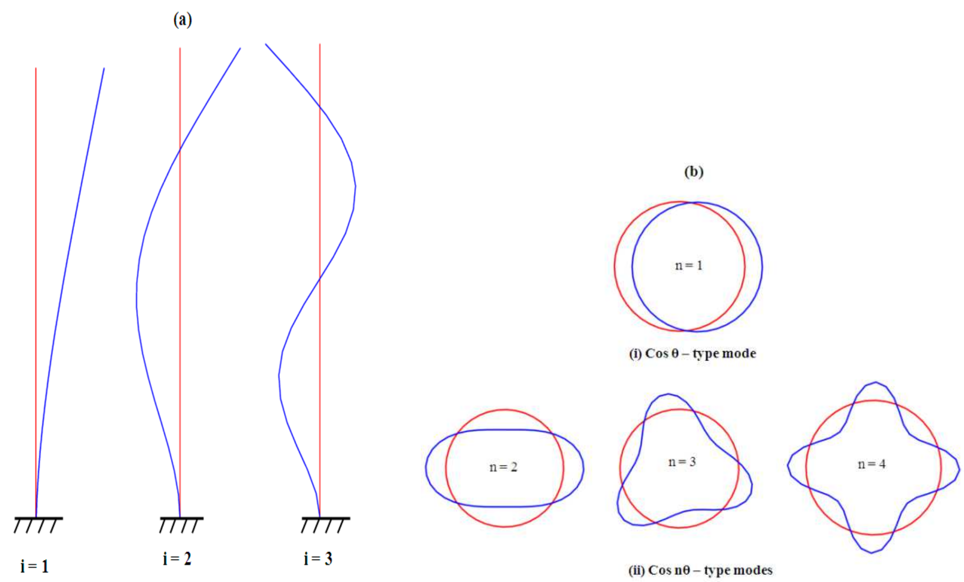


**Vertical nodal patterns** **circumferential nodal patterns**

**Figure 7.2: Fluid filled circular cylindrical shell vibrational modes**

the cos $\theta$-type modes for which there is a single cosine wave of deflection in the circumferential direction, and as the cos $n\theta$-type modes for which the deflection of the shell involves a number of circumferential waves higher than 1. These circumferential cos $n\theta$-type modes can be further denoted as beam-type modes because the shell behaves like a vertical cantilever beam across the length. Figure 7.2 shows the vertical nodal patterns and circumferential modes for a circular cylindrical shell filled with fluid. Table 7.2 and Table 7.3 shows the frequencies obtained for tall and broad shell respectively filled with 75% of fluid using

CAST3M. Eleven circumferential modes and respective first four beam bending modes for tall and broad tanks are listed in the tables.

**Table 7.2: Natural frequencies of 75% water filled tall tank in Hz**

| N | i =1 | i = 2 | i =3 | i =4 |
|---|---|---|---|---|
| 0 | 8.3900 | 21.7788 | 30.6000 | 37.0870 |
| 1 | 7.5664 | 19.0684 | 27.2553 | 34.7280 |
| 2 | 3.8778 | 13.3654 | 23.3592 | 30.6960 |
| 3 | 2.3316 | 9.2367 | 18.3713 | 26.1492 |
| 4 | 1.8390 | 6.8814 | 14.3715 | 22.1290 |
| 5 | 2.1403 | 5.6799 | 11.7428 | 18.9999 |
| 6 | 2.9151 | 5.5905 | 10.2408 | 16.7749 |
| 7 | 3.9289 | 6.6056 | 9.9507 | 15.4247 |
| 8 | 5.4472 | 8.0779 | 11.4522 | 15.1237 |
| 9 | 7.8278 | 7.8279 | 14.2709 | 16.9166 |
| 10 | 11.4890 | 11.4886 | 12.2500 | 13.2498 |

**Table 7.3: Natural frequencies of 75% water filled broad tank in Hz**

| N | i =1 | i = 2 | i =3 | i =4 |
|---|---|---|---|---|
| 0 | 7.6132 | 14.0437 | 16.6794 | 22.0095 |
| 1 | 7.7356 | 13.5557 | 18.0370 | 21.8886 |
| 2 | 6.7361 | 12.8303 | 17.7728 | 21.7119 |
| 3 | 5.7191 | 12.5201 | 17.4291 | 21.857 |
| 4 | 4.8012 | 11.8171 | 16.9818 | 21.3220 |
| 5 | 4.0513 | 11.1001 | 16.9560 | 20.8907 |
| 6 | 3.4553 | 10.2286 | 15.9066 | 20.3305 |
| 7 | 2.9916 | 9.3406 | 15.3397 | 19.8196 |
| 8 | 2.6485 | 8.5395 | 14.7584 | 19.4217 |
| 9 | 2.4242 | 7.8678 | 14.1782 | 19.1193 |
| 10 | 2.3253 | 7.3345 | 13.6227 | 18.8837 |

### 7.6.2 Dynamic stability of tall and broad fluid filled shells

In the present section dynamic stability analysis is carried out for the fluid-filled shells using Hsu's conditions as given in Eq. (7.40). Figure 7.2 and Figure 7.3 shows the dynamic stability chart of tall and broad shell respectively. The simple resonance regions are shown in blue colored lines and combination resonance regions are shown in red colored lines. From the stability charts it can be observed that, if the peak ground acceleration (PGA) of vertical base excitation exceeds approximately 0.2g, the tanks undergo parametric instability and below this excitation the tanks are stable. From the figures we can infer that, the instability regions are more dense and broad for tall tank compared to broad tank. Thus tall tank is more prone to dynamic instability under vertical excitation.

## 7.7 Summary

The dynamic stability of bottom clamped cylindrical shells filled with fluid under vertical base excitation is obtained using Hsu's stability criteria. The governing Mathieu-Hill equation is obtained by employing finite element formulation. Two tanks of different aspect ratio are taken and analysis is carried out in CAST3M.

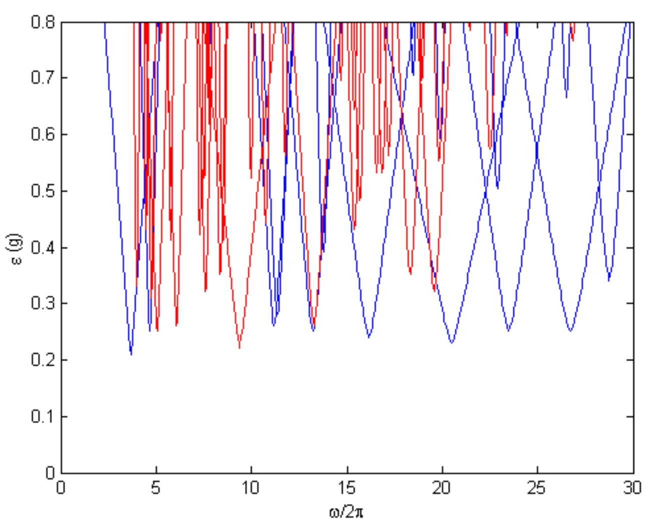


**Figure 7.3: Dynamic stability chart for tall tank**

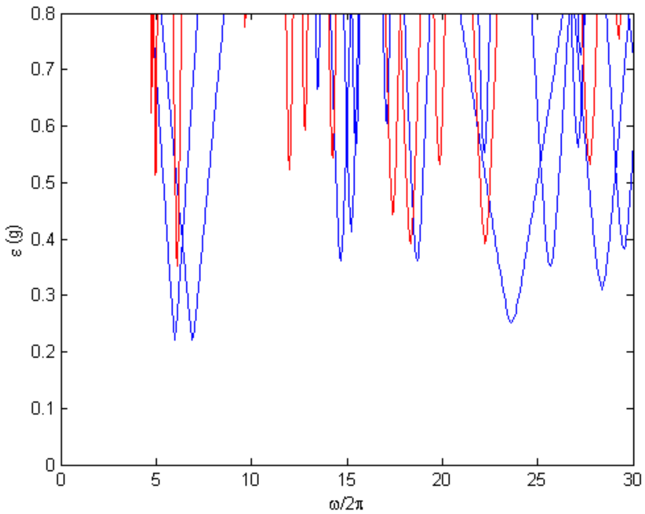


**Figure 7.4: Dynamic stability chart for broad tank**

# Chapter 8

# SUMMARY AND SCOPE FOR FUTURE STUDIES

## 8.1 Summary

The present work deals with the investigation of dynamic stability of elastic structures under parametric excitation. The governing equations of motion for the system have been derived using finite element method. The governing equation of motion to study parametric instability is classified as Hill's equation. The objective of solving Hill's equation is not to get the exact form of solution but to know under what parameters the system undergoes instability. This is done by plotting stability chart. Computer codes were written to plot the dynamic stability charts. The entire computational process has been accomplished by computer codes developed in MATLAB and CAST3M.

Chapter 1 introduces to parametric instability, its governing equation and mathematical methods to analyze parametric systems. Mathematical aspects and methodology of analyzing the stability of parametric systems is discussed. Floquet's theory, Bolotin's analytical and finite element approach and Hsu's stability approach are discussed along with pros and cons of each method.

In chapter 2 a SDOF parametric system i.e. a simple pendulum and an inverted pendulum are studied which serves in understanding the methodology and phenomenon of parametric stability and instability with ease.

Chapter 3, 4 and 5 respectively deal with dynamic stability analysis of simply supported slender beam, simply supported thin plates and bottom clamped thin cylindrical shell. The governing equations are derived using finite element method. Stability analysis was carried out using Bolotin's finite element approach and Hsu's stability criteria. The present computer codes are written so that any arbitrary boundary conditions can be given to the elastic structures.

Chapter 5 deals with dynamic stability of free-surface sloshing of liquid in rigid tanks under vertical excitations. The stability of the free-surface of the liquid is analyzed theoretically through the governing linearized equations. A finite element arbitrary Eulerian-Lagrangian formulation is developed [List of Publications, Journals, 1] for sloshing response under horizontal, vertical and combined excitations. The stability chart obtained is checked by simulating sloshing response using the finite element formulation and by an experiment on shake table. The numerical and experimental results were as expected from the stability chart. The same numerical model is extended to sloshing response in axisymmetric tanks [List of Publications, Journals, 2], sloshing response in tanks with submerged components [List of Publications, Conference Proceedings, 7] and to sloshing response in 3D rectangular tanks.

Chapter 6 deals with the dynamic stability of cylindrical shells filled with fluid taking fluid-structure-interaction into account. Dynamic stability chart is obtained employing Hsu's stability criteria. Numerical analysis is carried out in CAST3M.

## 8.2 Scope of future-work

Some of the possible areas for further research from the present work are given below.

1. The dynamic stability of the elastic structures with material non-linearity has to be explored.

2. Numerical formulation for dynamic stability of free-surface of liquid and for non linear sloshing response in tanks was studied assuming tanks as rigid. The numerical formulation for the same studies can be extended to flexible tanks.
3. The same numerical formulation can be extended to study the sloshing response in tanks subjected to rotational motion.
4. It would be interesting to study the sloshing response under vertical excitations of large amplitudes. For large amplitudes, the sloshing response can be chaotic and liquid can splash. These studies cannot be carried out with the present developed finite element formulation. Finite element method being a grid based method, it has its own limitations for very large amplitude sloshing response studies, it demands mesh less methods. Such studies have to be carried out using smoothed particle hydrodynamics (SPH).
5. Shake table experiments have to be conducted for studying dynamic stability of thin shells filled with fluid.
6. In the present work dynamic stability of fluid-filled shells are carried out assuming linearized free-surface boundary conditions of fluid. The dynamic stability studies of fluid-filled shells can be carried out with non-linear free-surface boundary conditions of fluid.

# REFERENCES


1. M. Faraday, On a peculiar class of acoustical figures; and on certain forms assumed by groups of particles upon vibrating elastic surfaces, *Philosophical Transactions Royal Society of London*, **121,** 299-340, 1831.
2. F. Melde, Concerning the generation of standing waves of a filamentous body, (Ueber die Erzeugung stehender Wellen eines fadenfÖrmigen Körpers), *Annals of Physics and Chemistry,* **109**, 193-215, 1860.
3. L. Rayleigh, *The Theory of Sound*, London: Macmillan, 1877.
4. L. Matthiessen, Acoustic experiments; the smallest transverse waves of fluids free-surface, (Akustische Versuche, die kleinsten Transversal wellen der Flüssigkeiten bctressend), *Annals of Physics,* **134**, 107-117, 1868.
5. L. Rayleigh, On maintained vibrations, *Philosophical Magazine,* **15**, 229-235, 1883a.
6. L. Rayleigh, On the crispations of fluid resting upon a vibrating support, *Philosophical Magazine,* **16,** 50-58, 1883b.
7. T. B. Benjamin, F. Ursell, The stability of the plane free-surface of a liquid in vertical periodic motion, *Proceedings of Royal Society of London,* **225 (A)**, 505-515, 1954.
8. N. W. Mc Lachlan, *Theory and Applications of Mathieu Functions*, Oxford University Press, New York, 1957.
9. N. M. Beliaev, Stability of prismatic rods subjected to variable longitudinal forces, *Collection of Papers: Engineering and Structural Mechanics,* 149-167, 1924.
10. N. M. Krylov and N. N. Bogoliubov, Calculations of the vibrations of frame construction with the consideration of normal forces and with the help of the methods of nonlinear mechanics, *Collection of Papers: Investigation of Vibration of Structures,* 5-24, 1935.
11. E. A. Beilin and G. U. Dzhanelidze, Survey of work on the dynamic stability of elastic systems, *Prikladnaya Matematika i Mekhanika*, **16 (5)**, 635-648, 1952.
12. J. J. Stoker, *Nonlinear Vibrations in Mechanical and Electrical Systems,* Interscience Publishers Limited, London, 1950.

13. S. Timoshenko and J. M. Gere, *Theory of Elastic Stability,* Mc Graw Hill Book Company, 1961.

14. V. V. Bolotin, *The Dynamic Stability of Elastic Systems,* Holden-Day, Inc, San Francisco, London, Amsterdam, 1964.

15. A. H. Nayfeh and D. T. Mook, *Nonlinear Oscillations,* John Willey & Sons, Inc., New York, 1979.

16. R. A. Ibrahim, *Parametric Random Vibration,* Research Studies Press Limited, England, 1985.

17. Matthew Cartmell, *Introduction to Linear, Parametric and Nonlinear Vibrations,* Chapman and Hall, 1990.

18. R. M. Evan Iwanoski, On the parametric response of structures, *Applied Mechanics Review,* **18**, 699-702, 1965.

19. S. T. Ariaratnam, Parametric resonance, *Proceedings of the tent U. S. National Congress of Applied Mechanics,* 1986.

20. G. J. Simitses, Instability of dynamically loaded structures, *Applied Mechanics Review,* **40**, 1403-1408, 1987.

21. W. Magnus and S. Winkler, *Hill's Equations,* Interscience Publishers, John Wiley & Sons, 1966.

22. L. Meirovitch, *Methods of Analytical Dynamics,* Mc Graw Hill Book Company, 1970.

23. H. D. Angelo, *Linear Time-Varying System: Analysis and Synthesis,* Allyn and Bacon, Inc., 1970.

24. J. A. Richards, *Analysis of Periodically Time-Varying Systems,* Springer-Verlag, 1983.

25. W. Szemplinska-Stupnicka, The generalized harmonic balance method for determining the combination resonance in the parametric dynamic systems, *Journal of Sound and Vibration,* **58 (3)**, 347-361, 1978.

26. Tadashi Kotera, A new method of determining regions of instability of a system with parametric excitations, *Bulletin of JSME,* **23 (177)**, 419- 424, 1980.

27. K. Takahashi, An approach to investigate the instability of the multi-degree-of-freedom parametric dynamic systems, *Journal of Sound and Vibration,* **78(4)**, 519-529, 1981.

28. K. Takahashi, Instability of parametric dynamic systems with non-uniform damping, *Journal of Sound and Vibration,* **85(2)**, 257-262, 1982.
29. S. T. Noah, G. R. Hopkins, A generalized Hill's method for the stability analysis of parametrically excited dynamic systems, *ASME Journal of Applied Mechanics*, **49**, 217-223, 1982.
30. O. Turhan, A generalized Bolotin's method for stability limit determination of parametrically excited systems, *Journal of Sound and Vibration,* **216 (5)**, 851-863, 1998.
31. C. S. Hsu, On the parametric excitation of dynamic system having multiple degrees of freedom, *ASME Journal of Applied Mechanics,* **30**, 367-372, 1963.
32. C. S. Hsu, Further results on parametric excitation of a dynamic system, *ASME Journal of Applied Mechanics,* **32**, 373-377, 1965.
33. J. E. Brown, J. M. Hutt, A. E. Salama, Finite element solution to dynamic stability of bars, *AIAA Journal*, **6**, 1423-1425, 1968.
34. S. Z. H. Burney, *Dynamic Stability of Plane Structures*, Doctoral Thesis, Department of Civil Engineering and Applied Mechanics, McGill University, 1971.
35. B. A. H. Abbas, Thomas, Dynamic stability of Timoshenko beams resting on an elastic foundation, *Journal of Sound and Vibration*, **60**, 33-44, 1978.
36. B. A. H. Abbas, Dynamic stability of a rotating Timoshenko beam with a flexible root, *Journal of Sound and Vibration*, **108**, 25-32, 1986.
37. B. P. Shastry, G. Venkateswara Rao, Dynamic stability of bars considering shear deformation and rotatory inertia, *Computers and Structures*, **19**, 823-827, 1984.
38. B. P. Shastry, G. Venkateswara Rao, Dynamic stability of a short cantilever column subjected to distributed axial loads, *Computers and Structures*, **22 (6)**, 1063-1064.
39. B. P. Shastry, G. Venkateswara Rao, Dynamic stability of cantilever columns resting on an elastic foundation, *Computers and Structures*, **25 (1)**, 157-158, 1987.
40. Y. Basar, C. Eller, W. B. Kratzig, Finite element procedures for parametric resonance phenomenon of arbitrary elastic shell structures, *Computational Mechanics*, **2**, 89-98, 1987.

41. G. Briseghella, C. E. Majorana, C. Pellegrino, Dynamic stability of elastic structures: a finite element approach, *Computers and Structures*, **69**, 11-25, 1998.

42. I. Svensson, Dynamic instability regions in a damped system, *Journal of Sound and Vibration*, **244**, 779-793, 2001.

43. F. Tisseur, K. Meerbergen, The quadratic eigenvalue problem, *SIAM Review*, **43 (2)**, 235-286, 2001.

44. R. A. Struble, *Nonlinear Differential Equations,* Mc Graw Hill Book Company, Inc., New York, 1962.

45. A. B. Pippard, The inverted pendulum, *European Journal of Physics*, **8**, 203-206, 1987.

46. A. James Blackburn, S. Vik, Wu. Binruo and H. J. T. Smith, Driven pendulum for studying chaos, *Review of Scientific Instruments,* **60 (3)**, 422-426, 1989.

47. F. M. Phelps, J. H. Hunter, An analytical solution of the inverted pendulum, *American Journal of Physics*, **33**, 285-295, 1965.

48. P. L. Kapitsa, Dynamic stability of a pendulum with a vibrating point of suspension, in collected papers by P. L. Kapitsa, *Peragmon*, *London*, **2**, 714-725, 1965.

49. D. J. Ness, Small oscillations of a stabilized, inverted pendulum, *American Journal of Physics,* **35**, 964-967, 1967.

50. H. P. Kalmus, The inverted pendulum, *American Journal of Physics*, **38**, 874-878, 1970.

51. R. W. Leven, B. Pompe, C. Wilke, B. P. Koch, Experiments on periodic and chaotic motions of a parametrically forced pendulum, *Physica*, **16D**, 371-384, 1985.

52. J. Miles, Directly forced oscillations of an inverted pendulum, *Physics Letters*, **A133**, 295-297, 1988.

53. J. A. Blackburn, H. J. T. Smith, N. Gronbech Jensen, Stability and Hopf bifurcations in an inverted pendulum, *American Journal of Physics*, **60**, 903-908, 1992.

54. H. J. T. Smith, J. A. Blackburn, Experimental study of an inverted pendulum, *American Journal of Physics*, **60**, 909-911, 1992.

55. D. J. Acheson, T. Mullin, Upside-down pendulums, *Nature*, **366**, 215-216, 1993.

56. D. J. Acheson, A pendulum theorem, *Proceedings of Royal Society of London,* **443**, 239-245, 1993.
57. G. Erdos, T. Singh, Stability of a parametrically excited damped inverted pendulum, *Journal of Sound and Vibration*, **198**, 643-650, 1996.
58. M. V. Bartuccelli, G. Gentile, K. V. Georgiou, On the dynamics of a vertically driven damped planar pendulum, *Proceedings of Royal Society of London*, **457**, 3007-3022, 2001.
59. R. M. Carbo, R. W. M. Smith, M. E. Poese, Stability of the parametrically excited damped inverted pendulum: Theory and experiment, *Journal of the Acoustical Society of America*, **128(4)**, 1623-1631, 2010.
60. T. Iwatsubo, M. Saigo, Parametric instability of clamped-clamped and clamped-simply supported columns under periodic axial load, *Journal of Sound and Vibration*, **30(1)**, 65-77, 1973.
61. T. Iwatsubo, T. Sugiyama, Simple and combination resonances of columns under periodic axial loads, *Journal of Sound and Vibration*, **33(2)**, 211-221, 1974.
62. Y. K. Lin, T. Y. Shih, Column response to horizontal-vertical earthquakes, *ASCE Journal of Engineering Mechanics*, **6**, 1099-1109, 1980.
63. F. Hara, Seismic vibration analysis of a vertical mechanical structure subjected to horizontal and vertical 2D random excitation, *International conference on structural mechanics in reactor technology (SMIRT)*, **M1-M2**, 135-140, 1985.
64. R. F. Fung, The effect of non-linear inertia on the steady state response of a beam system subjected to combined excitations, *Journal of Sound and Vibration*, **203(3)**, 373-387, 1997.
65. Han-II Park, Dong-Ho Jung, A finite element method for dynamic analysis of long slender marine structures under combined parametric and forcing excitations, *Ocean Engineering*, **29**, 1313-1325, 2002.
66. M. Chiba, Influence of horizontal excitations on dynamic stability of a slender beam under vertical excitations, *Experimental Mechanics*, **49**, 541-549, 2009.
67. Y. S. Hamed, M. Sayed, D. X. Cao, W. Zhang, Nonlinear study of the dynamic behavior of string-beam coupled system under combined excitations, *Acta Mechanica*, **27(6)**, 1034-1051, 2011.

68. R. D. Cook, D. S. Malkus, M. E. Plesha, R. J. Witt, *Concepts and applications of finite element analysis*, John Wiley & Sons, New York, 2007.
69. T. Yamamoto, A. Saito, On the oscillations of summed and differential types under parametric excitation (Vibratory systems with damping), (Printed in Japanese), *Transactions of the Japan Society of Mechanical Engineers*, **33**, 905-914, 1967.
70. K. J. Bathe, *Finite Element Procedures*, PHI Learning Private Limited, New Delhi.
71. J. M. Hutt and A. E. Salam, Dynamic stability of plates by finite elements, *ASCE Journal of Engineering Mechanics Division*, 879-899, 1971.
72. D. Krajcinovic and G. Herrmann, Numerical solutions of the dynamic stability problem, *International Journal of Numerical Methods in Engineering*, **2**, 551-561, 1970.
73. J. Tani and T. Nakamura, Dynamic stability of annular plates under periodic radial loads, *Journal of Acoustical Society of America*, **64**, 827-831, 1978.
74. R. S. Srinivasan and P. Chellapandi, Dynamic stability of rectangular laminated composited plates, *Computers and Structures*, **24**, 233-238, 1986.
75. K. Takahashi and Y. Konishi, Dynamic stability of a rectangular plate subjected to distributed in-plane dynamic force, *Journal of Sound and Vibration,* **123(1)**, 115-127, 1988.
76. L. W. Chen and J. Y. Yang, Dynamic stability of laminated composite plates by the finite element method, *Computers and Structures*, **36 (5)**, 845-851, 1990.
77. P. J. Deolasi and P. K. Datta, Simple and combination resonances of rectangular plates subjected to non-uniform edge loading with damping, *Engineering Structures*, **19(12)**, 1011-1017, 1997.
78. S. Sassi and G. L. Ostiguy, Effects of initial geometric imperfections on the interaction between forced and parametric vibrations, *Journal of Sound and Vibration*, **178(1)**, 41-54, 1994.
79. S. Sassi and G. L. Ostiguy, On the interaction between forced and combination resonances, *Journal of Sound and Vibration*, **187(1)**, 51-67, 1995.

80. S. Sassi, M. Thomas and F. Laville, Dynamic response obtained by direct numerical integration for pre-deformed rectangular plates subjected to in-plane loading, *Journal of Sound and Vibration*, **197(1)**, 67-83, 1996.
81. S. Sassi, H. Smaoui, M. Thomas and F. Laville, More details about the interaction of forced and parametric resonances arising from in-plane excitation of imperfect rectangular plates, *Journal of Sound and Vibration*, **243(3)**, 503-524, 2001.
82. O. C. Zienkiewicz and R. L. Taylor, *The finite element method*, McGraw Hill Book Company.
83. A. W. Leissa, *Vibration of plates*, U. S. Government Printing Office, NASA SP-160, 1969.
84. A. W. Leissa, Vibration and Buckling of a simply supported rectangular plate subjected to a pair of in-plant concentrated forces, *Journal of Sound and Vibration*, **127**,155- 171, 1988.
85. J. G. Teng, Buckling of thin shells: Recent advances and trends, *Applied Mechanics Review*, **49(4)**, 263-274, 1996.
86. A. W. Leissa, *Vibration of Shells*, American Institute of Physics, 1993.
87. J. C. Yao, Dynamic stability of cylindrical shells under static and periodic axial and radial loads, *American Institute of Aeronautics and Astronautics Journal*, **1**, 1391-1396, 1963.
88. J. D. Wood and L. R. Koval, Buckling of cylindrical shells under dynamic loads, *American Institute of Aeronautics and Astronautics Journal,* **1**, 2576-2582, 1963.
89. A. Vijayaraghavan and R. M. Evan-Iwanowski, Parametric instability of circular cylindrical shells, *ASME Journal of Applied Mechanics*, **E34**, 985-990, 1967.
90. N. Yamaki and K. Nagai, Dynamic stability of circular cylindrical shells under periodic shearing forces, *Journal of Sound and Vibration*, **45(4)**, 513-527, 1976.
91. N. Yamaki and K. Nagai, Dynamic stability of circular cylindrical shells under periodic compressive forces, *Journal of Sound and Vibration*, **58(3)**, 425-441, 1978.
92. C. Eller, Finite-element procedures for the stability analysis of nonlinear, parametric excited shell structures, *Computers & Structures*, **35**, 259-265, 1990.

93. K. Y. Lam and T. Y. Ng, Dynamic stability of cylindrical shells subjected to conservative periodic axial loads using different shell theories, *Journal of Sound and Vibration*, **207(4)**, 497-520, 1997.

94. Paulo B. Goncalves and Zenon J. G. N. Del Prado, Nonlinear oscillations and stability of parametrically excited cylindrical shells, *Meccanica*, **37**, 569-597, 2002.

95. Paulo B. Goncalves, Frederico M. A. Silva and Zenon J. G. N. Del Prado, Global stability analysis of parametrically excited cylindrical shells through the evolution of basin boundaries, *Nonlinear Dynamics*, **50**, 121-145, 2007.

96. F. Pellicano, K. V. Avramov, Linear and nonlinear dynamics of a circular cylindrical shell connected to a rigid disk, *Communications in Nonlinear Science and Numerical Simulation*, **12**, 496-518, 2007.

97. S. Ahmad, B. M. Irons and O. C. Zienkiewicz, Analysis of Thick and Thin Shell Structures by Curved Finite Elements, *International Journal of Numerical Mathematics*, **2**, 419-451, 1970.

98. H. N. Abramson, *The dynamic behaviour of liquid in moving containers*, NASA SP 106, 1996.

99. M. A. Haroun, (1980), *Dynamic analysis of liquid storage tanks*, California Institute of Technology Earthquake Engineering Research Laboratory, EERL 80-4.

100. M. D. Aslam, Finite Element Analysis of earthquake-induced sloshing in axisymmetric tanks, *International Journal for Numerical Methods in Engineering*, **17**, 159-170, 1981.

101. S. Mitra, Upadhyay and K. P. Sinhamahapatra, Slosh dynamics of inviscid fluids in two-dimensional tanks of various geometry using finite element method, *International Journal for Numerical Methods in Engineering*, **56**, 1625-1651, 2008.

102. H. J. P. Morand and R. Ohayon, *Fluid-Structure Interaction: Applied Numerical Methods*, Wiley: New York, 1995.

103. J. W. Miles, On the sloshing of liquid in a flexible tank, *Journal of Applied Mechanics*, **25 (2)**, 227-283, 1958.

104. H. N. Abramson, Dynamic behaviour of liquid in moving containers, ASME Applied Mechanics Reviews, 16(7), 501-506, 1963.

105. H. F. Bauer, *Theory of fluid oscillations in a circular cylindrical ring tank partially filled with liquid*, NASA-TN-D-557, 1960.

106. O. C. Zienkiewicz and P. Bettes, Fluid-structure dynamic interaction and wave forces-an introduction to numerical treatment, *International Journal of Numerical Methods in Engineering*, **13**, 1-16, 1978.

107. W. K. Liu and C. M. A. David, Coupling effect between liquid sloshing and flexible fluid-filled systems, *Nuclear Engineering and Design*, **72**, 345-357, 1982.

108. W. C. Muller, Simplified analysis of linear fluid–structure interaction, *International Journal for Numerical Methods in Engineering*, **17**, 113-121, 1981.

109. J. R. Cho, J. M. Song and J. K. Lee, Finite element techniques for the free-vibration and seismic analysis of liquid-storage tanks, *Finite Element in Analysis and Design*, **37**, 467-483, 2001.

110. O. M. Faltinsen, A numerical non-linear method of sloshing in tanks with two dimensional flow, *Journal of Ship Research*, **22**, 193-202, 1978.

111. O. M. Faltinsen, A nonlinear theory of sloshing in rectangular tanks, *Journal of Ship Research*, **18**, 224–241, 1974.

112. T. Nakayama and K. Washizu, The boundary element method applied to the analysis of two-dimensional nonlinear sloshing problems, *International Journal for Numerical Methods in Engineering*, **17**, 1631–1646, 1981.

113. J. L. Ortiz and A. A. Barhorst, Large-displacement non-linear sloshing in 2D circular rigid containers-prescribed motion of the container, *International Journal for Numerical Methods in Engineering*, **41**, 195-210, 1998.

114. G. X. Wu and R. E. Taylor, Finite element analysis of two-dimensional nonlinear transient water waves, *Applied Ocean Research*, **16**, 363-372, 1994.

115. G. X. Wu and R. E. Taylor, Time stepping solutions of the two-dimensional nonlinear wave radiation problem, *Ocean Engineering*, **8**, 785-798, 1995.

116. G. X. Wu, A. A. Ma and R. Eatock Taylor, Numerical simulation of sloshing waves in a 3D tank based on a finite element method, *Applied Ocean Research*, **20**, 337-355, 1998.

117. W. Chen, M. A. Haroun and F. Liu, Large amplitude liquid sloshing in seismically excited tanks, *Journal of Earthquake Engineering and Structural Dynamics*, **25**, 653-669, 1996.

118. M. S. Turnbull, A. G. L. Borthwick and R. Eatock Taylor, Numerical wave tank based on sigma-transformed finite element inviscid flow solver, *International Journal of Numerical Methods in Fluids*, **42**, 641-663, 2003.

119. J. B. Frandsen, Sloshing motions in the excited tanks, *Journal of Computational Physics*, **196**, 53-87, 2004.

120. J. R. Cho and H. W. Lee, Non-linear finite element analysis of large amplitude sloshing flow in two-dimensional tank, *International Journal for Numerical Methods in Engineering*, **61**, 514-531, 2004.

121. C. Z. Wang and B. C. Khoo, Finite element analysis of two-dimensional non-linear sloshing problems in random excitation, *Ocean Engineering*, **32**, 107-133, 2005.

122. V. Sriram, S. A. Sannasiraj and V. Sundar, Numerical simulation of 2D sloshing waves due to horizontal and vertical random excitation, *Applied Ocean Research*, **28**, 19-32, 2006.

123. K. C. Biswal, S. K. Bhattacharya and P. K. Sinha, Non-linear sloshing in partially liquid filled containers with baffles, *International Journal of Numerical Methods in Engineering*, **68**, 317-337, 2006.

124. W. Kanok-Nukulchai and B. T. Tam, Structure-fluid interaction model of tuned liquid dampers, *International Journal of Numerical Methods in Engineering*, **46**, 1541-1558, 1999.

125. R. A. Ibrahim, V. N. Pilipchuk and T. Ikeda, Recent advances in liquid sloshing dynamics, *ASME Applied Mechanics Review*, **54**, 133-199, 2001.

126. F. Dodge, T. Kana and H. Abramson, *Liquid free surface oscillations in longitudinally excited rigid cylindrical container*, Southwest Research Institute Technical Report 2, 1964.

127. J. W. Miles Nonlinear Faraday resonance, *Journal of Fluid Mechanics*, **146**, 285-302, 1984.

128. R. S. Khandelwal, N. C. Nigam, Parametric instabilities of a liquid free surface in a flexible container under vertical periodic motion, **Journal of Sound and Vibration**, **74(2)**, 243-249, 1981.

129. J. Miles and D. Henderson, Parametrically forced surface waves, *Annual Review of Fluid Mechanics*, **22**, 143–165, 1990.

130. M. Perlin and W. W. Schultz, Capillary effects on surface waves, *Annual Review of Fluid Mechanics*, **32**, 241-274, 2000.

131. L. Jiang, C. L. Ting, M. Perlin and W. W. Schultz, Moderate and steep faraday waves: instabilities, modulation and temporal asymmetries, *Journal of Fluid Mechanics*, **329**, 275-307, 1996.

132. J. B. Frandsen, A. G. L. Borthwick, Simulation of sloshing motions in fixed and vertically excited containers using a 2-D inviscid $\sigma$-transformed finite difference solver, *Journal of Fluids and Structures*, **18**, 197-214, 2003.

133. De-Zhi Ning, Wei-Hua Song, Yu-Long Liu and Bin Teng, A boundary element investigation of liquid sloshing in coupled horizontal and vertical excitation, *Journal of Applied Mathematics,* **Vol. 2012**, Article ID 340640, 2012. Doi:10.1155/2012/340640.

134. M. S. Longuet-Higgins and E. D. Cokelet, The deformation of steep surface waves on water: I. A numerical method of computation, *Proceedings of Royal Society of London A*, **350**, 1–26, 1976.

135. O. C. Zienkiewicz and J. Z. Zhu, The super convergent patch recovery and a postiori error estimates. Part 1: The recovery technique, *International Journal for Numerical Methods in Engineering*, **33,** 1331-1364, 1992.

136. B. N. Bublik and V. I. Merkulov, On the dynamic stability of thin elastic shells filled with a liquid, *Journal of Applied Mathematics and Mechanics* (*Prikl. Matem. Mekhan.*), **24**, 941-946, 1960.

137. D. D. Kana and J. F. Gormley, Longitudinal vibration of a modal space vehicle propellant tank, *Journal of Spacecraft*, **2**, 1585-1591, 1967.

138. D. D. Kana and R. R. Craig, Parametric oscillations of a longitudinally excited cylindrical shell containing liquid, *Journal of Spacecraft*, **5**, 13-21, 1968.

139. A. Vijayaraghavan and R. M. Evan-Iwanowski, Parametric instability of circular cylindrical shells, *ASME Journal of Applied Mechanics*, **34(4)**, 985-990, 1967.

140. Yu. S. Shkenev, Dynamic stability of an elastic shell filled with an ideal liquid, *Journal of Applied Mathematics and Mechanics* (*Prikl. Matem. Mekhan.*), **6(8)**, 128-132, 1970.

141. V. S. Pavlovskii and V. G. Filin, Parametric instability of cylindrical shells filled with a liquid, *Journal of Applied Mathematics and Mechanics* (*Prikl. Matem. Mekhan.*), **11(6)**, 72-81, 1975.

142. V. S. Pavlovskii and V. G. Filin, Nonlinear parametric vibrations of liquid-filled cylindrical shells with an initial deflection, *Journal of Applied Mathematics and Mechanics* (*Prikl. Matem. Mekhan.*), **21(3)**, 46-56, 1985.

143. J. Tani, Dynamic instability of truncated shells under periodic axial load, *International Journal of Solids and Structures,* **10**, 169-176, 1974.

144. N. Yamaki and K. Nagai, Dynamic stability of circular cylindrical shells under periodic shearing forces, *Journal of Sound and Vibration*, **45(4)**, 513-527, 1976.

145. M. A. Haroun and M. A. Tayel, Dynamic response of vertically excited liquid storage tanks, *Proceedings of 8$^{th}$ world conference on earthquake engineering*, 421-428, 1984.

146. A. S. Veletsos and A. K. Kumar, Dynamic response of vertically excited liquid storage tanks, *Proceedings of 8$^{th}$ world conference on earthquake engineering*, 453-460, 1984.

147. M. Chiba, N. Yamaki and J. Tani, Free vibration of a clamped-free circular cylindrical shell partially filled with liquid – Part I: Theoretical analysis, *Thin-Walled Structures*, **2**, 265-284, 1984.

148. M. Chiba, N. Yamaki and J. Tani, Free vibration of a clamped-free circular cylindrical shell partially filled with liquid – Part II: Numerical results, *Thin-Walled Structures*, **2**, 307-324, 1984.

149. M. Chiba, N. Yamaki and J. Tani, Free vibration of a clamped-free circular cylindrical shell partially filled with liquid – Part III: Experimental results, *Thin-Walled Structures*, **3**, 1-14, 1985.

150. M. Chiba, J. Tani, H. Hashimoto and S. Sudo, Dynamic stability of liquid-filled cylindrical shells under horizontal excitation, Part I: Experiment, *Journal of Sound and Vibration*, **104(2)**, 301-319, 1986.

151. M. Chiba, J. Tani and N. Yamaki, Dynamic stability of liquid-filled cylindrical shells under vertical excitation, Part I: Experimental results, *Earthquake Engineering and Structural Dynamics*, **15**, 23-36, 1987.

152. M. Chiba, J. Tani and N. Yamaki, Dynamic stability of liquid-filled cylindrical shells under vertical excitation, Part II: Theoretical Results, *Earthquake Engineering and Structural Dynamics*, **15**, 37-51, 1987.

153. W. K. Liu and R. A. Uras, Variational approach to fluid-structure interaction with sloshing, *Nuclear Engineering and Design*, **106**, 69-85, 1988.

154. W. K. Liu and R. A. Uras, Transient failure analysis of liquid-filled shells Part I: Theory, *Nuclear Engineering and Design*, **117**, 107-140, 1989.

155. W. K. Liu and R. A. Uras, Transient failure analysis of liquid-filled shells Part II: Applications, *Nuclear Engineering and Design*, **117**, 141-157, 1989.

156. R. A. Uras and W. K. Liu, Dynamic stability characteristics of liquid-filled shells, *Earthquake Engineering and Structural Dynamics*, **18**, 1219-1231, 1989.

157. R. A. Uras and W. K. Liu, Dynamic buckling of liquid-filled shells under horizontal excitation, *Journal of Sound and Vibration*, **141(3)**

158. K. Tsukimori, W. K. Liu, Y. H. Tsao and R. A. Uras, Dynamic stability characteristics of fluid-filled shells under multiple excitations, *Nuclear Engineering and Design,* **142**, 299-318, 1993.

159. K. Tsukimori, W. K. Liu and R. A. Uras, Formulation of dynamic stability of fluid-filled shells, *Nuclear Engineering and Design*, **142**, 267-297, 1993.

160. Jayaraj Kochupillai, N. Ganesan and Chandramouli Padmanabhan, Model reduction for parametric instability analysis in shells conveying fluid, *Journal of Sound and Vibration*, **262**, 633-649, 2003.

161. Jayaraj Kochupillai, N. Ganesan and Chandramouli Padmanabhan, Efficient computation of parametric instability regimes in systems with a large number of degrees-of-freedom, *Finite Elements in Analysis and Design*, **40**, 1123-1138, 2004.

162. Paulo. B. Goncalves, Zenon J. G. N. Del Prado, Nonlinear oscillations and stability of parametrically excited cylindrical shells, *Meccanica*, **37**, 569-597, 2002.

163. Fredericao M. A. Silva, Paulo B. Goncalves and Zenon. J. G. N. Del Prado, Nonlinear vibrations of axially loaded cylindrical shells partially filled with fluid, *DINCON'10 9th Brazilizn Conference on Dynamics, Control and their Applications*, June 07-11, 2010.

164. F. M. A. Silva, P. B. Goncalves and Z. J. G. N. Del Prado, Parametric instability and snap-through of partially fluid-filled cylindrical shells, *Procedia Engineering*, **14**, 598-605, 2011.

165. M. Amabili, *Nonlinear vibrations and Stability of shell and plates*, Cambridge Press, 2008.

166. C. Rajakumar, C. G. Rogers, The Lanczos algorithm applied to unsymmetric generalized eigenvalue problem, *International Journal of Numerical Methods in Engineering*, **32**, 1009-1026, 1991.

167. A. Combescure, Fluid-structure interaction: a general method used in the CEASEMT computer programs, *Computers and Structures*, **12**, 471-474, 1980.

168. http://www-cast3m.cea.fr/

169. Jean-Francois Sigrist, Daniel Broc and Chrisitan Laine, Dynamic analysis of a nuclear reactor with fluid-structure interaction Part I: Seismic loading, fluid added mass and added stiffness effects, *Nuclear Engineering and Design*, **236**, 2431-2443, 2006.

170. Jean-Francois Sigrist, Daniel Broc and Chrisitan Laine, Dynamic analysis of a nuclear reactor with fluid-structure interaction Part II: Shock loading, influence of fluid compressibility, *Nuclear Engineering and Design,* **237**, 289-299, 2007.

171. Jean-Francois Sigrist, Daniel Broc and Chrisitan Laine, Fluid-structure interaction effects modeling for the modal analysis of a nuclear pressure vessel, *Journal of Pressure Vessel Technology*, **129**, 1-6, 2007.

## Appendix-A

### A.1 Eigenvalue problem in the absence of damping

Eq. (1.29) and Eq. (1.30) are reduced to following generalized eigenvalue problems in the absence of damping respectively,

$$\left| K_e + K_{GS} - \frac{1}{2} K_{GD} - \frac{1}{4} \Omega^2 M \right| = 0 \qquad \text{(A.1)}$$

$$\left| K_e + K_{GS} + \frac{1}{2} K_{GD} - \frac{1}{4} \Omega^2 M \right| = 0 \qquad \text{(A.2)}$$

and

$$\left| K_e + K_{GS} - \Omega^2 M \right| = 0 \qquad \text{(A.3)}$$

$$\left| \begin{bmatrix} K_e + K_{GS} & K_{GD} \\ \frac{1}{2} K_{GD} & K_e + K_{GS} \end{bmatrix} - \Omega^2 \begin{bmatrix} 0 & 0 \\ 0 & M \end{bmatrix} \right| = 0 \qquad \text{(A.4)}$$

### A.2 On solving quadratic eigenvalue problem

Let the quadratic eigenvalue problem be of the form

$$\left( \lambda^2 A + \lambda B + C \right) v = 0 \qquad \text{(A.5)}$$

The quadratic eigenvalue problem Eq. (A.5) can be reduced to generalized eigenvalue problem using the enlarged eigenvector

$$U = \begin{bmatrix} \lambda V \\ V \end{bmatrix}. \qquad \text{(A.6)}$$

Substituting Eq. (A.5) into Eq. (A.4), it reduces to the following linear form

$$\left( \begin{bmatrix} A & 0 \\ 0 & C \end{bmatrix} - \lambda \begin{bmatrix} 0 & A \\ -A & -B \end{bmatrix} \right) U = 0. \qquad \text{(A.7)}$$

Eq. (A.7) can be solved for $\lambda$ by

$$\left| \begin{bmatrix} A & 0 \\ 0 & C \end{bmatrix} - \lambda \begin{bmatrix} 0 & A \\ -A & -B \end{bmatrix} \right| = 0 \tag{A.8}$$

## Appendix-B

The periodic solution with a period 2π can be written in the form

$$z(t) = \sum_{k=1,3,5}^{\infty} \left( a_k \sin\frac{kt}{2} + b_k \cos\frac{kt}{2} \right) \qquad \text{(B.1)}$$

Substituting the series above Eq. (B.1) into Eq. (6.18) and equating the coefficients of identical sine and cosine terms lead to the following system of linear homogenous algebraic equations

$$\begin{aligned} &\left(1+\frac{k_v}{2}-\frac{1}{4\Omega_n^2}\right)a_1-\frac{k_v}{2}a_3=0 \\ &\left(1-\frac{k^2}{4\Omega_n^2}\right)a_k-\frac{k_v}{2}\left(a_{k-2}+a_{k+2}\right)=0 \qquad k=3,5,7,\ldots \end{aligned} \qquad \text{(B.2)}$$

$$\begin{aligned} &\left(1-\frac{k_v}{2}-\frac{1}{4\Omega_n^2}\right)b_1-\frac{k_v}{2}b_3=0 \\ &\left(1-\frac{k^2}{4\Omega_n^2}\right)b_k-\frac{k_v}{2}\left(b_{k-2}+b_{k+2}\right)=0 \qquad k=3,5,7,\ldots \end{aligned} \qquad \text{(B.3)}$$

The periodic solution with period π can be expresses in Fourier series is given as

$$z(t) = b_0 + \sum_{k=2,4,6}^{\infty} \left( a_k \sin\frac{kt}{2} + b_k \cos\frac{kt}{2} \right) \qquad \text{(B.4)}$$

Substituting the series Eq. (B.4) into Eq. (6.18) and equating the coefficients of identical sine and cosine terms lead to the following system of linear homogenous algebraic equations

$$\begin{aligned} &\left(1-\frac{1}{\Omega_n^2}\right)a_2-\frac{k_v}{2}a_4=0 \\ &\left(1-\frac{k^2}{4\Omega_n^2}\right)a_k-\frac{k_v}{2}\left(a_{k-2}+a_{k+2}\right)=0 \qquad k=4,6,8,\ldots \end{aligned} \qquad \text{(B.5)}$$

$$
\begin{aligned}
& b_0 - \frac{k_v}{2} b_2 = 0 \\
& \left(1 - \frac{1}{\Omega_n^2}\right) b_2 - \frac{k_v}{2}\left(b_0 + b_4\right) = 0 \\
& \left(1 - \frac{k^2}{4\Omega_n^2}\right) b_k - \frac{k_v}{2}\left(b_{k-2} + b_{k+2}\right) = 0 \qquad k = 4, 6, 8, \ldots
\end{aligned} \tag{B.6}
$$

The system of linear homogenous Eqs. (B.2) - (B.3) and Eqs. (B.5) - (B.6) has a non-trivial solution when the determinant composed of the coefficients is zero. The determinants are written as

$$
\begin{vmatrix}
1 \pm \frac{k_v}{2} - \frac{1}{4\Omega_n^2} & -\frac{k_v}{2} & 0 & \cdots \\
-\frac{k_v}{2} & 1 - \frac{9}{4\Omega_n^2} & -\frac{k_v}{2} & \cdots \\
0 & -\frac{k_v}{2} & 1 - \frac{25}{4\Omega_n^2} & \cdots \\
\vdots & \vdots & \vdots & \ddots
\end{vmatrix} = 0 \tag{B.7}
$$

Eq. (B.7) gives determinant obtained from both the Eqs. (B.2)-(B.3) combined under the ± sign.

$$
\begin{vmatrix}
1 - \frac{1}{\Omega_n^2} & -\frac{k_v}{2} & 0 & \cdots \\
-\frac{k_v}{2} & 1 - \frac{4}{4\Omega_n^2} & -\frac{k_v}{2} & \cdots \\
0 & -\frac{k_v}{2} & 1 - \frac{16}{4\Omega_n^2} & \cdots \\
\vdots & \vdots & \vdots & \ddots
\end{vmatrix} = 0 \tag{B.8}
$$

$$\begin{vmatrix} 1 & -\frac{k_v}{2} & 0 & 0 & \cdots \\ -k_v & 1-\frac{1}{\Omega_n^2} & -\frac{k_v}{2} & 0 & \cdots \\ 0 & -\frac{k_v}{2} & 1-\frac{4}{\Omega_n^2} & -\frac{k_v}{2} & \cdots \\ 0 & 0 & -\frac{k_v}{2} & 1-\frac{16}{\Omega_n^2} & \cdots \\ \vdots & \vdots & \vdots & \vdots & \ddots \end{vmatrix} = 0 \qquad \text{(B.9)}$$

The determinants given above are called Hill determinants, they are of infinite order. The Hill determinants are tri-diagonal in nature. It is clear from these determinants that $\boldsymbol{\Omega}_n$ always appear on the diagonal of the matrices, one can invoke the analogy with the eigenvalue problem and refer $\boldsymbol{\Omega}_n$ as an eigenvalue. Then, for given values of $k_v$, it is possible to calculate values of $\boldsymbol{\Omega}_n$ corresponding to periodic solutions of period $\pi$ and $2\pi$. By solving the above eigenvalue problems, a stability chart is plotted.